

Summer 2010

Nonlinear Observers for Human-in-the-loop Control Systems

Samuel Kitchen McKinley

Embry-Riddle Aeronautical University - Daytona Beach

Follow this and additional works at: <https://commons.erau.edu/db-theses>



Part of the [Aviation Commons](#), and the [Engineering Physics Commons](#)

Scholarly Commons Citation

McKinley, Samuel Kitchen, "Nonlinear Observers for Human-in-the-loop Control Systems" (2010). *Theses - Daytona Beach*. 97.

<https://commons.erau.edu/db-theses/97>

This thesis is brought to you for free and open access by Embry-Riddle Aeronautical University – Daytona Beach at ERAU Scholarly Commons. It has been accepted for inclusion in the Theses - Daytona Beach collection by an authorized administrator of ERAU Scholarly Commons. For more information, please contact commons@erau.edu.

Nonlinear Observers for Human-in-the-loop Control Systems

By

Samuel Kitchen-McKinley

A thesis submitted to the Physical Sciences Department
In Partial Fulfillment of the Requirements of
Master of Science in Engineering Physics

Embry-Riddle Aeronautical University

Daytona Beach, FL 32114

Summer 2010

UMI Number: EP31910

INFORMATION TO USERS

The quality of this reproduction is dependent upon the quality of the copy submitted. Broken or indistinct print, colored or poor quality illustrations and photographs, print bleed-through, substandard margins, and improper alignment can adversely affect reproduction.

In the unlikely event that the author did not send a complete manuscript and there are missing pages, these will be noted. Also, if unauthorized copyright material had to be removed, a note will indicate the deletion.

UMI[®]

UMI Microform EP31910
Copyright 2011 by ProQuest LLC
All rights reserved. This microform edition is protected against
unauthorized copying under Title 17, United States Code.

ProQuest LLC
789 East Eisenhower Parkway
P.O. Box 1346
Ann Arbor, MI 48106-1346

Copyright by Samuel Kitchen-McKinley 2010

All Rights Reserved

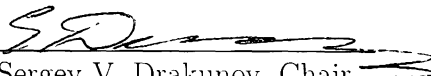
Nonlinear Observers for Human-in-the-loop Control Systems

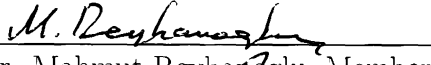
By Samuel Kitchen-McKinley

This thesis was prepared under the direction of the candidate's thesis committee chair, Dr. Sergey V Drakunov, Department of Physical Sciences, and has been approved by the members of his thesis committee. It was submitted to the Department of Physical Sciences and was accepted in partial fulfillment of the requirements for the


Degree of
Master of Science in Engineering Physics


THESIS COMMITTEE:

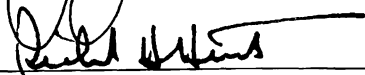

Dr. Sergey V. Drakunov, Chair


Dr. Mahmut Beyhanoglu, Member


Dr. John Hughes, Member


Dr. Erdman, MSEP Graduate Program Coordinator


Dr. Olivero, Department Chair, Physical Sciences


Dr. Richard Heist, Executive V.P. and C.A.O.


Date

Acknowledgments

I would like to thank my advisor, Dr. Sergey Drakunov, for providing me with this opportunity, and for his dedication, enthusiasm, and expertise towards the subject matter and completion of this thesis.

Abstract

The development of models for a human-in-the-loop with hardware is an area of ongoing research. The ability to simulate a human-in-the-loop with hardware provides a platform for better understanding the dynamics of human and machine cognition. A human-in-the-loop model provides information that can be used to design more efficient human interfaces and smarter autonomous assistant controllers. This can make a complex task such as flying an aircraft safer and more accessible. This thesis explores different possibilities for human operator models to be modeled in the loop with a vehicle. A human is modeled as a linear state feedback controller in the loop with the task of controlling a simple solid ball. The human arm is modeled controlling a joystick as the human is considered to control the ball with a joystick. Nonlinear sliding mode observers are developed to estimate the gains of a feedback control law and nonlinear sliding mode observers are developed to estimate the torques on the shoulder, elbow, and joystick joints. The nonlinear observers are simulated on a human-in-the-loop system to show the accuracy of the observers.

Contents

Acknowledgments	iv
Abstract	v
1 Introduction	1
1.1 Human and Machine Cognition	1
1.2 Semi-autonomous Control	2
1.2.1 Two Philosophies	3
1.2.2 Relevant Situations	5
1.3 Modeling the Human	7
1.4 Human-in-the-loop	8
1.5 Problem Statement	10
2 Mathematical Methods	12
2.1 State Space	12
2.2 Linear State Control	13
2.2.1 Linear Controllability	13
2.2.2 Stability	14
2.2.3 State Feedback Control	15
2.3 PID Controller	16

2.4	State Observers	18
2.4.1	Linear Observability	18
2.4.2	Linear State Observers	19
2.4.3	Sliding Mode	19
2.4.4	Sliding Mode State Observers	23
2.4.5	Sliding Mode Disturbance Observers	25
2.5	Least Square Method	27
2.6	Summary of Mathematical Methods	29
3	Human Decision Making Models	30
3.1	Introduction to Human models	30
3.2	Neural Networks	32
3.2.1	Neural Network Models	35
3.3	Human Chaotic Behavior	37
3.3.1	An Experiment	38
3.4	Human Based PID Controller	42
3.5	Summary of Human Models	49
4	Human Arm Models	52
4.1	Introduction to Human Motion	52
4.2	Human Arm Controlling a Joystick	55
4.3	Pitch Control Modeled with Arm and Joystick as One System	56
4.4	Pitch Control Modeled with Arm and Joystick as Two Systems	63
4.4.1	Joystick as an Inverted Pendulum	64
4.4.2	Human Arm as a Double Pendulum	67
4.5	Combining Arm and Joystick Systems	72

5	Vehicle System Model	74
5.1	Introduction	74
5.2	Aircraft Equations of Motion	75
5.2.1	Linearized Aircraft Model	78
5.3	Simple Case: Controlling A Solid Ball	83
6	Observers	88
6.1	Sliding Mode Observer for Inverted Pendulum	88
6.2	Sliding Mode Observer for Human Arm	90
6.3	Observer for PD Gains	92
7	Human-in-the-loop With Hardware	98
7.1	Results	99
7.2	Conclusion	107
8	Conclusions and Future Studies	110
8.1	Improve Models	110
8.2	Semi-Autonomous Control	112
A	Constants	119
B	Simulink Models	122
C	Matlab Code	130
	Bibliography	114

List of Tables

7.1	PD gain results.	107
A.1	Relative mass and length of select body segments as a percentage of total body mass and height for adult males [34].	119
A.2	Mass and length of select body segments as calculated from Table A.1 for typical total body mass and height of adult males.	119
A.3	Joystick constants.	121
A.4	Solid ball constants.	121

List of Figures

1.1	Block diagram of state feedback control.	9
1.2	Block diagram of human-in-the-loop with hardware.	10
2.1	Block diagram of a PID controller.	17
2.2	State trajectories for $\dot{x} = -\text{sign}(x)$ [7].	21
2.3	Sliding mode on the intersection of two surfaces with chattering [7].	21
3.1	Computer generated plots of a nonlinear function $Y = aX(1 - X)$	39
3.2	Plot of one subject's attempt to iterate equation (3.6) [36].	40
3.3	Plot of equation (3.6) with Gaussian noise [36].	40
3.4	Plot of equation (3.6) with "fuzzy" memory pair interpolation [36].	40
3.5	Block diagram of CMAC based controller method [19].	44
3.6	Block diagram of learning process [19].	44
3.7	Human and machine control results [19].	46
3.8	PID gains learned from the skilled human operator [19].	47
3.9	Block diagrams of PID controller with added disturbance.	51
4.1	Mobility of the human body [39].	53
4.2	Kinematic model of the human body [39].	54
4.3	Pitch control system diagram with arm and joystick.	56
4.4	Plot of elbow position as a function of joystick angle.	60

4.5	Angular relations of the shoulder, elbow and joystick.	62
4.6	Joystick as an inverted pendulum diagram with an arbitrary end-effector force.	64
4.7	Joystick as an inverted pendulum diagram with an end-effector force due to an applied torque.	66
4.8	Human arm as a double pendulum diagram with an arbitrary end-effector force.	67
5.1	Aircraft body axes reference [23].	76
5.2	Aircraft control results.	82
5.3	Solid ball diagram.	84
5.4	Ball control results.	86
7.1	Testing results of observers for applied torques.	100
7.2	Joystick torque observer results.	102
7.3	Shoulder torque observer results.	103
7.4	Elbow torque observer results.	104
7.5	Observable states of PD controlling solid ball.	105
7.6	Unobservable states of PD controlling solid ball.	106
7.7	Block diagram of human-in-the-loop with hardware.	108
A.1	Simulated and measured results for joystick motion.	120
B.1	Arm and joystick models and observers combined.	122
B.2	Arm Simulink model.	123
B.3	Arm Simulink observer.	124
B.4	Joystick Simulink model.	125
B.5	Solid ball Simulink model.	126

B.6	Solid ball control with PD and torque observers combined.	127
B.7	PD Simulink observer.	128
B.8	Observer vector V for PD Simulink observer.	129

Chapter 1

Introduction

1.1 Human and Machine Cognition

Everyday, humans interact with many kinds of machines. Most machines are designed with a particular function and then an interface is put in place so a human can interact with it. Some devices end up being more user friendly than others. In the case of motorized vehicles, when a human is controlling something that is beyond its own physical capabilities, the human interface becomes a large safety issue. An increase in the ability for the human to naturally control the vehicle will lead to a decrease in human related accidents. A machine could be designed for the purposes of helping a human perform a function, rather than designing a machine to do a function and then designing how the human controls the machine after the fact. This would be an example of human centered cognition where a product is designed to fit the human, rather than fitting a human to the product. A human controlled system should be designed such that the respective strengths are exploited and the respective weaknesses are mitigated [11]. There are many ways vehicle control could be modified to improve safety and efficiency for the human controller, whether driving a car, flying

an aircraft or controlling a spacecraft.

In particular, piloting an aircraft is an example of a situation where a human is required to process a lot of information in order to safely control the aircraft. This includes processing visual information from outside references as well as instruments inside the cockpit and auditory information from radio communication simultaneously while properly maintaining aircraft performance, orientation and collision avoidance. The workload on a pilot is very high. The safety and effectiveness of the pilot can be greatly increased by efficiently organizing the information into the most manageable form for a human [25].

There are many examples of how current aircraft interfaces can be improved. These improvements can be more passive or more active. A major example would be to change the format of the visual displays of the instrumentation. Another example would be to change the way information is sent to the pilot, such as a Tactile Situation Awareness System vest worn by the pilot [25]. The ability to implement any of these innovations is based on the fact that there are now very good models of aircraft in flight [11].

1.2 Semi-autonomous Control

In addition to these improvements, a more intelligent semi-autonomous autopilot could be developed to smoothly aid a human controlling an aircraft. This could be used to aid the human controller in emergency situations, such as an engine failure or a stall, where immediate and precise action is required. This could also be used in potentially dangerous situations where the pilot has become tired, distracted or incapacitated. It is important for the semi-autonomous control system to intelligently decide when it is appropriate to take control of the aircraft or when it is more ap-

propriate to just inform the pilot of an abnormal situation; there could also be a combination of the two. This is important so as not to impede the pilot's ability to control the aircraft when necessary.

1.2.1 Two Philosophies

With the progression of technology over the past century, technology has played a growing part in aviation. Part of this involves a growing amount of information available to the pilot and part of this involves a growing amount of automation. There are different philosophies debated about how much and what kind of automation should be used in aviation.

Two major aircraft manufactures have taken two opposing approaches to the use of automation in commercial aircraft. The argument basically comes down to whether the pilot or the autopilot should have the ultimate authority in regards to flying an aircraft. Airbus has chosen to design the flight computer to have the final authority, particularly when an aircraft reaches its design limits in an emergency. This way attempts to remove the human from the loop as much as possible under the pretense that human error is the cause of most accidents. Boeing takes the opposite approach, allowing the pilot to override the autopilot if the pilot deems it necessary.

This difference in philosophy really only resides in the phase of intervening with the pilot. Both aerospace companies have sophisticated autopilot control systems that can monitor the aircraft and calculate when it is unstable. Once the system has been determined to be close to instability, Boeing's aircraft will just warn the pilot of this but allow them to continue, while the Airbus aircrafts will implement a set of hard limits on the controls to keep the system from becoming unstable. This difference can be argued from a psychological standpoint about which way may be better to intervene with the pilot so as to produce the safer outcome.

Consider the example of a pilot performing an abrupt maneuver to avoid a mid air collision. In an Airbus plane, the pilot can simply pull the joystick to its limits (perhaps up and to the left) and the aircraft will respond by pitching up and to left as much as it can without exceeding the limitations of the aircraft that could make it unstable. In a Boeing plane, when the pilot avoids the collision, the pilot will only be warned if the aircraft is exceeding stability limits, but the pilot still has full control and can exceed the limits if they choose. Both ways have advantages and disadvantages. The Airbus design alleviates the workload on the pilot and removes pilot error in an emergency situation and provides the plane with the best chance for success. This reasoning comes from the point of view that if the limits have to be exceeded in order to avoid the collision then there was no way to avoid it. Boeing would argue that the pilot should have the ability to exceed the limits just enough so as to make the difference that could end up avoiding the collision. This is because the limitations are based on the design of the aircraft and have built in margins for error. Exceeding the limits does not necessarily mean instant instability or instant structural failure. Or it may be to the point that some structural failure might be manageable and worth avoiding the collision.

Having the ability to monitor the human-in-the-loop may provide access to a hybrid of both Boeing's and Airbus's autopilot implementation. The pilot could be allowed to continue beyond the aircraft limitations, like Boeing, but only if it is determined that the human is still in proper control. If it is determined that human is not in proper control, then the autopilot could take over like in Airbus. The ability to make this determination could help in the situation where the plane is heading to an unstable configuration, but with two different pilot configurations. Consider an example of the extremes where an aircraft is determined to be flying beyond its design limitations and it could be determined whether the pilot was maintaining

proper control of the aircraft or has just fallen unconscious on the control stick. The ability to monitor and determine the human's performance and the corrective action that should be taken are still two separate issues. But this information could be used to help the flight computer make a more informed decision.

1.2.2 Relevant Situations

There are many examples of situations when an autopilot should have full control, when the pilot should have full control and when a combination of the two would be best. Examples where autopilot is most useful involve situations where maintaining aircraft stability in straight and level flight become a monotonous task for the pilot. This is true because sustained monotonous activity can tire a human out. This also alleviates the pilot to be able to concentrate on other tasks such as navigation and radio communication. This implementation is commonly used on commercial flights. Examples where human control is more useful is in situations where more complex maneuvers are required such as take off and landing. The human can better adapt to unforeseen changing variables in the system.

The more interesting examples involve situations where a mix between human control and autopilot control are more useful. One example of this could be in the situation of an engine failure. For a single engine plane, an engine failure means complete loss of forward thrust. The highest priority of a pilot is to fly the aircraft. In this case flying the aircraft means establishing and maintaining the best glide airspeed. Best glide speed is always the same for a particular aircraft and provides the maximum horizontal distance per vertical height lost during powered off flight. The best glide speed is maintained through attitude control. Emergency procedures during an engine failure calls for the pilot to maintain best glide speed, search for the closest suitable landing site, attempt to restart the engine and use the radios to

provide others with information about the emergency. Obviously all this provides a heavy work load on the pilot during a stressful situation. An automatic “co-pilot” could provide support for the pilot in command. The simplest way would be for the autopilot to detect the engine failure and immediately establish best glide speed, relieving the pilot of this continuous task which takes up so much of the pilot’s concentration.

Other examples include cases where a pilot becomes tired, distracted or incapacitated. The autopilot could be used in these cases as a pilot monitor that can detect when the pilot is not responding correctly and take corrective action, which may include alerting the pilot or taking over control. A simple example of this kind is when a pilot is maintaining straight and level flight while looking inside the cockpit to do navigation calculations. The pilot’s hand remains on the yoke and may begin to drop slightly causing the plane to drift off course and possibly into an unusual attitude with no way for the pilot to know. In this situation the control of the human-in-the-loop could be monitored and the pilot could be alerted when the aircraft begins to drift towards an unstable position. If the pilot does not respond the autopilot could then take corrective action by actively controlling the aircraft.

An autopilot as described in the previous examples would be less of an autopilot that is switched either on or off, and more of a computer based “co-pilot” that monitors the system and the human-in-the-loop and smoothly assists the pilot in command to help mitigate the workload associated with flying an aircraft. The first step to designing a more intelligent control system as such involves the ability to observe the state of the human-in-the-loop with the hardware. In this case a model of the human must be known and included. In order to better design a system around the human, a better understanding of the human-in-the-loop is required.

1.3 Modeling the Human

The human being is a very complex system, and therefore it is very difficult to predict and model. The human is in part complex because of its controlling center, the brain, which is a highly complex neural nodal structure [3]. It is therefore common to model the brain as an artificial neural network. A neural network has the ability to process and learn information from the environment by recognizing common inputs, recognizing common relationships between inputs, and recognizing common associations between inputs and outputs. Different states or features are stored in different nodes of the neural network and the relationships between nodes can be reinforced by increasing the weights or values between nodes based on information from the environment. Neural networks therefore rely on temporal information as well, in that previous states are measured against current states to make decisions [12, 13, 15, 16].

Because a complete and general model of a human would be so complex and so chaotic, it would seldom be useful in practice. A more reasonable approach is to build a human model based on a particular situation or a particular task that the human would be performing. A human model could also be simplified by breaking down the human into different aspects. In total, the human model involves a series of outputs based on a series of inputs. The inputs could be the state of the environment and the outputs could be the actions, behaviors, or decisions of the human. The state of the environment is known through the senses and processed in the brain [12, 13]. The environment can be manipulated by the human through the body. In general a human acts in a heuristic manner. The same person in the same situation does not necessarily behave the same way [36].

For the purpose of this thesis, the human can be simplified to only be modeled as its function as a controller of a vehicle. In this way, the human operator can be

modeled as a standard linear feedback control. The human corrects the states of the system, the vehicle, to some desired state. Human operators are commonly modeled as a standard PID state feedback controller [18, 19, 26, 27]. A PID controller works by multiplying PID gains by the errors of the *Proportional*, *Integral* and *Derivative* states of the system. If it is assumed that human controls a vehicle with this scheme, then it could be said that a skilled operator uses optimal gains to correct the system to a desired location. The limitations of using this approximation are the same limitations that arise when using linear state feedback controllers. The linear feedback controller will only work well for the conditions the gains are designed for. If the states of the system are changing too quickly or are too far off from the desired states then the system could become too unstable for the feedback control system to compensate. At this point the PID model for the human would become inaccurate because the human can in fact adapt to the changing conditions and in a sense reprogram itself with a new control law that can compensate for a different environment.

In any case the feedback control law is built and processed in the brain. The brain measures the states of the system through the senses and controls the system mechanically with the body. The manipulation of the system, in the case of the aircraft, comes from the manipulation of the joystick which controls the aerodynamic surfaces on the aircraft. Therefore a complete model of the human pilot should include the brain as a state feedback controller and the mechanical actuator dynamics of a human arm controlling a joystick.

1.4 Human-in-the-loop

By developing a model of a human operator, it is now possible to model a human-in-the-loop with a vehicle. Understanding how the human controls a vehicle is crucial

in developing a semi-autonomous control system that can smoothly aid a human in the control of a vehicle.

A standard feedback control system is shown in Figure 1.1. The feedback control law, u , is designed to drive the error of the states of the system, \bar{y} , to zero in order to move the system to some desired state, y^* , by manipulating the input actuators of the system.

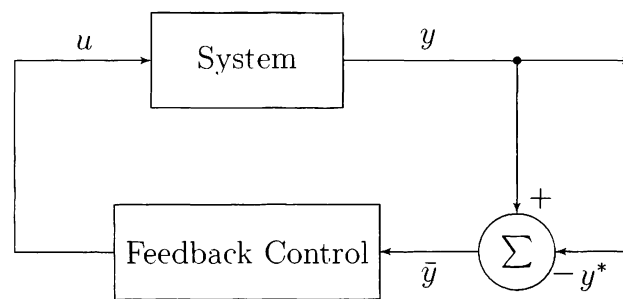


Figure 1.1: Block diagram of state feedback control.

For modeling a human-in-the-loop, a human is placed in the feedback loop much like the feedback control law in Figure 1.1. Figure 1.2 shows a human-in-the-loop with a system. The “Feedback Control” block is replaced by the model of a human. The complete model of the human is shown as three parts: the “Senses”, the “Human Brain” and the “Human Arm”. The “Senses” block simply identifies the method by which the human gathers information about the system. The “Human Brain” block contains the control law and may additionally decide the desired configuration of the system along with the method for determining the error of the system. The “Human Arm” block represents the mechanical method of interaction that the control law of the brain has with the system. The “System” block in Figure 1.1 is broken down into two parts in Figure 1.2: the “Controls” block and the “Vehicle” block. The “Controls” block represents the step between the human and the control inputs of the “Vehicle”. For instance, a human does not move the wheels of a car, but instead moves the

steering wheel which moves the wheels. In an aircraft the human manipulates a joystick which moves the aerodynamic control surfaces of the aircraft. The “Human Arm” and the “Controls” represents a step between the “Human Brain” and the “Vehicle” which has particular dynamics that the brain must then incorporate into the control law.

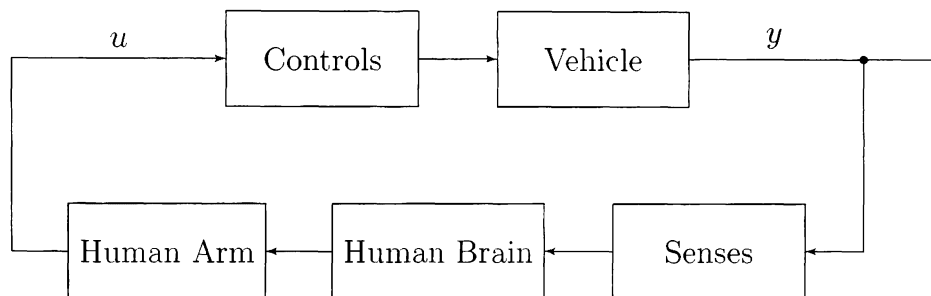


Figure 1.2: Block diagram of human-in-the-loop with hardware.

The ability to simulate a human controlling a vehicle offers a quantitative way to develop observers that could identify important parameters of a real human controlling a vehicle and possibly predict human behavior in certain situations. This could also be used to obtain information about the human, which in turn could be used to determine how an autopilot could best assist the human operator.

1.5 Problem Statement

A human-in-the-loop cannot always perform as well as a computer controller, and a computer controller cannot always perform as well as a human controller. This becomes more substantial as the complexity of the system to be controlled increases. This is particularly true in the case of a human flying an aircraft. A better understanding of the dynamics of a human-in-the-loop can provide insight into designing vehicle interfaces and semi-autonomous assistant controllers that could amplify the

strengths and mitigate the weaknesses of both the human and the computer controller.

A better understanding of human-in-the-loop dynamics relies on the ability to simulate the human-in-the-loop with hardware. This requires a model of the human controller. This thesis explores different types of decision making models and mechanical models that could be used to describe the human operator.

The ability to simulate the human-in-the-loop provides a model that can be used to identify key parameters and predict human behavior. This thesis will develop nonlinear sliding mode observers that can estimate unmeasurable states of the human. With a model of the human-in-the-loop these observers can now be designed and tested and could eventually be used to observe those parameters of a real human controlling a vehicle.

This thesis will develop nonlinear observers that can estimate the torques involved in a human arm operating a joystick. Nonlinear observers will also be developed to estimate the gains of a linear feedback control system that is designed for controlling a simple solid ball.

Chapter 2

Mathematical Methods

This chapter provides the key mathematical concepts used throughout this thesis. This includes linear control theory, linear and nonlinear observer theory, and the least square method.

2.1 State Space

To begin with, the equations that describe a system should be given in *state-space* form. Consider a differential equation of the form

$$\dot{x} = f(x). \tag{2.1}$$

where $x = (x_1, \dots, x_n)^T$ and $f = (f_1, \dots, f_n)^T$. The n -dimensional vector space is called *state-space*, where x is the *state vector* and f is the *vector field* [38].

Linear control and observer methods commonly use a linear time invariant state-

space system represented in the form

$$\dot{x} = Ax + Bu \quad (2.2a)$$

$$y = Cx, \quad (2.2b)$$

where $x \in \mathbb{R}^n$, $y \in \mathbb{R}^m$, and $u \in \mathbb{R}^q$ are the state, output, and input vectors, respectively. A is a constant $n \times n$ matrix, B is a constant $n \times q$ matrix, and C is a constant $m \times n$ matrix [38].

2.2 Linear State Control

Given a linear time invariant system in state-space form.

$$\dot{x} = Ax + Bu. \quad (2.3)$$

a control law input u can be designed so that the state vector of the system x is driven to some desired point x^*

2.2.1 Linear Controllability

A system is considered controllable if there exists an input $u(t)$ that will transfer any state $x(t_0)$ to any state $x(t_1)$ in a finite time $t_1 > t_0$. The controllability of the system from equation (2.3) can be tested by determining the rank of the controllability matrix. The controllability matrix is an $n \times (nq)$ matrix of the form

$$\begin{bmatrix} B & AB & A^2B & \dots & A^{n-1}B \end{bmatrix}. \quad (2.4)$$

The system is controllable if and only if the controllability matrix has rank n [38]. In this case, rank n also denotes full rank. Full rank means that all the rows are linearly independent.

2.2.2 Stability

Consider a nonlinear dynamic system described as

$$\dot{x} = f(x, t), \quad (2.5)$$

where $x = (x_1, \dots, x_n)^T$ is the state vector. An equilibrium point is denoted by x^* , where

$$f(x^*, t) = 0 \quad (2.6)$$

for all t .

An isolated equilibrium point has *Lyapunov stability* if for any $\epsilon > 0$ there exists a real positive number $\delta(\epsilon, t_0)$ such that for all $t \geq t_0$

$$\|x(t_0) - x^*\| \leq \delta \Rightarrow \|x(t) - x^*\| \leq \epsilon, \quad (2.7)$$

where $\|x\|$ denotes the Euclidean norm of the vector x defined as

$$\|x\| \equiv \sqrt{x^T x}. \quad (2.8)$$

An isolated equilibrium point is *locally asymptotically stable* if it has *Lyapunov stability* and

$$\|x(t_0) - x^*\| \leq \delta \Rightarrow x(t) \rightarrow x^* \quad (2.9)$$

as $t \rightarrow \infty$.

An equilibrium point is *globally asymptotically stable* if it has *Lyapunov stability* and

$$x(t) \rightarrow x^* \quad (2.10)$$

as $t \rightarrow \infty$ for any initial condition $x(t_0)$.

A linear system is stable about an equilibrium point x^* if all eigenvalues of matrix A have non-positive real parts and no repeated eigenvalues on the imaginary axis [38].

2.2.3 State Feedback Control

Consider a linear time-invariant dynamic system described in terms of the errors.

$$\dot{\bar{x}} = A\bar{x} + B\bar{u}, \quad (2.11)$$

where \bar{x} and \bar{u} denote the error defined as

$$\bar{x} = x - x^* \quad (2.12)$$

$$\bar{u} = u - u^* \quad (2.13)$$

and where x^* is the desired state and u^* is the feedforward control and where $x \in \mathfrak{R}^n$ and $u \in \mathfrak{R}^q$. The feedforward control input u^* should be chosen to satisfy the equation

$$\dot{x}^* = Ax^* + Bu^* \quad (2.14)$$

The control input u can be designed such that a control gain matrix K multiplies the state vector x and drives the system to some desired state x^* as

$$\bar{u} = -K\bar{x}, \quad (2.15)$$

where $K \in \mathfrak{R}^{q \times n}$. From equations (2.13) and (2.15) it follows that the full state feedback and feedforward control law is

$$u = \bar{u} + u^* \quad (2.16)$$

or

$$u = -K\bar{r} + u^* \quad (2.17)$$

The closed loop system then becomes

$$\dot{\bar{x}} = (A - BK)\bar{x} \quad (2.18)$$

and the characteristic equation becomes

$$|sI - A + BK| = 0. \quad (2.19)$$

Here, K can be chosen so the closed loop system is stable using the method of *pole placement*. Pole placement arbitrarily chooses the eigenvalues of $(A - BK)$ to have negative real parts and complex conjugate pairs so that the system is stable. The characteristic equation can then be used to calculate K . The eigenvalues can arbitrarily be chosen with the previously stated conditions if the system is controllable [38].

2.3 PID Controller

The most basic form of feedback control is one in which the output is proportional to the error given as [22]

$$u = K_P \bar{x}. \quad (2.20)$$

where the error, $\bar{x} \equiv e(t)$, and where

$$e(t) = r(t) - y(t) \quad (2.21)$$

as shown in Figure 2.1, where r is the reference signal and y is the output of the system. However this may not be able to control steady-state error. The steady-state can be controlled by introducing an integral component to the control given as [22]

$$u = K_P \bar{x} + K_I \int \bar{x} dt. \quad (2.22)$$

Adding a derivative component can have the advantage of providing large corrections before the error becomes too large [22]. It can also improve the transient state response. Adding the derivative component is described as [24]

$$u = K_P \bar{x} + K_I \int \bar{x} dt + K_D \dot{\bar{x}}. \quad (2.23)$$

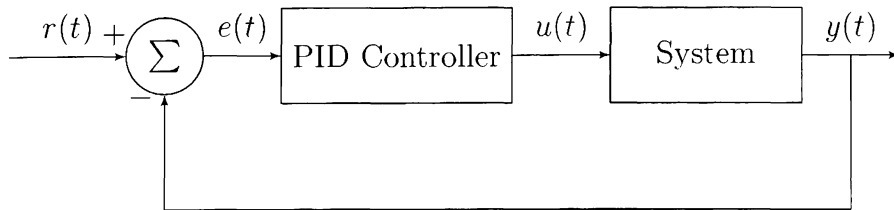


Figure 2.1: Block diagram of a PID controller.

The resultant controller is known as a proportional-integral-derivative, or PID controller. The PID controller is one of the most common feedback control laws [38]. It can be implemented as the control for many systems. The gains of the PID control law, given as K_P , K_D , and K_I , are what need to be determined and tuned to best

control any particular system. The PID controller can be implemented into a system as shown in Figure 2.1.

2.4 State Observers

This section explores methods for designing both linear and nonlinear observers. The goal of an observer is to estimate the states of a system that cannot be measured.

2.4.1 Linear Observability

Consider a linear time invariant state-space system,

$$\dot{x} = Ax + Bu \tag{2.24a}$$

$$y = Cx, \tag{2.24b}$$

where $x \in \mathbb{R}^n$, $u \in \mathbb{R}^q$, and $y \in \mathbb{R}^m$ and where y is the output vector of the measured states. A system is considered observable at t_0 if the knowledge of the control input $u(t)$ and the output $y(t)$ over a finite time period $t_0 \leq t \leq t_1$, suffices to determine the state $x(t_0)$. The observability of the system from equation (2.24) can be tested by determining the rank of the observability matrix. The observability matrix is a $(qn) \times n$ matrix of the form

$$\begin{bmatrix} C \\ AC \\ A^2C \\ \vdots \\ A^{n-1}C \end{bmatrix} \tag{2.25}$$

The system is observable if the observability matrix has rank n [38].

2.4.2 Linear State Observers

A state estimator, or observer, can be used to estimate the states of a system that cannot be directly measured. Consider a linear system,

$$\dot{x} = Ax + Bu \tag{2.26a}$$

$$y = Cx, \tag{2.26b}$$

where $x \in \mathbb{R}^n$, $y \in \mathbb{R}^m$, and $u \in \mathbb{R}^q$ and matrix C denotes which output variables are measured. Consider an asymptotic state observer.

$$\dot{\hat{x}} = A\hat{x} + Bu + L(y - C\hat{x}), \tag{2.27}$$

where \hat{x} denotes an estimate of x , and L denotes the gain matrix with dimensions $n \times q$. The error between the actual state and the estimated state, \bar{x} , is defined as

$$\bar{x} = x - \hat{x}. \tag{2.28}$$

The estimate error equation can then be described as

$$\dot{\bar{x}} = (A - LC)\bar{x}. \tag{2.29}$$

If the gain matrix L is chosen such that the eigenvalues of $(A - LC)$ have negative real parts, then the error, \bar{x} , is driven to zero [38].

2.4.3 Sliding Mode

Sliding mode control uses a variable structure control with a high speed switched feedback. The switching control law drives the states of a system to a predetermined

sliding surface, σ , in state-space. The switching control law works by having two gains: one for when the state trajectory is “above” the surface one for when the state trajectory is “below” the surface. Sliding mode control is therefore inherently discontinuous [7]. This is accomplished by implementing the sign function given as

$$\text{sign}(r) = \begin{cases} -1 & \text{if } x < 0 \\ +1 & \text{if } x > 0 \end{cases} \quad (2.30)$$

Consider a first order system

$$\dot{x}(t) = u(x), \quad (2.31)$$

with the control law

$$u(x, t) = -\text{sign}(x), \quad (2.32)$$

so that

$$\dot{x} = -\text{sign}(x), \quad (2.33)$$

as shown in Figure 2.2. Here the control $u(x, t)$ switches around the surface $\sigma(x, t) = x = 0$ so that for any initial condition x_0 there exists a finite time t_1 for which $x(t) = 0$ for all $t \geq t_1$. Ideally, once the sliding surface is intercepted, the state trajectory will remain on the sliding surface: the system is then considered to be in *sliding mode* [7]

An ideal sliding mode exists only when the state trajectory $x(t)$ satisfies $\sigma(x(t), t) = 0$ at every $t \geq t_1$ for some t_1 . However an ideal sliding mode requires infinitely fast switching to have the trajectory exactly remain on the surface, and real switching control systems will be limited to a finite frequency. As such the trajectory will oscillate within the vicinity of the sliding surface. This is called *chattering* and is shown in Figure 2.3. If the frequency is sufficiently high enough relative to the dynamic response of the system, the chattering may become negligible [7].

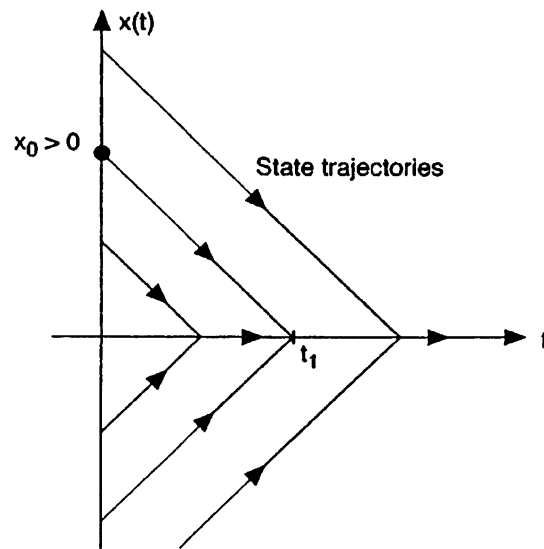


Figure 2.2: State trajectories for $\dot{x} = -\text{sign}(x)$ [7].

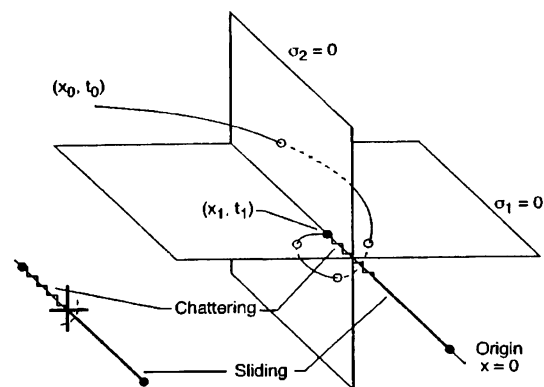


Figure 2.3: Sliding mode on the intersection of two surfaces with chattering [7].

For the explanation of equivalent control, consider the nonlinear system

$$\dot{x}(t) = f(x, t) + B(x, t)u(x, t), \quad (2.34)$$

where $x(t) \in \mathbb{R}^n$, $u(t) \in \mathbb{R}^q$ and $B \in \mathbb{R}^{n \times q}$. Equivalent control is the continuous form of sliding mode control when the system is on the sliding surface. As such, since $\sigma(x(t), t) = 0$ for all $t \geq t_1$, it follows that $\dot{\sigma}(x(t), t) = 0$. Using the chain rule, the equivalent control, u_{eq} , becomes the input for

$$\dot{\sigma} = \frac{\partial \sigma}{\partial t} + \frac{\partial \sigma}{\partial x} \dot{x} = \frac{\partial \sigma}{\partial t} + \frac{\partial \sigma}{\partial x} f(x, t) + \frac{\partial \sigma}{\partial x} B(x, t)u_{eq} = 0. \quad (2.35)$$

If $\frac{\partial \sigma}{\partial x} B(x, t)$ is nonsingular for all x and t , u_{eq} can be calculated as

$$u_{eq} = - \left[\frac{\partial \sigma}{\partial x} B(x, t) \right]^{-1} \left(\frac{\partial \sigma}{\partial t} + \frac{\partial \sigma}{\partial x} f(x, t) \right) \quad (2.36)$$

The dynamics of the system under these conditions can then be written as

$$\dot{x}(t) = \left[I - B(x, t) \left[\frac{\partial \sigma}{\partial x} B(x, t) \right]^{-1} \frac{\partial \sigma}{\partial x} \right] f(x, t) - B(x, t) \left[\frac{\partial \sigma}{\partial x} B(x, t) \right]^{-1} \frac{\partial \sigma}{\partial t}. \quad (2.37)$$

The equivalent control can be used to determine the dynamics of the system on the sliding surface [7].

The equivalent value is denoted as $[\dots]_{eq}$. For sliding mode control, $[\text{sign}(x)]_{eq}$ is an average value of the chattering as described earlier. The value $[\text{sign}(x)]_{eq}$ can be obtained by using a low pass filter tuned sufficiently so as to be large enough to eliminate the high frequency component caused by unideal switching but not too large as to eliminate the slow component of the motion which is the equivalent control [10].

Sliding mode observers are analogous to sliding mode controllers, just like linear state feedback controllers and observers, in that controllers attempt to drive a system to a desired point, $x \rightarrow x^*$, and observers attempt to drive the state estimates of a system to the actual states as $\hat{x} \rightarrow x$. For sliding mode this means that the sliding mode surface of an observer is the actual trajectory of the system and the estimate of the states should converge on that sliding surface. Design of a sliding mode observer is described in general in Section 2.4.4 and then for the specific case of estimating a disturbance in Section 2.4.5.

2.4.4 Sliding Mode State Observers

A sliding mode observer has the advantage of being more robust and applicable to nonlinear systems as compared to standard full order observers. A sliding mode observer can be used on a linear system, as denoted by equation (2.2), similar in form to equation (2.27) as

$$\dot{\hat{x}} = A\hat{x} + Bu + L\text{sign}(y - C\hat{x}). \quad (2.38)$$

With a suitable choice of the gain matrix L , the sliding vector $(y - C\hat{x})$ will converge to zero [10].

Now consider a nonlinear system,

$$\dot{x} = f(x) \quad (2.39a)$$

$$y = h(x). \quad (2.39b)$$

where $x \in \mathbb{R}^n$, $y \in \mathbb{R}^m$, and

$$f(x) = \begin{bmatrix} f_1(x) \\ f_2(x) \\ f_3(x) \\ \vdots \\ f_n(x) \end{bmatrix}. \quad (2.40)$$

In general the sliding mode observer can be designed in terms of the estimated states of the system, \hat{x} , by implementing the formula

$$\dot{\hat{x}} = \left(\frac{\partial H(\hat{x})}{\partial x} \right)^{-1} L(\hat{x}) \text{sign}(V(t) - H(\hat{x})). \quad (2.41)$$

The $H(x)$ vector is comprised of the output function $h(x)$ and its repeated Lie derivatives where

$$H(x) = \begin{bmatrix} h_1(x) \\ h_2(x) \\ h_3(x) \\ \vdots \\ h_n(x) \end{bmatrix} = \begin{bmatrix} h(x) \\ L_f h(x) \\ L_f^2 h(x) \\ \vdots \\ L_f^{n-1} h(x) \end{bmatrix} = \begin{bmatrix} h(x) \\ \frac{\partial h_1(x)}{\partial x} f(x) \\ \frac{\partial h_2(x)}{\partial x} f(x) \\ \vdots \\ \frac{\partial h_{n-1}(x)}{\partial x} f(x) \end{bmatrix}, \quad (2.42)$$

and where $L_f^i h$ is the i^{th} Lie derivative of the output function h along the vector f

The matrix $L(\hat{x})$, is a diagonal $n \times n$ matrix of gains shown as

$$L = \begin{bmatrix} L_1(\hat{x}) & & & & \\ & L_2(\hat{x}) & & & \\ & & L_3(\hat{x}) & & \\ & & & \ddots & \\ & & & & L_n(\hat{x}) \end{bmatrix}. \quad (2.43)$$

where $L_i(\hat{x}) > 0$ must be suitably large enough to reach sliding mode. The vector $V(t)$ is the observer vector shown as

$$V(t) = \begin{bmatrix} v_1(t) \\ v_2(t) \\ v_3(t) \\ \vdots \\ v_n(t) \end{bmatrix} = \begin{bmatrix} y(t) \\ [L_1(\hat{x})\text{sign}(v_1(t) - h_1(\hat{x}))]_{eq} \\ [L_2(\hat{x})\text{sign}(v_2(t) - h_2(\hat{x}))]_{eq} \\ \vdots \\ [L_{n-1}(\hat{x})\text{sign}(v_{n-1}(t) - h_{n-1}(\hat{x}))]_{eq} \end{bmatrix}, \quad (2.44)$$

where $[\dots]_{eq}$ denotes the equivalent value of a discontinuous function in sliding mode [9]. There are two drawbacks to this method. One drawback is that the Jacobian of the vector $H(\hat{x})$, $\frac{\partial H(x)}{\partial x}$, must remain nonsingular so that it is invertible. The other drawback is that observer vector $V(t)$ is determined by successive steps of taking the equivalent value. This can lead to a propagation of chattering noise produced by a finite frequency of the switching feature of the sliding mode observer.

2.4.5 Sliding Mode Disturbance Observers

Sliding mode observers have the ability to observe a disturbance on the system without having to know the functional form of the disturbance. Consider a nonlinear system with a disturbance described as

$$M(x)\ddot{r} = f(r, \dot{x}) + \xi, \quad (2.45)$$

where the functional form of the disturbance ξ is unknown. Equation (2.45) can be solved for \ddot{r} which produces

$$\ddot{r} = M^{-1}(x)f(x, \dot{x}) + M^{-1}(x)\xi. \quad (2.46)$$

Equation (2.46) can then be represented in state-space by letting

$$x_1 = x \quad (2.47a)$$

$$x_2 = \dot{x}. \quad (2.47b)$$

and so is described in the form

$$\dot{x}_1 = x_2 = \dot{x} \quad (2.48a)$$

$$\dot{x}_2 = M^{-1}(x_1)f(x_1, x_2) + M^{-1}(x_1)\xi. \quad (2.48b)$$

Assuming all the states of the system can be measured, x and \dot{x} , the disturbance ξ can be estimated using an observer of the form

$$\dot{\hat{x}}_1 = \hat{x}_2 + L_1 \text{sign}(x_1 - \hat{x}_1) \quad (2.49a)$$

$$\dot{\hat{x}}_2 = M^{-1}(\hat{x}_1)f(\hat{x}_1, \hat{x}_2) + M^{-1}(\hat{x}_1)L_2 \text{sign}(x_2 - \hat{x}_2). \quad (2.49b)$$

The errors between the observed states and the actual states can be expressed as

$$\bar{x}_1 = x_1 - \hat{x}_1 \quad (2.50a)$$

$$\bar{x}_2 = x_2 - \hat{x}_2. \quad (2.50b)$$

The equations from (2.49) can be expressed in terms of the errors as

$$\dot{\bar{x}}_1 = \bar{x}_2 + L_1 \text{sign}(\bar{x}_1) \quad (2.51a)$$

$$\dot{\bar{x}}_2 = M^{-1}(x_1)f(x_1, x_2) - M^{-1}(\hat{x}_1)f(\hat{x}_1, \hat{x}_2) + M^{-1}(\hat{x}_1)L_2 \text{sign}(\bar{x}_2) + M^{-1}(x_1)\xi. \quad (2.51b)$$

When sliding mode begins the errors are driven to zero,

$$\bar{x}_1 = x_1 - \hat{x}_1 \rightarrow 0 \quad (2.52a)$$

$$\bar{x}_2 = x_2 - \hat{x}_2 \rightarrow 0. \quad (2.52b)$$

and so the first two terms in equation (2.51b) will then cancel and $\dot{\hat{x}}_2$ will also go to zero, shown as

$$\begin{aligned} \dot{\hat{x}}_2 &\rightarrow 0 \\ M^{-1}(x_1)f(x_1, x_2) - M^{-1}(\hat{x}_1)f(\hat{x}_1, \hat{x}_2) &\rightarrow 0. \end{aligned} \quad (2.53)$$

This leaves equation (2.51b) as

$$0 = 0 + M^{-1}(\hat{x}_1)L_2\text{sign}(\bar{x}_2) + M^{-1}(x_1)\xi. \quad (2.54)$$

And so when rearranged the disturbance can now be calculated as [10]

$$\xi = [L_2\text{sign}(x_2 - \hat{x}_2)]_{eq}. \quad (2.55)$$

Therefore by using a sliding mode observer it is possible to estimate a disturbance on a system without the need for a functional form of the disturbance. This method could be described as having the ability to measure a system with a known model and estimate a disturbance that deviates the system from some expected trajectory.

2.5 Least Square Method

The least square method is a mathematical tool derived from linear algebra that can calculate the “best fit” line of a set of data points. Given a linear equation of the

form

$$XC = B, \quad (2.56)$$

where X is an $N \times n$ matrix, C is an $n \times 1$ matrix and B is an $N \times 1$ matrix shown generally as

$$\begin{bmatrix} x_1(1) & \dots & x_n(1) \\ \vdots & \cdot & \vdots \\ x_1(N) & \dots & x_n(N) \end{bmatrix} \begin{bmatrix} c_1 \\ \vdots \\ c_n \end{bmatrix} = \begin{bmatrix} b_1 \\ \vdots \\ b_N \end{bmatrix}. \quad (2.57)$$

Matrix C can be solved for as

$$XC = B \quad (2.58)$$

$$X^T XC = X^T B \quad (2.59)$$

$$C = (X^T X)^{-1} X^T B. \quad (2.60)$$

If $X^T X$ is nonsingular and so invertible, then there exists a *least square solution*, C_{opt} , by minimizing the error $\|E\|^2 \rightarrow \min$, where the error is described as

$$E = XC - B. \quad (2.61)$$

So the least square solution is given by [20]

$$C_{opt} = (X^T X)^{-1} X^T B \quad (2.62)$$

where C_{opt} is a vector of the optimal solution for the coefficients that describe a “best fit” line for a series of data points.

2.6 Summary of Mathematical Methods

The methods described in this chapter will be used in this thesis to investigate the ability to observe important parameters of a human-in-the-loop that cannot be directly measured. The particular states of interest include the feedback control gains a human-in-the-loop uses that would be calculated and processed in the brain and the torques involved in the human motion dynamics of a human arm controlling a joystick. The observers rely on the ability, in a sense, to observe the deviation of a system's trajectory from an expected trajectory. To do this, it is then required to have a model of the system. And so the next chapters aim to investigate different models that can be used for the human brain, the human arm and different vehicles that a human can control.

Chapter 3

Human Decision Making Models

3.1 Introduction to Human models

In order to be able to simulate a human-in-the-loop control system, a model of the human is essential. As discussed in Section 1.4, the model of the human can be split into two major parts; human motion, which represents the human's ability to mechanically interact with the environment, and the human brain, which represents the control center for processing information, decision making and subsequently controlling human motion through the muscular system. This chapter will focus on different model considerations for the human brain and then human motion will be discussed in Chapter 4.

There are many different approaches to designing accurate models of the human brain which may be more or less useful depending on the type of application for which it is going to be used. There are biologically inspired neural networks [16], biologically inspired macroscopic neural populations [17], mathematically inspired neural network models [5, 6, 15, 21, 32], mathematical models describing the brain as a mapping of inputs to outputs, where human behavior is described as a path from perception

to processing to action [12, 13], the states of the human could be described by the measurements of EEG (Electroencephalography) data [3, 17, 31], or the brain could be modeled as a decision making center for only specific tasks. The brain could be modeled analogous to a control system if the human is in the loop with a system and the human is only tasked with controlling that system. It is common to then describe the human mathematically as a PID controller [18, 19, 26, 27].

In general the human brain is made up of many complex connections between many neurons in a large neural network [3]. The network is chaotic on the neural level and highly dynamical on a large scale due to the coupling of neurons in both physical space and time. Any mathematical model that attempts to map out this network must consist of nonlinear differential equations taking the chaos into account [3, 12, 13, 17, 30, 36, 37]. With these main parameters in place, the mathematical model can take different forms. It may include properties of neurotransmitters, neurons, and chemical reactions that take place within the brain. This would be an example of a biologically inspired model [15, 17, 30]. Other forms may just consist of theoretical mathematics that could be applied in general to many types of networks [5, 6, 21, 32].

Another important aspect of an efficient and accurate model is its ability to adapt and change itself to better suite the changing sensory input coming from a changing environment. This can include the use of pattern storage and recognition instead of storing every bit of sensory data. A competitive network is also an important aspect to include so as to have the system itself decide what sensory input should be saved or thrown out. This can be helpful not only to throw out bad data, such as low signal to noise input or supersaturated input, but also to determine which inputs are useful or relevant bits of information. In this way, what is relevant will also be assessed by how it matches the current pattern. So the pattern and competitive nature of the network would work in tandem [12, 15, 16].

3.2 Neural Networks

The success of a neural network depends on neurons working in a competitive form. The neurons are subject to upper and lower bounds of signal saturation and low signal to noise. In a competitive system the neuron or population of neurons with the strongest intact signal can be chosen and all others can be dismissed [16]. Small signal to noise can be typical given that neurons operate near the quantum range. If the signal is too strong it could be spread over a population of interacting neurons, or perhaps shunted so as to reduce the signal below the upper threshold. If the signal is low a feedback amplification function could be used to increase the signal more than it would increase the noise. One such model can work well at both these processes by using a Sigmoid function [15].

Friston describes the brain as an collection of dynamical systems relating inputs to outputs. The model to describe this neural activity sufficiently must consist of activity at the current time and its recent history. An important aspect to the description of the brain is the idea that “the dynamics of neural systems can be viewed as a succession of transient spatiotemporal patterns of activity that mediate perceptual synthesis and adaptive sensorimotor integration.” The description will only be useful with an explicit temporal domain. A problem with describing the complexities of the brain is that not all of the state variables are directly observable. However, measurements of whole cells or populations could be possible. The two main points to the adequate description of brain activity are a mathematical relationship between the inputs and outputs and the fact that the measurable output of one system is the input of other systems [13].

Neural activity of the brain is stochastic in nature. It is a complex dynamical system including a significant portion of random noise. This can biologically come

from random opening ion channels or synaptic conductance and voltage noise. Because of the degree of randomness in the system, it is necessary to use a numerical computational model in computer simulation to accurately model neural activity in the brain [30].

The nebulous cartesian system is probabilistic description of states as cloudy packets obeying quantum rules. A description of the brain-body-mind construct must include uncertain causalities and multiple uncertain causalities. This is because of the nonlinear behavior of the neuronal electricity which can be seen as chaotic behavior measured by EEG. The “Nebulous Cartesian System” is even a step above a hyper-probabilistic construct by including aspects of sentiments, emotions and creativity. The nebulous system is a description that aims to predict future behaviors through probabilities [3].

Macroscopic neural populations is an appropriate level for modeling neural functions in perception, cognition and consciousness. Nonlinear dynamics can be used to describe the neural mechanics by which large scale patterns of brain activity are self organized. Brains are chaotic systems that do more than just filter and process sensory input; chaotic dynamics give rise to intelligence and creative powers [12].

The brain has a fundamental uncertainty in its states analogous to the Heisenberg uncertainty principle in quantum physics. There are a number of reasons why the brain behaves as a chaotic system. There are several structures of the brain that are made up of several groups of neural oscillators in at least five frequency channels. Therefore, the brain has a large number of degrees of freedom related to those activities. Also the dimension of possible states of the substructures of the brain or the brain as a whole is high. These facts lead to a chaotic system in which small changes in initial conditions may give way to large changes in the trajectories of the system. At the other end of the spectrum, the uncertain behavior of the brain structure can be

seen by observing only a few neurons. This is not a chaotic matter, but a probabilistic outcome as in the quantum efficiency of a neuron to fire or not fire when excited [3].

Freeman describes one type of perception that starts with the sensing of a stimuli. Then there is a binding of parallel activity of multiple features to represent objects that are filtered, normalized and matched with retrieved representations from storage. Perception is the binding of the representations of an object from multiple sensory systems. Another mode of perception that is more intentional is organized by large scale neural interactions whereby representations are formed within an existing framework constructed from experiences. Patterns are formed with the guidance of a chaotic attractor. Perceptions are shaped by connectivity patterns from past learning [12].

Cortical activity is the product of interactions among neuronal populations. The macroscopic features of cortical activity can be modeled in terms of the microscopic behavior of neurons. Another proposal aims use a model of neural activity to estimate physiological parameters from electrophysical data. The model assumes neurons are dynamical, random units organized into populations of similar biological properties and response characteristics. Multiple populations then can interact to form a network. This uses the idea of a changing probability density in state-space. The trajectories correspond to the state of a neuron. By taking the expectation of these probability densities, measurements can be modeled. The dynamics of a neuron can be highly random but the dynamics of the density may not be random [17].

The coupling among hierarchies of neural populations lead to neural responses and sensory information propagated through the system. Biophysical parameters can control this coupling. Electroencephalography (EEG) measures electrical activity generated by the brain. The electrochemical activity of coupled neurons generate a distribution of current sources in the cortex. This is based on the electrical properties

of the nervous tissues. These electrical traces can give an interesting expression of large scale coordinated patterns of electrical potential [17].

Nonlinear chaotic mathematical modeling of neural networks can be applied to and help make sense of data from EEGs. Understanding the chaos in EEG readings in patients can be used to help understand how epilepsy and depression can manifest in the human brain [31].

3.2.1 Neural Network Models

In Cohen and Grossberg's "Absolute Stability of Global Pattern Formation and Parallel Memory Storage by Competitive Neural Networks" [6], the process by which input patterns are transformed and stored by competitive neural networks is considered. The model which can exhibit the absolute stability property is

$$\frac{dx_i}{dt} = a_i(x_i) \left[b_i(x_i) - \sum_{k=1}^n c_{ik} d_k(x_k) \right]. \quad (3.1)$$

where $i = 1, 2, \dots, n$, and the matrix $C = ||c_{ik}||$ is symmetric and the system as a whole is competitive. The model is capable of approaching one of perhaps infinitely many equilibrium points in response to arbitrary input patterns and initial data. The global Liapunov function used to analyze the system used was

$$V(x) = -\sum_{i=1}^n \int_0^{x_i} b_i(\xi_i) d'_i(\xi_i) d\xi_i + \frac{1}{2} \sum_{j,k=1}^n c_{jk} d_j(x_j) d_k(x_k). \quad (3.2)$$

The analysis showed that all the trajectories converge. But each trajectory would not necessarily converge to a unique equilibrium point [6].

Another consideration of the Cohen-Grossberg model is made by Liao et. al. [21]. They use a modified model that includes distributed delays. The importance of the

distributed delayed feedback provides an approximation of propagated delays due to the physical separations between large numbers of neurons in a network. Their neural network model is

$$\dot{x}(t) = -a_i(x_i(t)) \left[b_i(x_i(t)) - \sum_{j=1}^n w_{ij} s_j(x_j(t)) - \sum_{j=1}^n w_{ij}^{\tau} \int_{-\infty}^t K_{ij}(t-s) s_j(x_j(s)) ds + J_i \right], \quad (3.3)$$

where $i = 1, 2, \dots, n$, J_i denotes the constant inputs from outside of the system, $\tau_{ij} \geq 0$ are the delays caused during the switching and transmission processes. $a_i(x_i(t)) \geq 0$ is the amplification function. $b_i(x_i(t))$ is the self-signal function, w_{ij} is the delayed connection weight matrix. s_j are the neuron activation functions. and K_{ij} are the delay kernels. They have also developed and shown criteria and conditions for global exponential stability [21].

The dynamic causal model for neural networks that can be used as the framework for inferring neural mechanisms from fMRI (functional Magnetic Resonance), EEG and MEG (Magnetoencephalography) measurements is described by

$$\frac{dx}{dt} = \left(A + \sum_{i=1}^m u_i B^{(i)} + \sum_{j=1}^n u_j D^{(j)} \right) x + C u, \quad (3.4)$$

where matrix A represents the fixed strength of connections between the modeled regions, matrix B represents the context-dependent modulation of these connections. and matrix C represents the influence of external inputs such as sensory stimuli [32].

The model discussed by Chumbly is also based on use for application in brain imaging such fMRIs and EEGs described as

$$\dot{z} = \left(A + \sum_{i=1}^m u_t B^i \right) z_t + C u_t, \quad (3.5)$$

where z_t is the neuronal activity, u_t is the input, and matrix A describes input inde-

pendent or “regional” connectivity among the states. Some of the parameters may be biological. Because in reality neuronal networks cannot diverge exponentially to infinity, the real component of the eigenvalues of matrix A must be negative. In fact when the largest real eigenvalue is negative, the stable mode is a point attractor [5].

3.3 Human Chaotic Behavior

Human behavior is both unpredictable and nonrandom. The behavior of a person does not come from external cause. This includes the physiological state of a person. The implication of no external cause makes the behavior of a human unpredictable. And yet a human cannot behave randomly when asked to do so. One description of this is that humans behave in a heuristic manner. A heuristic procedure does not guarantee the correctness of a solution to a particular problem. This would be opposite to an algorithm. Heuristic behavior could mean that the same person in the same situation would not necessarily behave the same way. The person could behave unpredictably but not randomly. The decision of a human is based on what comes to mind first. This could be based on the nodal structure of the neural network of that person [36].

Ward and West explored the possibility of a human responding randomly by developing a model that could simulate a human attempting to mimic a nonlinear system. The system used was a logistic difference equation,

$$Y_{n+1} = aY_n(1 - Y_n), \quad (3.6)$$

where a is a constant and therefore the current value of Y_{n+1} is produced from a previous value Y_n . The chaotic attractor, a , determines how random the series appears to be. Values between 3.5 and 4 are where the function appears most random. Ward

and West chose a to be 3.66 [36].

3.3.1 An Experiment

Subjects were asked to respond with the next number in the series based on the previous “seed” number. The subjects were trained by the nonlinear function

$$Y = aX(1 - X). \quad (3.7)$$

The subjects would make a guess based on a given seed, X , and presented with the correct response, Y , as feedback. This was iterated until the subject’s accuracy became asymptotic [36]. Once the subjects had sufficiently learned with feedback, they then tried to iterate equation (3.6) without feedback. Starting with an initial random seed, each subsequent response was used as the seed for the next response. Figure 3.1 shows a computer generation of equation (3.7) with n number of iterations, where $n = 100$, $a = 3.66$, and $Y_{initial} = 0.5$. Each value was multiplied by 1000 before being plotted. Figure 3.1(a) shows the logistic map generated from equation (3.7). Figure 3.1(b) shows the logistic map generated by iterating equation (3.6). And Figure 3.1(c) shows the output of equation (3.6) as per iteration. This shows how Figure 3.1(b) is generated in time. Notice that this could appear as the values chaotically “jumping” around the function and would be difficult for a human to accurately reproduce. If a subject was to perfectly iterate the function the logistic map would match Figure 3.1(b) [36].

Figure 3.2 shows how close the subject approximated the logistic iteration. In order to quantify the accuracy, Ward and West best fitted equation (3.7) to the subject’s data by adjusting the value of a . The subject from Figure 3.2 approximated a chaotic attractor of 3.47 with an adjusted R^2 value of 0.851 [36].

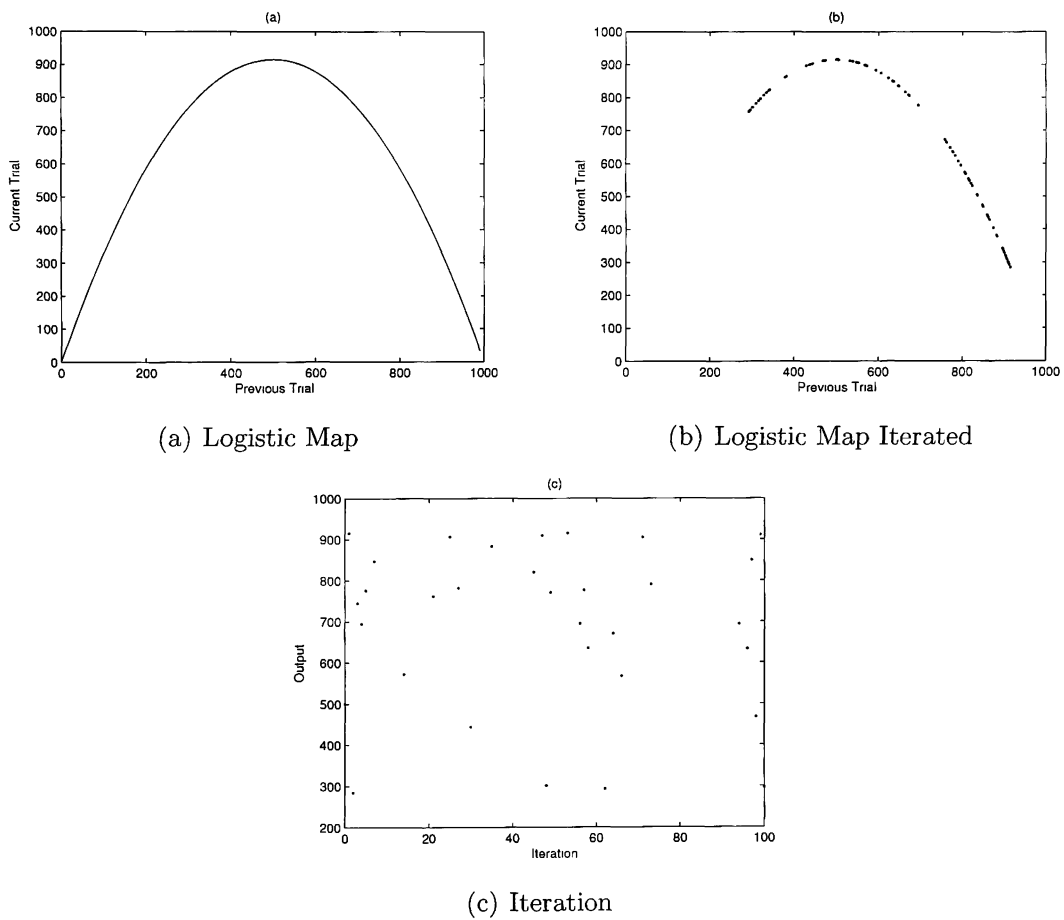


Figure 3.1: Computer generated plots of a nonlinear function $Y = aX(1 - X)$.

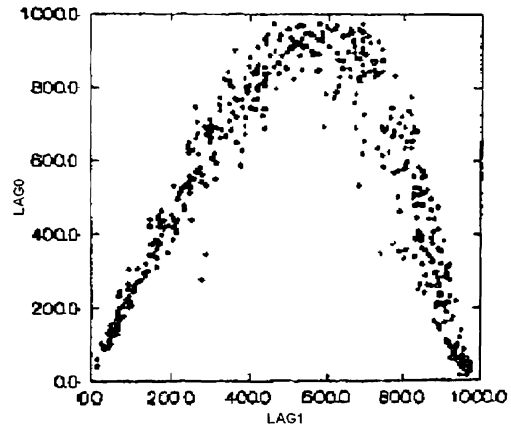


Figure 3.2: Plot of one subject's attempt to iterate equation (3.6) [36].

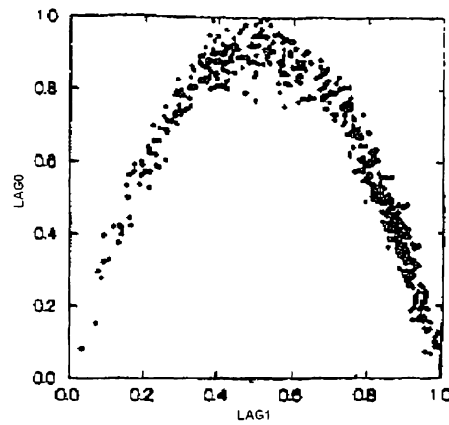


Figure 3.3: Plot of equation (3.6) with Gaussian noise [36].

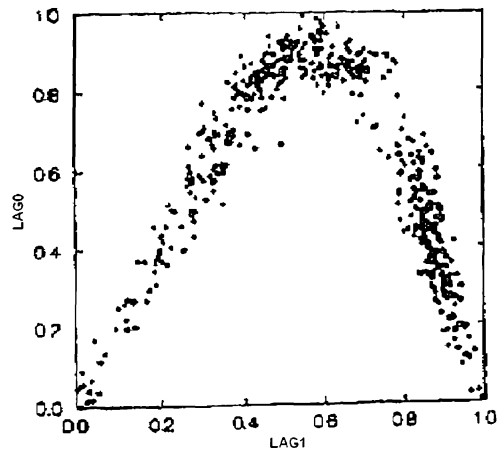


Figure 3.4: Plot of equation (3.6) with "fuzzy" memory pair interpolation [36].

Two approaches were then taken to reproduce the plot of Figure 3.2 in order to gain some insight into the decision making of the human. The first approach was to simply add γ , a Gaussian noise distribution with a mean of zero, to equation (3.6) as [36]

$$Y_{n+1} = aY_n(1 - Y_n) + \gamma. \quad (3.8)$$

Figure 3.3 shows the results when adding a Gaussian distribution with a standard deviation of 50%. Figure 3.3 shows some clear resemblance to Figure 3.2, but there are some key differences. By having the added noise, the model more closely resembles the human, Figure 3.2, than the computer, Figure 3.1b, and so can account for the unpredictability in the heuristics of the human. However, the added noise is an overgeneralization [36].

In order to more precisely mimic the human, Ward and West attempted to map out the decision making method of the human. They employed a memory pair interpolation scheme along with a “fuzzy” memory scheme. The memory pairs and interpolation precision was catered to each of the subjects individually by inspection of their data set. This is because the memory pairs come about from each subject’s learning history. The memory pairs were also “fuzzified” by adding Gaussian noise with a standard deviation of 40% to each subject in order to account for the non-precision of the human. The results of this approach can be seen in Figure 3.4, and clearly shows the fuzzy memory pair scheme can closely reproduce the subject’s data plot [36].

The fuzzy memory pair model can represent certain psychological processes, such as memory, calculation, and decision. The drawback is that it cannot be represented by a nonlinear difference equation. Its behavior could be described by equation (3.8) with parameter a approximating the particular memory pairs used by a certain sub-

ject. But more importantly, the unpredictable aspect of the subject's behavior comes from the noisy term and not the nonlinear function part of equation (3.8). The chaotic factor comes from a combination of human memory and performance limitations. During complex tasks, a human will perform heuristic behavior to approximate a desired output [36].

3.4 Human Based PID Controller

Modeling the human operator as a linear controller of a vehicle has been a developing area of study for many decades [18].

Basing the function of a human on a PID controller depends on designing the gains of the controller so that it would mimic the actions of a human in its place. A controller based on the input of skilled human is developed developed by Koiwai, et. al [19]. Neural networks could be an effective design for controlling such nonlinear systems. but Koiwai, et. al. [19], suggest a Cerebellar Model Articulation Controller (CMAC) that can be used in place of an artificial neural network. It has the advantage of a faster learning time and is based on a simpler structure. In particular, it can be used as a learning center for a human based PID controller. The gains of the PID controller can be tuned based on the input of a human expert in a particular skill. With enough data from the human expert, the system could continue to be controlled autonomously. This method could be used in many applications for autonomous control of systems normally controlled by a human operator [19]. The PID controller

is developed as

$$\begin{aligned}
 u(t) &= u(t-1) \\
 &+ K_P \{y(t-1) - y(t)\} \\
 &+ K_I e(t) \\
 &+ K_D \{2y(t-1) - y(t) - y(t-2)\},
 \end{aligned} \tag{3.9}$$

where $e(t)$ is the error defined as

$$e(t) \equiv r(t) - y(t). \tag{3.10}$$

and $r(t)$ is the reference signal. Each CMAC computes the weights from $r(t)$, $e(t)$, and $\Delta e(t)$. The change in the error, $\Delta e(t)$, is defined as

$$\Delta e(t) \equiv e(t) - e(t-1). \tag{3.11}$$

The gains of the PID controller, (K_P, K_I, K_D) , are each tuned by the weights of three CMACs,

$$K_P = \sum_{h=1}^K W_{P,h}(t) \tag{3.12a}$$

$$K_I = \sum_{h=1}^K W_{I,h}(t) \tag{3.12b}$$

$$K_D = \sum_{h=1}^K W_{D,h}(t). \tag{3.12c}$$

where $h = 1, 2, \dots, K$, and K is the total number of weights selected from the CMAC. The weights are driven so that $u(t)$ approaches $u^*(t)$ by the following steepest descent

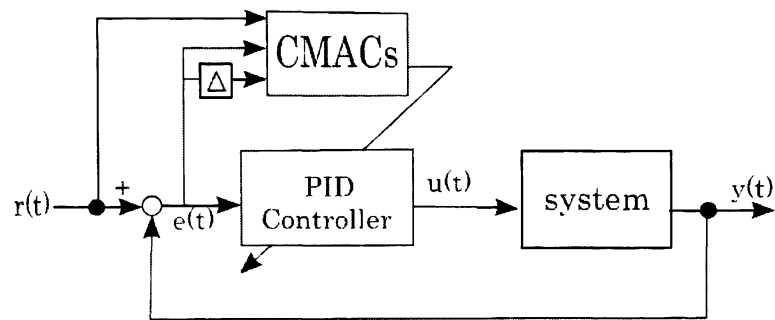


Figure 3.5: Block diagram of CMAC based controller method [19].

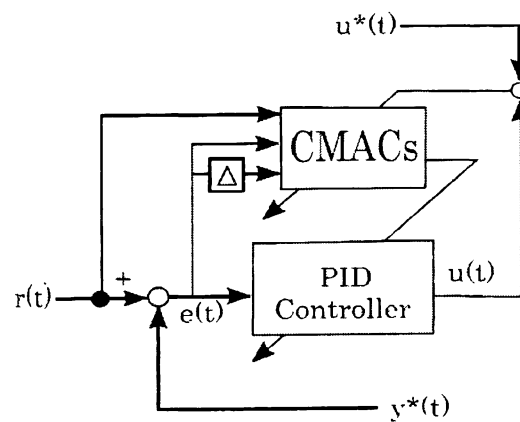


Figure 3.6: Block diagram of learning process [19].

method

$$W_{P,h}^{new}(t) = W_{P,h}^{old}(t) - g(t) \frac{\partial J}{\partial K_P} \frac{1}{K} \quad (3.13a)$$

$$W_{I,h}^{new}(t) = W_{I,h}^{old}(t) - g(t) \frac{\partial J}{\partial K_I} \frac{1}{K} \quad (3.13b)$$

$$W_{D,h}^{new}(t) = W_{D,h}^{old}(t) - g(t) \frac{\partial J}{\partial K_D} \frac{1}{K}, \quad (3.13c)$$

where $g(t)$ and J are defined as

$$g(t) = \frac{1}{c + a \cdot e^{(-b|u^*(t)-u(t)|)}} \quad (3.14)$$

$$J \equiv \frac{1}{2} \epsilon(t)^2 \quad (3.15)$$

$$\epsilon = u^*(t) - u(t), \quad (3.16)$$

and where a, b, c are the appropriate positive constant. Each partial differential from equation (3.13) is developed as

$$\frac{\partial J}{\partial K_P} = \frac{\partial J}{\partial \epsilon(t)} \frac{\partial \epsilon(t)}{\partial u(t)} \frac{\partial u(t)}{\partial K_P} = \epsilon(t) \{y(t) - y(t-1)\} \quad (3.17a)$$

$$\frac{\partial J}{\partial K_I} = \frac{\partial J}{\partial \epsilon(t)} \frac{\partial \epsilon(t)}{\partial u(t)} \frac{\partial u(t)}{\partial K_I} = -\epsilon(t) e(t) \quad (3.17b)$$

$$\frac{\partial J}{\partial K_D} = \frac{\partial J}{\partial \epsilon(t)} \frac{\partial \epsilon(t)}{\partial u(t)} \frac{\partial u(t)}{\partial K_D} = \epsilon(t) \{y(t) - 2y(t-1) + y(t-2)\}. \quad (3.17c)$$

The results from Koiwai et. al. [19] are shown in Figures 3.7 and 3.8. Figure 3.7 shows the controlled trajectory of the skilled human, y^* , to a desired trajectory, r , and the machine trajectory y based on the learned control gains which are shown in Figure 3.8. These results show that training a CMAC with multiple trails from a skilled operator can optimize the gains of the control law which a machine can then repeat by implementing the measured control law. It is important to note that

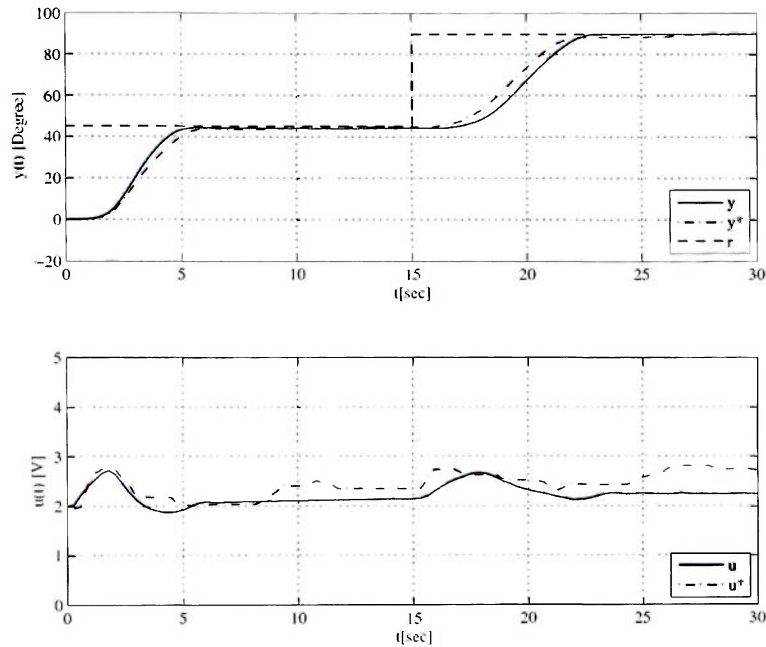


Figure 3.7: Human and machine control results [19].

although PID control is normally a linear control with constant gains, the results of Koiwai et. al. [19] show that the skilled human operator used variable PID gains based on the assumption that the human was actually acting as a PID controller.

Phatak and Weinert [26] attempt to identify human operator parameters from measured data for an optimal control model. The control is based on standard plant dynamics

$$\dot{x}(t) = Ax(t) + bu(t) + w(t) \quad (3.18a)$$

$$y(t) = Cx(t) + v(t), \quad (3.18b)$$

where $w(t)$ and $v(t)$ are zero-mean, Gaussian white noise with covariance matrices W and V , respectively. Phatak and Weinert [26] also postulate that the human chooses

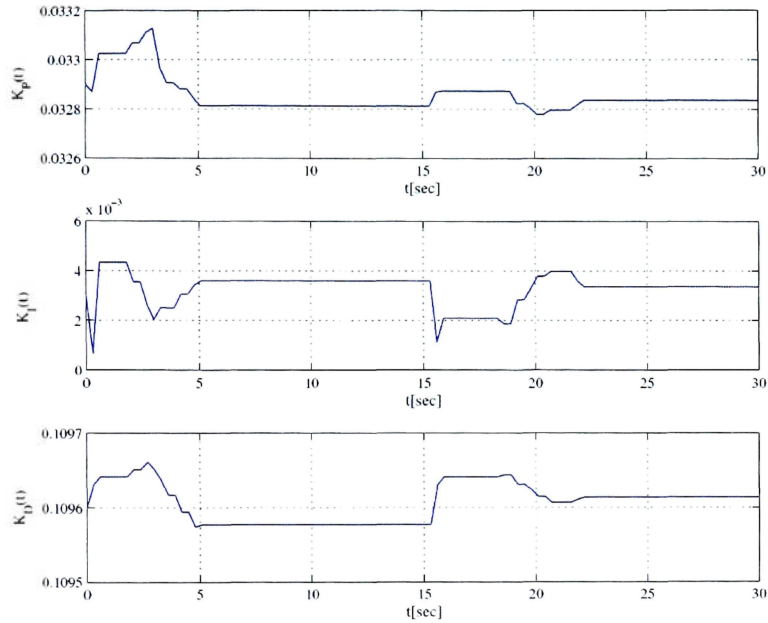


Figure 3.8: PID gains learned from the skilled human operator [19].

a feedback control law that specifically minimizes a quadratic cost function

$$J = E\{(x, Qx) + gu^2\}, \quad (3.19)$$

where Q is a constant non-negative definite matrix and g is a positive constant. The proposed optimal control law is then given by

$$u(t) = -\lambda^T x_d(t), \quad (3.20)$$

where λ is the optimal gain vector and $x_d(t)$ is the solution to the Kalman filter equation,

$$\dot{x}_d(t) = Ax_d(t) + bu(t) + K\nu(t) \quad (3.21)$$

$$\nu(t) = y(t) - Cx_d(t), \quad (3.22)$$

where K is the steady-state Kalman gain. The optimal control model for the human operator is made up of equations (3.20) and (3.21) and combined into

$$\dot{x}_d = \tilde{A}x_d + K\nu, \quad (3.23)$$

where $\tilde{A} = A - b\lambda'$ [26].

Phillips and Repperger [27] propose an informatic model of a human operator as a linear, time invariant function, that can describe a feed-forward human control system involving a single input with a single output. The model incorporates the time delay of the human operator including reaction time and movement time as

$$y_o = A [1 - e^{-\alpha_M(t-T_D)}], \quad (3.24)$$

where the output y_o depends on A , the unit-step input magnitude, α_M , the movement informatic frequency, and T_D , the reaction time delay. The human response, or action time (AT), is a sum of the reaction time (RT) and the movement time (MT) given as $AT = RT + MT$ [27].

Anderson [1] also proposes a linear feedback control model of a human operator. Anderson uses a mix between a “cross-over” model in frequency space and an “optimal control” model based on the linear-quadratic-gaussian control in state-space. The cross over model is given by

$$P(s) = H(s)e^{-\tau s}, \quad (3.25)$$

where $P(s)$ is the human operator, τ is the time delay and $H(s)$ is the control function described as

$$H(s) = K_p \frac{\tau_L s + 1}{\tau_I s + 1}, \quad (3.26)$$

where K_p is the static gain, τ_L is a lead time constant and τ_I is a lag time constant.

3.5 Summary of Human Models

As evident from this chapter there are many different approaches describing the human brain. The neural networks may provide a more complete or accurate model of the human brain but the complexities present a level of chaos with so many variables and are not necessarily useful for describing a human operator.

Several examples of papers were given that provided a human operator model as a linear feedback controller and different methods were proposed for learning the specific gains of a human operator. This is a reasonable assumption for a human only tasked with the function of controlling a vehicle. Many autonomous control systems for vehicles and other systems use linear feedback control successfully.

However, this may only be accurate for relatively stable conditions. The value of a human-in-the-loop control system is the human's ability to adapt to changing environment and learn new control methods for unforeseen disturbances. For instance, a human could be modeled with the added feature of being able to learn a disturbance and add an additional control law to compensate as shown in Figure 3.9 and by the following equations:

$$\dot{y} = Ay + Bu. \quad (3.27a)$$

$$u = K_P \bar{y} + K_I \int \bar{y} + K_D \dot{\bar{y}}, \quad (3.27b)$$

$$\dot{y} = Ay + Bu + f. \quad (3.28a)$$

$$u = K_P \bar{y} + K_I \int \bar{y} + K_D \dot{\bar{y}}. \quad (3.28b)$$

$$\dot{y} = Ay + Bu + f, \quad (3.29a)$$

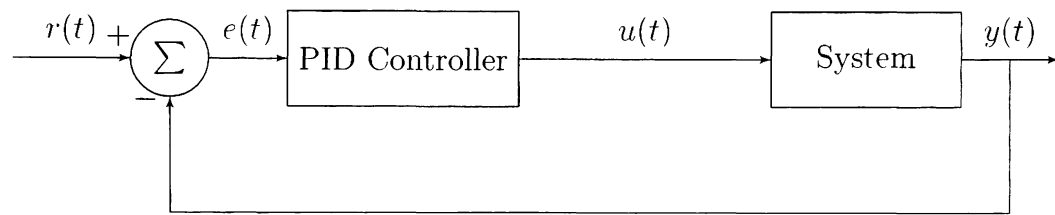
$$u = K_P \bar{y} + K_I \int \bar{y} + K_D \dot{\bar{y}} + u_f, \quad (3.29b)$$

where $\bar{y} \equiv e(t)$ is the error defined as

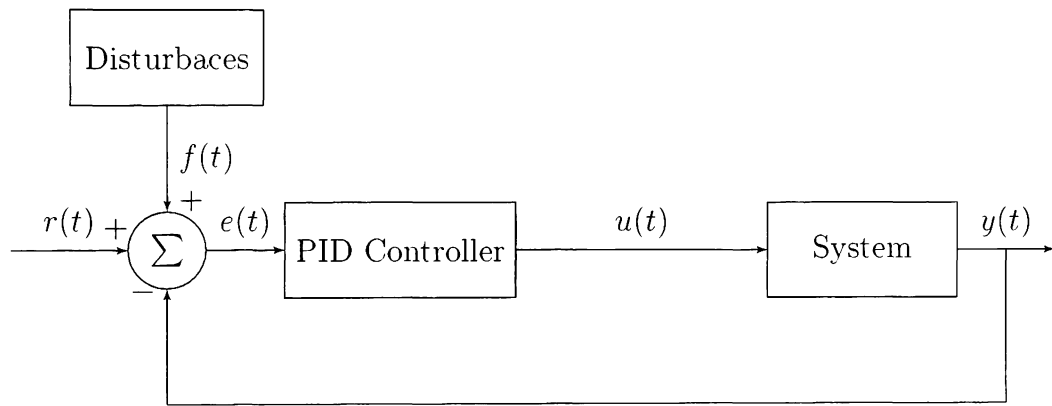
$$\bar{y} = |y - y^*|, \quad (3.30)$$

and $y^* \equiv r(t)$ is the desired state. Equation (3.27) shows a standard system and a standard PID controller and refers to Figure 3.9(a). Equation (3.28) shows a standard system with an added disturbance, f , and a standard PID controller and refers to Figure 3.9(b). Equation (3.29) shows a standard system with the added disturbance and a standard PID controller with an added term, u_f , designed to compensate for the disturbance. This refers to Figure 3.9(c).

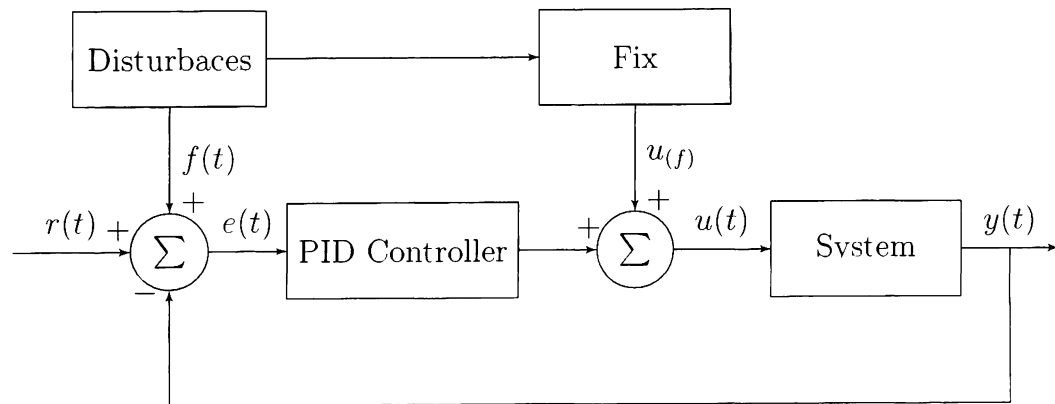
Future study of human-in-the-loop control should also base the human operator on a nonlinear multiparameter model that can include the features of adaptation and learning.



(a)



(b)



(c)

Figure 3.9: Block diagrams of PID controller with added disturbance.

Chapter 4

Human Arm Models

4.1 Introduction to Human Motion

Modeling human motion through the medium of mathematical equations of motion is an area of ongoing research that has produced many useful mathematical descriptions of human motion. The human body can be described as a system of rigid links connected by joints. The assumption that each body part is a rigid body is a good approximation for the purposes of studying human motion. However, since the human body can be modeled as a system of 148 links, it still proves to be a very complex system [39].

The complete human body can be modeled with as many as 148 movable bones connected by 147 joints as shown in Figure 4.1. Figure 4.1 shows one side of the body with each joint numbered. There are three classes of joints; there are 29 3rd class joints with 3 DOF (Degrees of Freedom), 33 4th class joints with 2 DOF and 85 5th class joints with 1 DOF. The total DOF can be calculated from the following formula [39]:

$$F = 6N - \sum_{i=3}^5 \nu_j. \quad (4.1)$$

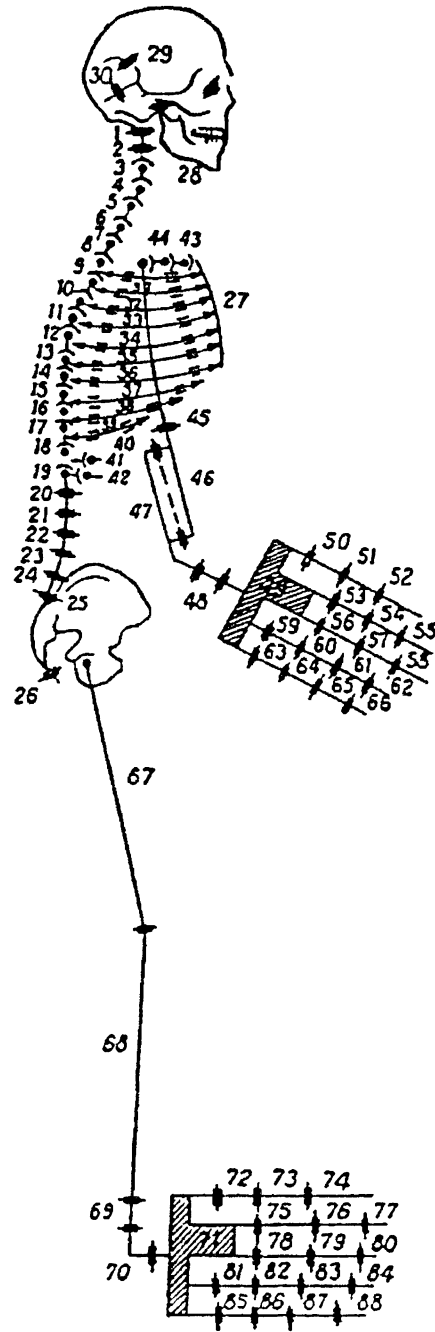


Figure 4.1: Mobility of the human body [39].

where F is the total number of DOF, N is the number of movable bones, ι is the class of the joint, and j_ι is the number of joints of class ι . The class of the joint is calculated as $\iota = 6 - f$ where f is the number of DOF. The complete human body can then be calculated to have 244 DOF [39]. The complete human body described as such provides a highly redundant skeletal system. With 244 DOF and a maneuverability of 238, the brain must specify 244 variables to place an end-effector in space where 238 variables are redundant and can be used to perform the motor task in an optimal way [39].

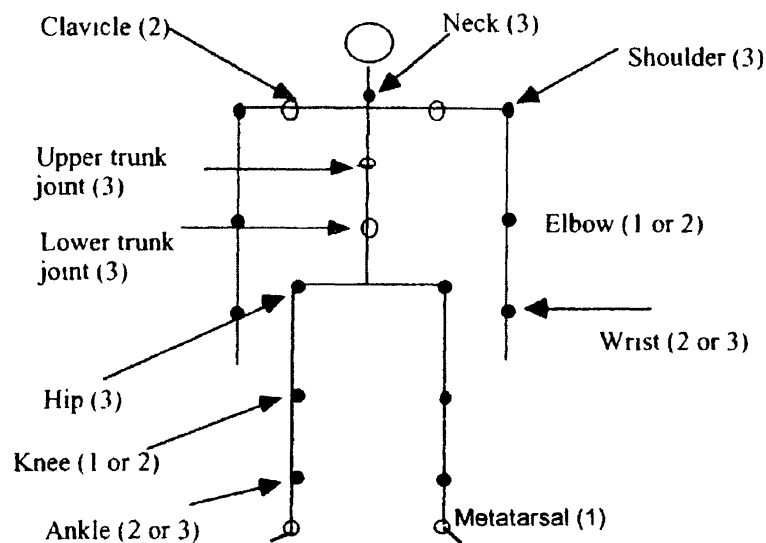


Figure 4.2: Kinematic model of the human body [39].

Figure 4.2 shows a kinematic model of the human body where the filled circles represent joints that are usually included in models and the open circles represent joints that are only included in some models. The numbers in the parentheses show the number of DOF for that joint. This simplified model has a maximum of 18 segments connected by 17 joints for a total 41 DOF. This is known as gross body model where many of the smaller joints are not included. Using this reduced model the human arm has 7 DOF. This still allows for a redundant system where there are

many joint angle solutions for the same end-effector motion [4, 28, 39].

4.2 Human Arm Controlling a Joystick

The human arm is the mechanical link between the control law calculated by the human brain and the actuator control of the system. It is an important step for a human-in-the-loop because the control law calculated in the brain must take all the actuator dynamics into account. Flying an aircraft involves the pilot's arm manipulating a joystick where the joystick's position is proportional to the control surfaces of the aircraft [22]. To more accurately understand the control law of the human brain, a model of the human arm controlling a joystick needs to be developed.

Manipulation of the joystick by the human arm is accomplished mechanically through the application of torques and forces placed on the various joints and connection points of the system. The human accomplishes this through contraction and extension of muscles in the arm. The movement of these muscles is controlled by the brain through signals sent back and forth along the central nervous system [4, 39]. In this case, input control for the position of the arm are the torques placed on the shoulder and elbow joints which results in a net force placed on the end of the joystick by the hand [14]. This net force placed on the end of the joystick by the arm results in a torque placed on the joystick which controls the angle of the joystick. From all of this it is a reasonable approximation to say that the control law designed in the human brain controls the torques to achieve a desired joystick position which results in the desired aircraft configuration. This is analogous to a robotic arm controlled by the output torques of electric motors placed at the joints [14, 39].

The total system can be simplified from a three dimensional system so as to be studied as two separate two dimensional systems. One system for aircraft roll control

and one system for aircraft pitch control. Only the system for pitch control will be considered in this thesis.

4.3 Pitch Control Modeled with Arm and Joystick as One System

One way to model a human arm manipulating a joystick for pitch control is to represent the system as a three link chain fixed at each endpoint. In this way the system would only have 1 DOF. With the endpoints fixed, the angles of the upper arm and forearm would depend on the angle of the joystick.

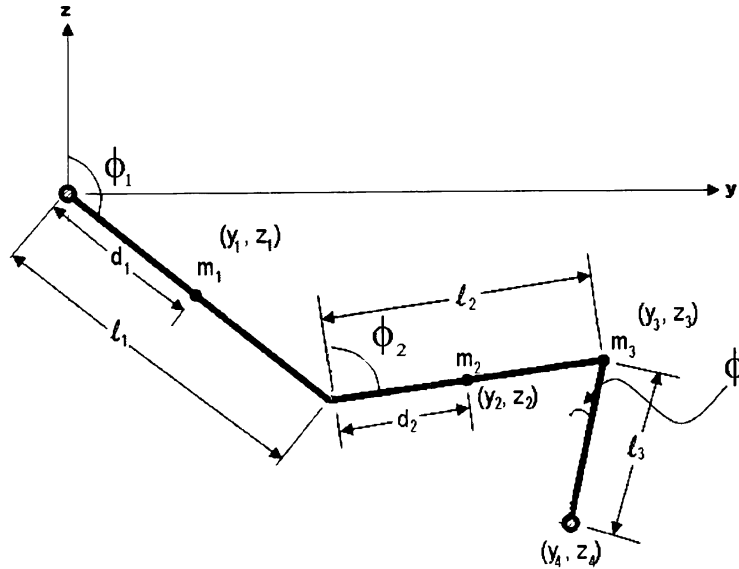


Figure 4 3: Pitch control system diagram with arm and joystick.

Figure 4.3 represents the system where l_1 is the length of the upper arm, l_2 is the length of the forearm, and l_3 is the length of the joystick. The length d_1 locates the center of mass of the upper arm and d_2 locates the center of mass of the forearm. The masses m_1 and m_2 are the masses of the upper arm and forearm, respectively, and

m_3 is the mass of the hand and the joystick. The location, in Cartesian coordinates, of m_1 , m_2 , m_3 , and the base of the joystick are denoted by (y_1, z_1) , (y_2, z_2) , (y_3, z_3) , and (y_4, z_4) , respectively. The shoulder is located at the origin. The shoulder and base of the joystick are fixed positions. The angle ϕ_1 is the angle between the z -axis and the upper arm. The angle ϕ_2 is the angle between a base line from the elbow in the z direction and the forearm. The angle ϕ is the angle between a base line from the base of the joystick in the z direction and the joystick.

The equations of motion can be derived using the Lagrangian of the system defined as [2]

$$L = T - V, \quad (4.2)$$

where T is the kinetic energy and V is the potential energy of the system. For the system shown in Figure 4.3, the Lagrangian becomes

$$L = \frac{1}{2} [m_1(\dot{y}_1^2 + \dot{z}_1^2) + m_2(\dot{y}_2^2 + \dot{z}_2^2) + m_3(\dot{y}_3^2 + \dot{z}_3^2)] - g [m_1 d_1 \cos \phi_1 + m_2(l_1 \cos \phi_1 + d_2 \cos \phi_2) + m_3 l_3 \cos \phi], \quad (4.3)$$

where g is the acceleration due to gravity. The angles ϕ_1 , ϕ_2 and ϕ are the angles of the shoulder, elbow and joystick, respectively. The Cartesian coordinates of the system are defined by

$$\begin{aligned} y_1 &= d_1 \sin \phi_1, & z_1 &= d_1 \cos \phi_1, \\ y_2 &= l_1 \sin \phi_1 + d_2 \sin \phi_2, & z_2 &= l_1 \cos \phi_1 + d_2 \cos \phi_2, \\ y_3 &= l_1 \sin \phi_1 + l_2 \sin \phi_2, & z_3 &= l_1 \cos \phi_1 + l_2 \cos \phi_2. \end{aligned} \quad (4.4)$$

The time derivatives of the equations from (4.4) become

$$\begin{aligned} \dot{y}_1 &= d_1 \cos \phi_1 \dot{\phi}_1, & \dot{z}_1 &= -d_1 \sin \phi_1 \dot{\phi}_1, \\ \dot{y}_2 &= l_1 \cos \phi_1 \dot{\phi}_1 + d_2 \cos \phi_2 \dot{\phi}_2, & \dot{z}_2 &= -l_1 \sin \phi_1 \dot{\phi}_1 - d_2 \sin \phi_2 \dot{\phi}_2, \\ \dot{y}_3 &= l_1 \cos \phi_1 \dot{\phi}_1 + l_2 \cos \phi_2 \dot{\phi}_2, & \dot{z}_3 &= -l_1 \sin \phi_1 \dot{\phi}_1 - l_2 \sin \phi_2 \dot{\phi}_2. \end{aligned} \quad (4.5)$$

For the purpose of substitution, $\dot{y}_i^2 + \dot{z}_i^2$, for each, $i = 1, 2, 3$, become

$$(\dot{y}_1^2 + \dot{z}_1^2) = d_1^2 \dot{\phi}_1^2, \quad (4.6a)$$

$$(\dot{y}_2^2 + \dot{z}_2^2) = l_1^2 \dot{\phi}_1^2 + d_2^2 \dot{\phi}_2^2 + l_1 d_2 \dot{\phi}_1 \dot{\phi}_2 \cos(\phi_1 - \phi_2), \quad (4.6b)$$

$$(\dot{y}_3^2 + \dot{z}_3^2) = l_1^2 \dot{\phi}_1^2 + l_2^2 \dot{\phi}_2^2 + l_1 l_2 \dot{\phi}_1 \dot{\phi}_2 \cos(\phi_1 - \phi_2). \quad (4.6c)$$

By substituting the equations from (4.6) into equation (4.3), L can be written in terms of $\phi_1, \phi_2, \phi, \dot{\phi}_1$, and $\dot{\phi}_2$ as

$$\begin{aligned} L &= \frac{1}{2} (m_1 d_1^2 + m_2 l_1^2 + m_3 l_1^2) \dot{\phi}_1^2 + \frac{1}{2} (m_2 d_2^2 + m_3 l_2^2) \dot{\phi}_2^2 \\ &+ \frac{1}{2} (m_2 l_1 d_2 + m_3 l_1 l_2) \dot{\phi}_1 \dot{\phi}_2 \cos(\phi_1 - \phi_2) - (m_1 d_1 + m_2 l_2) g \cos \phi_1 \\ &- m_2 d_2 g \cos \phi_2 - m_3 l_3 g \cos \phi. \end{aligned} \quad (4.7)$$

The equations of motion can then be found using the Lagrangian method as [2]

$$-\frac{\partial L}{\partial \phi} + \frac{d}{dt} \left(\frac{\partial L}{\partial \dot{\phi}} \right) = \tau, \quad (4.8)$$

where by the chain rule, $\frac{\partial L}{\partial \phi}$ and $\frac{\partial L}{\partial \dot{\phi}}$ are defined as

$$\frac{\partial L}{\partial \phi} = \sum_{i=1}^2 \left(\frac{\partial L}{\partial \phi_i} \frac{\partial \phi_i}{\partial \phi} + \frac{\partial L}{\partial \dot{\phi}_i} \frac{\partial \dot{\phi}_i}{\partial \phi} \right) \quad (4.9)$$

and

$$\frac{\partial L}{\partial \dot{\phi}} = \sum_{i=1}^2 \frac{\partial L}{\partial \dot{\phi}_i} \frac{\partial \dot{\phi}_i}{\partial \dot{\phi}}. \quad (4.10)$$

Because the system is a closed three link chain, a relationship between ϕ_1 , ϕ_2 and ϕ can be derived geometrically. Two equations can to be derived, $\phi_1(\phi)$, where ϕ_1 depends only on ϕ , and $\phi_2(\phi)$, where ϕ_2 depends only on ϕ . These two equations need to be derived to solve the components of equations (4.9) and (4.10).

Two independent equations can be written from Figure 4.3 as

$$y^2 + z^2 = l_1^2 \quad (4.11)$$

$$(y - y_3)^2 + (z - z_3)^2 = l_2^2 \quad (4.12)$$

Equation (4.11) describes the circle traced out by the elbow rotating about the shoulder fixed at the origin. Equation (4.12) describes the circle traced out by the elbow rotating about the hand centered the point (y_3, z_3) . This system of equations can be solved with two unique solutions to the location of the elbow, (y, z) . These two solutions would be at the intersection of the two circles. One solution places the elbow locked in the upper position and one solution places the elbow locked in the lower position. For the purposes of modeling the human arm only the lower position of the elbow will be considered. This solution is unique based on a unique angle, ϕ , as y_3 and z_3 depend on ϕ . Clearly, y_3 and z_3 are expressed as

$$y_3 = y_4 + l_3 \sin \phi \quad (4.13)$$

$$z_3 = z_4 + l_3 \cos \phi. \quad (4.14)$$

By substitution and separation of variables of equations (4.11) and (4.12), z can be

written in terms of y_3 and z_3 as

$$\begin{aligned} z = & \frac{1}{2(y_3^2 + z_3^2)} [l_1^2 z_3 - l_2^2 z_3 + y_3^2 z_3 + z_3^3 \\ & - [-y_3^2(l_1^4 + (-l_2^2 + y_3^2 + z_3^2)^2 \\ & - 2l_1^2(l_2^2 + y_3^2 + z_3^2))]^{1/2}], \end{aligned} \quad (4.15)$$

and therefore be written in terms of ϕ as

$$\begin{aligned} z = & \frac{1}{2((y_4 + l_3 \sin \phi)^2 + (z_4 + l_3 \cos \phi)^2)} [l_1^2 (z_4 + l_3 \cos \phi) \\ & - l_2^2 (z_4 + l_3 \cos \phi) + (y_4 + l_3 \sin \phi)^2 (z_4 + l_3 \cos \phi) + (z_4 + l_3 \cos \phi)^3 \\ & - [-(y_4 + l_3 \sin \phi)^2 (l_1^4 + (-l_2^2 + (y_4 + l_3 \sin \phi)^2 + (z_4 + l_3 \cos \phi)^2)^2 \\ & - 2l_1^2 (l_2^2 + (y_4 + l_3 \sin \phi)^2 + (z_4 + l_3 \cos \phi)^2))]^{1/2}]. \end{aligned} \quad (4.16)$$

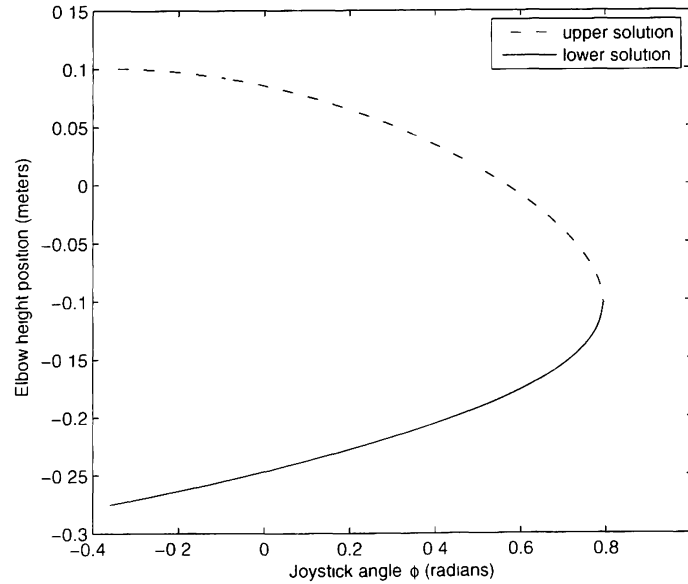


Figure 4.4: Plot of elbow position as a function of joystick angle.

Figure 4.4 shows the height of the elbow position, z , as a function of the joystick angle, ϕ . Since equation (4.16) is a quadratic formula there are two solutions to the height of the elbow position. The lower height position represents the more realistic solution for the human arm. Note that when both solutions are equal the arm is straight at maximum extension.

Since z can also be written in terms of ϕ_1 as

$$z = l_1 \cos \phi_1, \quad (4.17)$$

the angle ϕ_1 can be written as a function of ϕ as

$$\begin{aligned} \phi_1(\phi) = \cos^{-1} & \left[\frac{1}{2l_1((y_4 + l_3 \sin \phi)^2 + (z_4 + l_3 \cos \phi)^2)} [l_1^2(z_4 + l_3 \cos \phi) \right. \\ & - l_2^2(z_4 + l_3 \cos \phi) + (y_4 + l_3 \sin \phi)^2(z_4 + l_3 \cos \phi) + (z_4 + l_3 \cos \phi)^3 \\ & - [-(y_4 + l_3 \sin \phi)^2(l_1^4 + (-l_2^2 + (y_4 + l_3 \sin \phi)^2 + (z_4 + l_3 \cos \phi)^2)^2 \\ & \left. - 2l_1^2(l_2^2 + (y_4 + l_3 \sin \phi)^2 + (z_4 + l_3 \cos \phi)^2))]^{1/2} \right]. \end{aligned} \quad (4.18)$$

Since z_4 can be expressed as

$$z_4 = l_1 \cos \phi_1 + l_2 \cos \phi_2 + l_3 \cos \phi, \quad (4.19)$$

the angle ϕ_2 can be solved in terms of ϕ and ϕ_1 and therefore in terms of only ϕ by

substitution of (4.18) as

$$\begin{aligned}
 \phi_2(\phi) = \cos^{-1} & \left[-\frac{1}{2l_2((y_4 + l_3 \sin \phi)^2 + (z_4 + l_3 \cos \phi)^2)} [l_1^2(z_4 + l_3 \cos \phi) \right. \\
 & - l_2^2(z_4 + l_3 \cos \phi) + (y_4 + l_3 \sin \phi)^2(z_4 + l_3 \cos \phi) + (z_4 + l_3 \cos \phi)^3 \\
 & - [-(y_4 + l_3 \sin \phi)^2(l_1^4 + (-l_2^2 + (y_4 + l_3 \sin \phi)^2 + (z_4 + l_3 \cos \phi)^2)^2 \\
 & - 2l_1^2(l_2^2 + (y_4 + l_3 \sin \phi)^2 + (z_4 + l_3 \cos \phi)^2))]^{1/2}] \\
 & + \frac{z_4}{l_2} - \frac{l_3}{l_2} \cos \phi].
 \end{aligned} \tag{4.20}$$

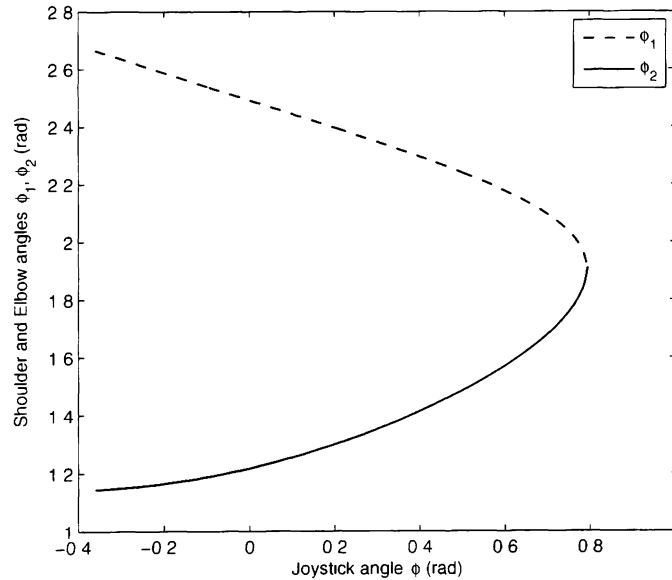


Figure 4.5: Angular relations of the shoulder, elbow and joystick.

Figure 4.5 shows the shoulder and elbow angles, ϕ_1 and ϕ_2 , respectively, as functions of the joystick angle, ϕ . Note that when both angles are equal the arm is straight at maximum extension. However, the maximum range for the joystick at $\pm 0.36 \text{ rad}$ from Table A.3 shows that the arm would never fully extend to control the joystick.

Using equations (4.18) and (4.20) the components of equations (4.9) and (4.10) can be then be derived as

$$\frac{\partial L}{\partial \phi_1} = -\frac{1}{2} (m_2 l_1 d_2 + m_3 l_1 l_2) \phi_1 \dot{\phi}_2 \sin(\phi_1 - \phi_2) + (m_1 g d_1 + m_2 g l_2) \sin \phi_1, \quad (4.21)$$

$$\frac{\partial L}{\partial \phi_2} = -\frac{1}{2} (m_2 l_1 d_1 + m_3 l_1 l_2) \phi_1 \dot{\phi}_2 \sin(\phi_1 - \phi_2) + m_2 g d_2 \sin \phi_2, \quad (4.22)$$

$$\frac{\partial L}{\partial \dot{\phi}_1} = (m_1 d_1^2 + m_2 l_1^2 + m_3 l_1^2) \dot{\phi}_1 + \frac{1}{2} (m_2 l_1 d_2 + m_3 l_1 l_2) \dot{\phi}_2 \cos(\phi_1 - \phi_2), \quad (4.23)$$

$$\frac{\partial L}{\partial \dot{\phi}_2} = (m_1 d_1^2 + m_2 l_1^2 + m_3 l_1^2) \dot{\phi}_2 + \frac{1}{2} (m_2 l_1 d_2 + m_3 l_1 l_2) \dot{\phi}_1 \cos(\phi_1 - \phi_2). \quad (4.24)$$

The other components, $\frac{\partial \phi_1}{\partial \phi}$, $\frac{\partial \dot{\phi}_1}{\partial \phi}$, $\frac{\partial \phi_2}{\partial \phi}$, $\frac{\partial \dot{\phi}_2}{\partial \phi}$, and $\frac{\partial \phi}{\partial \phi}$, can all be evaluated but prove to be very large equations as $\phi_1(\phi)$ and $\phi_2(\phi)$ are very large equations. Because ϕ_1 and ϕ_2 depend on ϕ , the model of a three link closed chain proves to be very complex.

4.4 Pitch Control Modeled with Arm and Joystick as Two Systems

Another approach to modeling the system this two dimensional system is to model the arm and the joystick separately and then constrain ends of each together. The arm can be modeled as two link, planer, double pendulum with 2 DOF [40], and the joystick can be modeled as an inverted pendulum with 1 DOF. The ends of each pendulum are then constrained to be at the same location by using equations (4.18) and (4.20) which constrain the shoulder and elbow angles. ϕ_1 and ϕ_2 , respectively, to be only dependent on the angle of the joystick, ϕ . The end-effector forces for each pendulum are taken into account and become a reaction force placed on the end of the other pendulum.

4.4.1 Joystick as an Inverted Pendulum

This section develops the model of the joystick based on a modified inverted pendulum. Figure 4.6 shows just the joystick portion of Figure 4.3 with the torques and forces added, where τ_3 is the net torque placed on the joystick and F is an arbitrary force on the end the joystick. F_y and F_x are the Cartesian components of the force F . The forces F_{τ_y} and F_{τ_z} are the components of F_y and F_x perpendicular to the joystick, respectively.

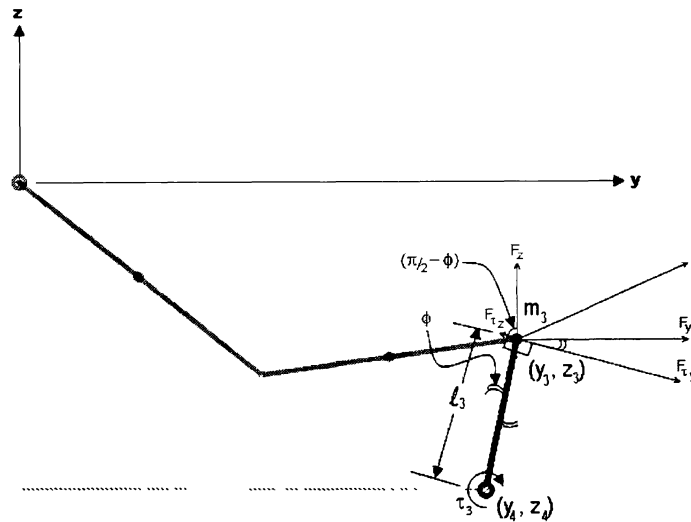


Figure 4.6: Joystick as an inverted pendulum diagram with an arbitrary end-effector force.

The equations of motion of an inverted pendulum are [2]

$$m_3 l_3^2 \ddot{\phi} = m_3 g l_3 \sin \phi + \tau_3. \quad (4.25)$$

where m_3 , l_3 , ϕ , and τ_3 are shown in Figure 4.6. Clearly, τ_3 would be any additional torque placed on the inverted pendulum. Equation (4.25) assumes a point mass at the end of a pendulum. To complete the model of the joystick, the restoring force of

the spring and friction should be added to the equations of motion as

$$m_3 l_3^2 \ddot{\phi} = m_3 g l_3 \sin \phi - k_s \phi - k_\mu \dot{\phi} + \tau_3, \quad (4.26)$$

where k_s is the spring constant and k_μ is the coefficient of friction.

The applied torque to the system, τ_3 , could be applied by either an actuator at the base of the joystick, or as the result of an applied force at the end of the joystick. It is useful to derive both the torque as a function of the end-effector force, $\tau_3(F)$, and the end-effector force as a function of the torque, $F(\tau_3)$.

The torque as a function of the end-effector force, $\tau_3(F)$, can be derived by inspection from Figure 4.6 as

$$\tau_3 = l_3 (F_{y_\tau} - F_{z_\tau}), \quad (4.27)$$

where F_{y_τ} and F_{z_τ} can be calculated as

$$F_{y_\tau} = F_y \cos(\phi) \quad (4.28)$$

$$F_{z_\tau} = F_z \cos(\pi/2 - \phi) = F_z \sin(\phi). \quad (4.29)$$

Equation (4.29) can then be subtracted from equation (4.28) to form

$$F_{y_\tau} - F_{z_\tau} = F_y \cos \phi - F_z \sin \phi. \quad (4.30)$$

Equation (4.30) can then be substituted into (4.27) to conclude

$$\tau_3 = l_3 (F_y \cos \phi - F_z \sin \phi) \quad (4.31)$$

Equation (4.31) can then be substituted into equation (4.26) so that the equations of

motion of the joystick can be written as

$$m_3 l_3^2 \ddot{\phi} = m_3 g l_3 \sin \phi - h_s \dot{\phi} - h_\mu \phi + l_3 (F_y \cos \phi - F_z \sin \phi), \quad (4.32)$$

so as to include end-effector force terms.

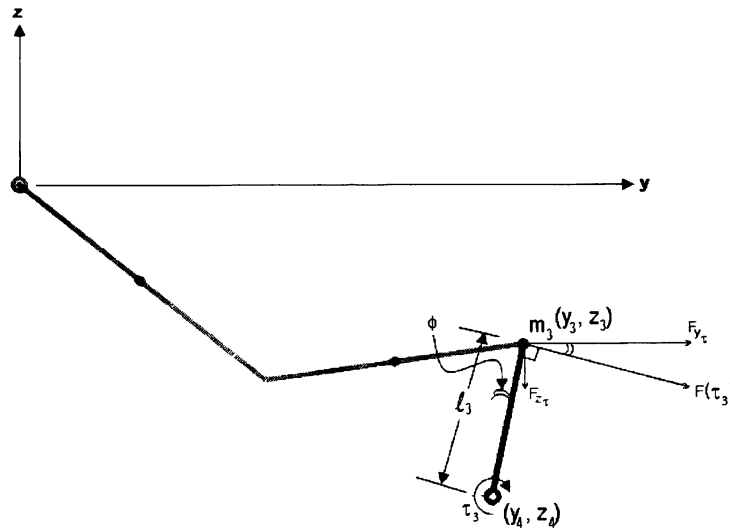


Figure 4.7: Joystick as an inverted pendulum diagram with an end-effector force due to an applied torque.

Figure 4.7 is similar to Figure 4.6 but with the end-effector force, $F(\tau_3)$, due to an applied torque, τ_3 . F_{y_τ} and F_{z_τ} are the Cartesian components of the force $F(\tau_3)$. The end-effector force as a function of the torque, $F(\tau_3)$, can be derived by inspection from Figure 4.7 as

$$\tau_3 = l_3 F(\tau_3). \quad (4.33)$$

Equation (4.33) can be rearranged and substituted with the Cartesian components

as

$$F_{y\tau} = \frac{\tau_3}{l_3} \cos(-\phi) \quad (4.34)$$

$$F_{z\tau} = \frac{\tau_3}{l_3} \sin(-\phi), \quad (4.35)$$

where $F_{y\tau}$ and $F_{z\tau}$ are the Cartesian components of the force applied at the end of the joystick due to an applied torque, τ_3 , at the base of the joystick.

4.4.2 Human Arm as a Double Pendulum

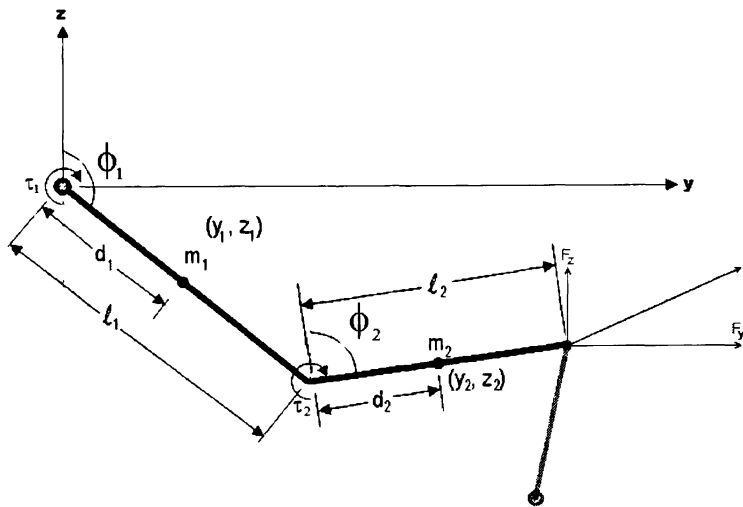


Figure 4.8: Human arm as a double pendulum diagram with an arbitrary end-effector force.

The human arm can be modeled as a double pendulum with 2 DOF. Figure 4.8 shows just the arm portion of Figure 4.3 with the torques and forces added, where τ_1 and τ_2 are the net torques placed on the shoulder and elbow, respectively, and F is an arbitrary force placed on the end of the arm. F_y and F_z are the Cartesian components of the force F .

A simple double pendulum is classically defined to have the center of mass of each link at the end of that link. For the purpose of modeling the human arm, it is accurate to observe the center of mass of each segment located at a specific point along the segment [40]. The location of the center of mass of each segment is denoted by the distance, d , from the beginning of each link as shown in Figure 4.8.

The equations of motion for the double pendulum can once again be solved from the Lagrangian of the system as [2]

$$L = T - V, \quad (4.36)$$

where T is the kinetic energy and V is the potential energy of the system. For the system shown in Figure 4.8, the Lagrangian becomes

$$\begin{aligned} L = & \frac{m_1}{2}(\dot{y}_1^2 + \dot{z}_1^2) + \frac{m_2}{2}(\dot{y}_2^2 + \dot{z}_2^2) \\ & - m_1 g d_1 \cos \phi_1 + m_2(l_1 \cos \phi_1 + d_2 \cos \phi_2), \end{aligned} \quad (4.37)$$

where g is the acceleration due to gravity, and ϕ_1 , ϕ_2 and ϕ are the angles of the shoulder, elbow and joystick, respectively. The Cartesian coordinates of the system are defined by

$$\begin{aligned} y_1 &= d_1 \sin \phi_1, & z_1 &= d_1 \cos \phi_1, \\ y_2 &= l_1 \sin \phi_1 + d_2 \sin \phi_2, & z_2 &= l_1 \cos \phi_1 + d_2 \cos \phi_2. \end{aligned} \quad (4.38)$$

The time derivatives of the equations from (4.38) become

$$\begin{aligned} \dot{y}_1 &= d_1 \cos \phi_1 \dot{\phi}_1, & \dot{z}_1 &= -d_1 \sin \phi_1 \dot{\phi}_1, \\ \dot{y}_2 &= l_1 \cos \phi_1 \dot{\phi}_1 + d_2 \cos \phi_2 \dot{\phi}_2, & \dot{z}_2 &= -l_1 \sin \phi_1 \dot{\phi}_1 - d_2 \sin \phi_2 \dot{\phi}_2. \end{aligned} \quad (4.39)$$

For the purpose of substitution, $\dot{y}_i^2 + \dot{z}_i^2$, for each, $i = 1, 2$, become

$$(\dot{y}_1^2 + \dot{z}_1^2) = d_1^2 \dot{\phi}_1^2, \quad (4.40a)$$

$$(\dot{y}_2^2 + \dot{z}_2^2) = l_1^2 \dot{\phi}_1^2 + d_2^2 \dot{\phi}_2^2 + l_1 d_2 \dot{\phi}_1 \dot{\phi}_2 \cos(\phi_1 - \phi_2). \quad (4.40b)$$

By substituting the equations from (4.40) into equation (4.37), L can be written in terms of ϕ_1 , ϕ_2 , ϕ , $\dot{\phi}_1$, and $\dot{\phi}_2$ as

$$\begin{aligned} L = & \frac{1}{2} (m_1 d_1^2 + m_2 l_1^2) \dot{\phi}_1^2 + \frac{m_2 d_2}{2} (d_2 \dot{\phi}_2^2 + l_1 \dot{\phi}_1 \dot{\phi}_2 \cos(\phi_1 - \phi_2)) \\ & - (m_1 d_1 + m_2 l_2) g \cos \phi_1 - m_2 d_2 g \cos \phi_2. \end{aligned} \quad (4.41)$$

The equations of motion can then be found using the Lagrangian method as [2]

$$-\frac{\partial L}{\partial \phi_i} + \frac{d}{dt} \left(\frac{\partial L}{\partial \dot{\phi}_i} \right) = \tau_i, \quad (4.42)$$

where $i = 1, 2$ for each joint. Each component can be derived separately for joint 1 as

$$\frac{\partial L}{\partial \phi_1} = -\frac{1}{2} m_2 d_2 l_1 \dot{\phi}_1 \dot{\phi}_2 \sin(\phi_1 - \phi_2) + (m_1 d_1 + m_2 l_2) g \sin \phi_1, \quad (4.43)$$

$$\frac{\partial L}{\partial \dot{\phi}_1} = (m_1 d_1^2 + m_2 l_1^2) \dot{\phi}_1 + \frac{m_2 d_2}{2} l_1 \dot{\phi}_2 \cos(\phi_1 - \phi_2). \quad (4.44)$$

$$\begin{aligned} \frac{d}{dt} \left(\frac{\partial L}{\partial \dot{\phi}_1} \right) = & (m_1 d_1^2 + m_2 l_1^2) \ddot{\phi}_1 + \frac{1}{2} m_2 d_2 l_1 \ddot{\phi}_2 \cos(\phi_1 - \phi_2) \\ & - \frac{1}{2} m_2 d_2 l_1 \dot{\phi}_2 \sin(\phi_1 - \phi_2) (\dot{\phi}_1 - \dot{\phi}_2). \end{aligned} \quad (4.45)$$

By substituting each of the previous components into equation (4.42) the total equa-

tion for joint 1 becomes

$$\begin{aligned}
 (m_1 d_1^2 + m_2 l_1^2) \ddot{\phi}_1 + \frac{1}{2} m_2 d_2 l_1 \phi_2 \cos(\phi_1 - \phi_2) \\
 + \frac{1}{2} m_2 d_2 l_1 \dot{\phi}_2^2 \sin(\phi_1 - \phi_2) - (m_1 d_1 + m_2 l_2) g \sin \phi_1 = \tau_1.
 \end{aligned} \tag{4.46}$$

Each component can be derived separately for joint 2 as

$$\frac{\partial L}{\partial \phi_2} = \frac{1}{2} m_2 d_2 l_1 \dot{\phi}_1 \dot{\phi}_2 \sin(\phi_1 - \phi_2) + m_2 g d_2 \sin \phi_2, \tag{4.47}$$

$$\frac{\partial L}{\partial \dot{\phi}_2} = m_2 d_2 \left(d_2 \dot{\phi}_2 + \frac{1}{2} l_1 \dot{\phi}_1 \cos(\phi_1 - \phi_2) \right), \tag{4.48}$$

$$\begin{aligned}
 \frac{d}{dt} \left(\frac{\partial L}{\partial \dot{\phi}_2} \right) = m_2 d_2^2 \ddot{\phi}_2 + \frac{1}{2} m_2 d_2 l_1 \ddot{\phi}_1 \cos(\phi_1 - \phi_2) \\
 - \frac{1}{2} m_2 d_2 l_1 \dot{\phi}_1 \sin(\phi_1 - \phi_2) (\dot{\phi}_1 - \dot{\phi}_2).
 \end{aligned} \tag{4.49}$$

By substituting each of the previous components into equation (4.42) the total equation for joint 2 becomes

$$\begin{aligned}
 m_2 d_2^2 \ddot{\phi}_2 + \frac{1}{2} m_2 d_2 l_1 \ddot{\phi}_1 \cos(\phi_1 - \phi_2) \\
 - m_2 g d_2 \sin \phi_2 - \frac{1}{2} m_2 d_2 l_1 \dot{\phi}_1^2 \sin(\phi_1 - \phi_2) = \tau_2.
 \end{aligned} \tag{4.50}$$

Equations (4.46) and (4.50) can then be rearranged and combined into the general state-space form of [28]

$$M(\Phi) \ddot{\Phi} = C(\Phi, \dot{\Phi}) + T_A, \tag{4.51}$$

where $M(\Phi)$ is the inertia matrix defined as

$$M(\Phi) = \begin{bmatrix} m_1 d_2^2 + m_2 l_2^2 & \frac{1}{2} m_2 d_2 l_1 \cos(\phi_1 - \phi_2) \\ \frac{1}{2} m_2 d_2 l_1 \cos(\phi_1 - \phi_2) & m_2 d_2^2 \end{bmatrix}, \tag{4.52}$$

Φ is the angle vector defined as

$$\ddot{\Phi} = \begin{bmatrix} \ddot{\phi}_1 \\ \ddot{\phi}_2 \end{bmatrix}, \quad (4.53)$$

$C(\Phi, \dot{\Phi})$ is the coriolis forces matrix. including gravity, and T_A are the input torques on the system defined as

$$C(\Phi, \dot{\Phi}) + T_A = \begin{bmatrix} (m_1gd_1 + m_2gl_2) \sin \phi_1 - \frac{1}{2}m_2d_2l_1\dot{\phi}_2^2 \sin(\phi_1 - \phi_2) \\ m_2gd_2 \sin \phi_2 + \frac{1}{2}m_2d_2l_1\dot{\phi}_1^2 \sin(\phi_1 - \phi_2) \end{bmatrix} + \begin{bmatrix} \tau_{A1} \\ \tau_{A2} \end{bmatrix} \quad (4.54)$$

Missing from equation (4.51) are the friction forces and the external constraining forces. For the purposes of this thesis the frictional forces will be neglected. The external constraining forces can be added by the relationship between a force placed at the end of the two link chain and the resulting torques placed at each joint. This relationship can be expressed by the transpose of the chain jacobian as [40]

$$T_F = J^T F. \quad (4.55)$$

For a planer, two link chain, equation (4.55) can be expressed by as

$$\begin{bmatrix} \tau_{F1} \\ \tau_{F2} \end{bmatrix} = \begin{bmatrix} -l_1 \cos \phi_1 - l_2 \cos \phi_2 & l_1 \sin \phi_1 + l_2 \sin \phi_2 \\ -l_2 \cos \phi_2 & l_2 \sin \phi_2 \end{bmatrix} \begin{bmatrix} F_y \\ F_z \end{bmatrix} \quad (4.56)$$

By adding the external forces to the system. the general equation becomes

$$M(\Phi)\ddot{\Phi} = C(\Phi, \dot{\Phi}) + T_F(\Phi) + T_A. \quad (4.57)$$

4.5 Combining Arm and Joystick Systems

The human arm equation of motion and the joystick equation of motion can be combined into one system first by constraining the the shoulder and elbow angles, ϕ_1 and ϕ_2 , respectively, to be dependent on the angle of the joystick, ϕ , by the equations (4.18) and (4.20). In addition to this the end-effector force from a torque placed on the joystick, $F(\tau_3)$, will be placed on the end-effector of the arm as a reaction force so that $F = -F(\tau_3)$. Combining the equations for $F(\tau_3)$ from Section 4.4.1.

$$F_{y_\tau} = \frac{\tau_3}{l_3} \cos(-\phi) \quad (4.58)$$

$$F_{z_\tau} = \frac{\tau_3}{l_3} \sin(-\phi). \quad (4.59)$$

and the end-effector force equations for $T_F = J^T F$ from Section 4.4.2.

$$\begin{bmatrix} \tau_{F_1} \\ \tau_{F_2} \end{bmatrix} = \begin{bmatrix} -l_1 \cos \phi_1 - l_2 \cos \phi_2 & l_1 \sin \phi_1 + l_2 \sin \phi_2 \\ -l_2 \cos \phi_2 & l_2 \sin \phi_2 \end{bmatrix} \begin{bmatrix} F_y \\ F_z \end{bmatrix}. \quad (4.60)$$

the resulting $T_F(\Phi)$ from the general human arm equation,

$$M(\Phi)\ddot{\Phi} = C(\Phi, \dot{\Phi}) + T_F(\Phi) + T_A. \quad (4.61)$$

can be combined as

$$\begin{bmatrix} \tau_{F_1} \\ \tau_{F_2} \end{bmatrix} = \begin{bmatrix} -l_1 \cos \phi_1 - l_2 \cos \phi_2 & l_1 \sin \phi_1 + l_2 \sin \phi_2 \\ -l_2 \cos \phi_2 & l_2 \sin \phi_2 \end{bmatrix} \begin{bmatrix} -\frac{\tau_3}{l_3} \cos(\phi) \\ \frac{\tau_3}{l_3} \sin(\phi) \end{bmatrix}. \quad (4.62)$$

The equations are combined as such for the purpose of designing observers that can observe τ_3 and subsequently τ_1 and τ_2 , by measuring only the angle of the joystick.

ϕ . The observers will be described in Chapter 6. The observers are designed that way because it is more practical to measure the angle of the joystick rather than the angle of each joint of the arm while a pilot is flying a plane.

Chapter 5

Vehicle System Model

5.1 Introduction

A model of a human-in-the-loop with a vehicle obviously requires a model of the vehicle. The parameters of a human modeled as a controller depend on the system that the human is controlling. In order to model a human as a feedback control system, as discussed in Chapter 3, the model of the system is required to calculate the gains of the feedback control law. If common environmental disturbances to the vehicle are known, additional compensating control laws could be included to improve the model of the human. Perhaps more importantly, these standard parameters need to be calculated so that when appropriately designed observers estimate the parameters of a real human controller, it is possible to determine if that human is performing within safety limits.

In addition to this, the human controller must take into account the actuator dynamics. This includes the mechanical dynamics between the human and the controlling device, such as a steering wheel or a joystick, as discussed in Chapter 4. This also includes the actuator dynamics between the controlling device and the control

inputs of the vehicle which are inherent to the vehicle.

As discussed in Chapter 1, the aircraft presents an interesting vehicle for a human pilot to control. The pilot must configure the aircraft in three dimensional space for both orientation and position. In addition to this, the three stability axes are coupled so that many maneuvers require precise, simultaneous control of all the control surfaces. And of course the state of the aircraft is nonlinearly dependent on aerodynamic forces and in turn atmospheric conditions which can be unpredictable and chaotic. Because of all these facts, designing an autopilot becomes a difficult task. In fact, different control laws would need to be designed for different situations. A human controller can learn to fly a plane in all conditions. The aircraft is one of the most prevalent complicated systems that humans control. Because of all this, the aircraft is an excellent and relevant place to study the relationship between an autonomous control system and a human-in-the-loop. The aircraft system is discussed in Section 5.2.

For the purposes of developing and testing nonlinear observers that could eventually be developed for a human-in-the-loop with an aircraft, a simple system is chosen as the system for a human to control. Section 5.3 presents a solid ball where the attitude of the ball is controlled by a single thruster. This system is used to demonstrate linear feedback control and subsequent estimation of the gains of that linear feedback control law.

5.2 Aircraft Equations of Motion

The configuration of an aircraft can be described with rigid body dynamics and aerodynamic forces. These equations are common and can be found in “The Control Handbook” [23]. The equations of motion are set up from the body frame references

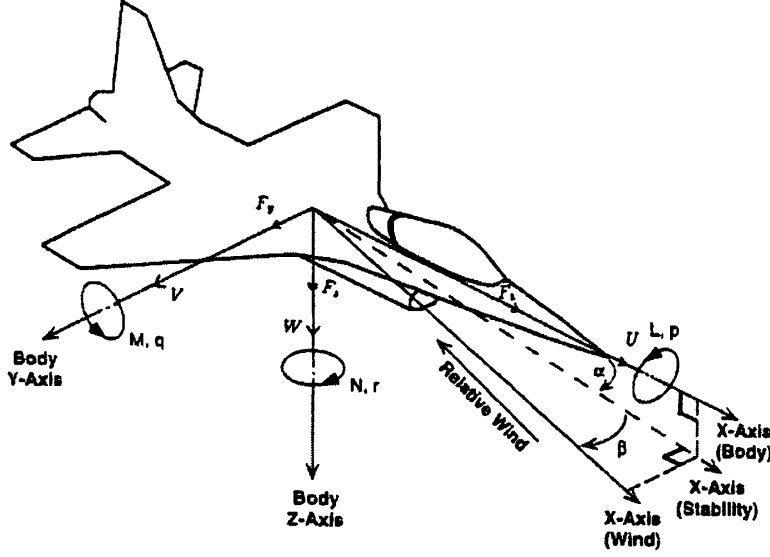


Figure 5.1: Aircraft body axes reference [23].

shown in Figure 5.1, and constructed in the force equations (5.1), the momentum equations (5.2), and the kinematic equations (5.4). The force equations are

$$\dot{U} = VR - WQ + \frac{1}{m} \sum F_x, \quad (5.1a)$$

$$\dot{V} = WP - UP + \frac{1}{m} \sum F_y, \quad (5.1b)$$

$$\dot{W} = UQ - VP + \frac{1}{m} \sum F_z, \quad (5.1c)$$

where m is the mass of the aircraft and U , V , and W are the components of the aircraft's velocity vector, and P , Q , and R are the components of the aircraft's body rotation speed as shown in Figure 5.1. The momentum equations are

$$\dot{P} = \frac{I_{xz}}{D} (I_x - I_y + I_z) PQ + \frac{1}{D} (I_y I_z - I_z^2 - I_{xz}^2) QR + \frac{I_z}{D} \sum L + \frac{I_{xz}}{D} \sum N, \quad (5.2a)$$

$$\dot{Q} = \frac{I_z - I_x}{I_y} PR + \frac{I_{xz}}{I_y} (R^2 - P^2) + \frac{1}{I_y} \sum M, \quad (5.2b)$$

$$\dot{R} = \frac{1}{D} (I_x^2 - I_x I_z + I_{xz}^2) PQ + \frac{I_{xz}}{D} (I_y - I_x - I_z) QR + \frac{I_{xz}}{D} \sum L + \frac{I_x}{D} \sum N. \quad (5.2c)$$

where I is the aircraft's inertia tensor and D is defined as

$$D = I_x I_z - I_{xz}^2. \quad (5.3)$$

The kinematic equations using Euler's angles are

$$\dot{\theta} = Q \cos \phi - R \sin \phi. \quad (5.4a)$$

$$\dot{\phi} = P + Q \sin \phi \tan \theta - R \cos \phi \tan \theta. \quad (5.4b)$$

$$\dot{\psi} = Q \frac{\sin \phi}{\cos \theta} - R \frac{\cos \phi}{\cos \theta}. \quad (5.4c)$$

where ϕ , θ , and ψ are the rotational angles about the x , y , and z body axes, respectively.

The external forces acting on the aircraft, such as gravity, g , aerodynamic and propulsive forces, including pilot control inputs, are contained in the force and momentum equations below. The aerodynamic forces are determined by air density, ρ , relative airspeed, \bar{U} , angle of attack, α , and sideslip angle, β . Parameters are introduced to nondimensionalize the aerodynamic forces. S is the wing's area, c is the wing's mean aerodynamic chord, b is the wing's span, and \bar{q} is dynamic pressure given as

$$\bar{q} = \frac{1}{2} \rho (U^2 + V^2 + W^2) = \frac{1}{2} \rho \bar{U}^2 \quad (5.5)$$

The pilot control inputs are given as the control surface deflections, δ_a , δ_e , δ_r , and δ_T , which represent the aileron, elevator, rudder deflections and throttle position,

respectively. The force and momentum summation equations are

$$\sum L = \bar{q}Sb\left(\frac{b}{2\bar{U}}C_{l_p}P + \frac{b}{2\bar{U}}C_{l_r}R + C_{l_\beta}\beta + C_{l_{\delta_a}}\delta_a + C_{l_{\delta_r}}\delta_r\right), \quad (5.6a)$$

$$\sum M = \bar{q}Sc\left(C_{m_0}P + C_{m_\alpha}\alpha + \frac{c}{2\bar{U}}C_{m_q}Q + \frac{c}{2\bar{U}}C_{m_\alpha}\dot{\alpha} + C_{m_{\delta_e}}\delta_e\right), \quad (5.6b)$$

$$\sum N = \bar{q}Sb\left(\frac{b}{2\bar{U}}C_{n_p}P + \frac{b}{2\bar{U}}C_{n_r}R + C_{n_\beta}\beta + C_{n_{\delta_a}}\delta_a + C_{n_{\delta_r}}\delta_r\right), \quad (5.6c)$$

$$\sum F_y = mg \sin \phi \cos \theta + \bar{q}S\left(\frac{b}{2\bar{U}}C_{y_p}P + \frac{b}{2\bar{U}}C_{y_r}R + C_{y_\beta}\beta + C_{y_{\delta_r}}\delta_r\right). \quad (5.6d)$$

$$\sum F_z = mg \cos \phi \cos \theta + T_z + \bar{q}S\left(-C_{z_\alpha}\alpha_{0L} + C_{z_\alpha}\alpha + \frac{c}{2\bar{U}}C_{z_q}Q + \frac{c}{2\bar{U}}C_{z_\alpha}\dot{\alpha} + C_{z_{\delta_e}}\delta_e\right), \quad (5.6e)$$

$$\sum F_x = -mg \sin \theta + C_{x_{\delta_T}}\delta_T + \bar{q}SC_x, \quad (5.6f)$$

where T_z is the z -axis component of thrust and α_{0L} is the zero lift angle of attack referenced from the x -stability axis. The coefficients represented by C represent nondimensional force and moment coefficients particular to a certain aircraft.

5.2.1 Linearized Aircraft Model

In order to design a control system it is common to first linearize the system about a nominal operation point and design the control to counteract small perturbations or deviations from that point. All the variables of the equations of motion can be replaced with the reference value plus some small disturbance shown as [22]

$$\begin{aligned} U &= U_0 + \Delta U, & V &= V_0 + \Delta V, & W &= W_0 + \Delta W, \\ P &= P_0 + \Delta P, & Q &= Q_0 + \Delta Q, & R &= R_0 + \Delta R, \\ X &= X_0 + \Delta X, & Y &= Y_0 + \Delta Y, & Z &= Z_0 + \Delta Z, \\ M &= M_0 + \Delta M, & N &= N_0 + \Delta N, & L &= L_0 + \Delta L, \\ \delta &= \delta_0 + \Delta\delta. \end{aligned} \quad (5.7)$$

The momentum equations (5.2) can be rewritten in terms of L , M , and N as

$$L = I_x \dot{P} - I_{xz} \dot{R} + QR(I_z - I_y) - I_{xz}PQ, \quad (5.8a)$$

$$M = I_y Q + RP(I_x - I_z) + I_{xz}(P^2 - R^2), \quad (5.8b)$$

$$N = -I_{xz} \dot{P} + I_z \dot{R} + PQ(I_y - I_x) + I_{xz}QR. \quad (5.8c)$$

And the force equations (5.1) can be rewritten in terms of X , Y , and Z as

$$X = mg \sin \theta + m(\dot{U} + QW - RV), \quad (5.9a)$$

$$Y = -mg \cos \theta \sin \phi + m(\dot{v} + RU - PW), \quad (5.9b)$$

$$Z = -mg \cos \theta \sin \phi + m(\dot{w} + PV - QU). \quad (5.9c)$$

To simplify the model further, only longitudinal control is considered and therefore

$$\phi = \psi = P = R = 0. \quad (5.10)$$

The momentum equations can then be linearized around the point reference point where

$$M_0 = 0. \quad (5.11)$$

This assumes that roll and yaw are steady in straight flight. The moment pitching equation can then be reduced to

$$\Delta M = I_y \Delta \ddot{\theta}. \quad (5.12)$$

The remaining states of interest are forward translation in the x direction, U , vertical translation in the z direction, W , pitch angle, θ and rate of change of pitch angle.

Q . The linearized equations of motion could then be written in state-space form in general as

$$\dot{x} = Ax + Bu \quad (5.13)$$

where x is the state vector, u is the control vector, and matrices A and B contain the aircraft's dimensional and stability derivatives. The linearized state-space form of the equations of motion are

$$\begin{bmatrix} \Delta \dot{U} \\ \Delta \dot{W} \\ \Delta \dot{Q} \\ \Delta \dot{\theta} \end{bmatrix} = \begin{bmatrix} X_u & X_w & 0 & -g \\ Z_u & Z_w & u_0 & 0 \\ M_u + M_{\dot{w}}Z_u & M_w + M_{\dot{w}}Z_w & M_q + M_{\dot{w}}U_0 & 0 \\ 0 & 0 & 1 & 0 \end{bmatrix} \begin{bmatrix} \Delta U \\ \Delta W \\ \Delta Q \\ \Delta \theta \end{bmatrix} + \begin{bmatrix} X_\delta & X_{\delta_T} \\ Z_\delta & Z_{\delta_T} \\ M_\delta + M_{\dot{w}}Z_\delta & M_{\delta_T} + M_{\dot{w}}Z_{\delta_T} \\ 0 & 0 \end{bmatrix} \begin{bmatrix} \Delta \delta \\ \Delta \delta_T \end{bmatrix}, \quad (5.14)$$

where the longitudinal derivatives are defined as

$$\begin{aligned}
X_u &= \frac{-(C_{D_u} + 2C_{D_0})\bar{q}S}{mU_0}, & X_w &= \frac{-(C_{D_\alpha} - C_{L_0})\bar{q}S}{mU_0}, \\
Z_u &= \frac{-(C_{L_u} + 2C_{L_0})\bar{q}S}{mU_0}, & & \\
Z_w &= \frac{-(C_{L_\alpha} + C_{D_0})\bar{q}S}{mU_0}, & Z_w &= C_{z_\alpha} \frac{\bar{c}}{2U_0} \bar{q}S / (U_0 m), \\
Z_\alpha &= U_0 Z_w, & Z_\alpha &= U_0 Z_w, \\
Z_q &= C_{z_q} \frac{\bar{c}}{2U_0} \bar{q}S / m, & Z_{\delta_e} &= C_{z_{\delta_e}} \bar{q}S / m, \\
M_u &= C_{m_u} \frac{(\bar{q}S\bar{c})}{U_0 I_y}, & & \\
M_w &= C_{m_\alpha} \frac{(\bar{q}S\bar{c})}{U_0 I_y}, & M_w &= C_{m_\alpha} \frac{\bar{c}}{2U_0} \frac{\bar{q}S\bar{c}}{U_0 I_y}, \\
M_\alpha &= U_0 M_w, & M_\alpha &= U_0 M_w, \\
M_q &= C_{m_q} \frac{\bar{c}}{2U_0} (\bar{q}S\bar{c}) / I_y, & M_{\delta_e} &= C_{m_{\delta_e}} (\bar{q}S\bar{c}) / I_y.
\end{aligned} \tag{5.15}$$

With a linearized model of the aircraft it is possible to design a linear feedback control law using the pole placement method described in Section 2.2.3. The pole placement method can be used to calculate the optimal values for any or all of the PID control gains depending on the level of control needed.

Accurately modeling of an aircraft proves to be difficult given the large number of aerodynamic coefficients. The aerodynamic coefficients are specific to a particular aircraft and they are non trivially dependent on atmospheric conditions. In addition to this the coefficients that relate the human control inputs to the control surfaces are not widely available.

A model for an aircraft can be modeled in Simulink using the “complete aircraft” block from the Aerosim blockset made by “Unmanned Dynamics” This blockset also includes the necessary parameters for a Navion aircraft along with a PI controller

for bank angle and a PID controller for airspeed. Figure 5.2 shows the successful convergence of the airspeed and bank angle to a desired value. The desired airspeed was 55m/s . The desired bank angle was 0° . The attitude required to maintain the desired airspeed is also shown. There were no winds. The PI controller for the bank angle is fed to the aileron control surface and the PID controller for the airspeed is fed to the elevator control surfaces.

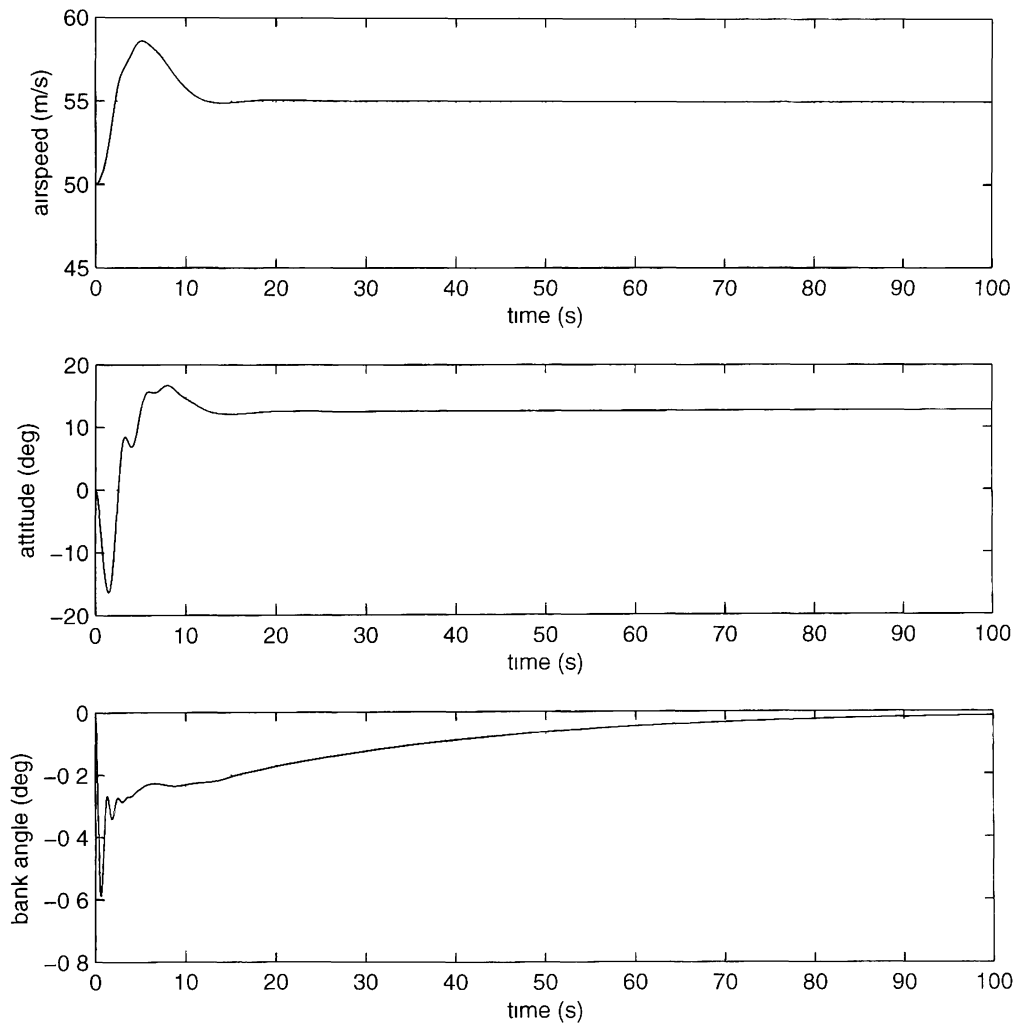


Figure 5.2: Aircraft control results.

5.3 Simple Case: Controlling A Solid Ball

As the aircraft is a complex nonlinear model it is more practical to test observer methods on a simple system. The solid ball with uniformly distributed mass is considered as a simple system with no external forces. This system would more closely represent a spacecraft in orbit. The system is further simplified by only considering attitude control in one dimension.

The equation of motion of a solid ball with one degree of freedom is represented as

$$J\ddot{\theta} = \tau_b, \quad (5.16)$$

where

$$\tau_b = r_b \times F_T, \quad (5.17)$$

and where

$$J = \frac{2}{5}m_b r_b^2. \quad (5.18)$$

where m_b is the mass of the ball, r_b is the radius of the ball. J is the moment of inertia of a solid ball, and τ_b is the net torque on the ball. The torque placed on the ball could be controlled by a thruster on the surface of the ball that could produce a variable force, F_T , tangent to the ball and in either direction. The equation of motion can be rearranged as

$$\dot{\theta} = \frac{r_b}{J}u. \quad (5.19)$$

where $u = F_T$ is the control input. In general linear state-space is written in the form

$$\dot{x} = Ax + Bu \quad (5.20a)$$

$$y = Cx. \quad (5.20b)$$

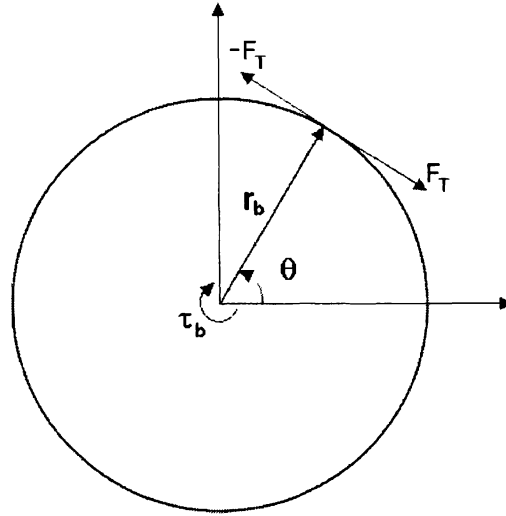


Figure 5.3: Solid ball diagram.

By making the following substitutions:

$$\begin{aligned} x_1 &= \theta, & \dot{x}_1 &= x_2, \\ x_2 &= \dot{\theta}, & \dot{x}_2 &= \ddot{\theta}, \end{aligned} \tag{5.21}$$

equation (5.19) can be represented in state-space form as

$$\begin{bmatrix} \dot{x}_1 \\ \dot{x}_2 \end{bmatrix} = \begin{bmatrix} 0 & 1 \\ 0 & 0 \end{bmatrix} \begin{bmatrix} x_1 \\ x_2 \end{bmatrix} + \begin{bmatrix} 0 \\ \frac{r_b}{J} \end{bmatrix} u, \tag{5.22}$$

where

$$A = \begin{bmatrix} 0 & 1 \\ 0 & 0 \end{bmatrix}, \tag{5.23}$$

$$B = \begin{bmatrix} 0 \\ \frac{r_b}{J} \end{bmatrix}, \tag{5.24}$$

and

$$C = \begin{bmatrix} 1 & 0 \\ 0 & 1 \end{bmatrix}, \quad (5.25)$$

indicating that all states are measured in the system. This is also known as full state feedback. The linear feedback control can be designed as described in Section 2.2.3 as

$$u = -K\bar{x}. \quad (5.26)$$

where $\bar{x} = x - x^*$. and for this case

$$u = \begin{bmatrix} k_p & k_d \end{bmatrix} \begin{bmatrix} \bar{x}_1 \\ \bar{x}_2 \end{bmatrix}. \quad (5.27)$$

where k_p and k_d are the proportional and derivative gains. K can then be chosen such that the eigenvalues of $(A - BK)$ have negative real parts. For this example let the mass and radius of the ball be $m_b = 2.5kg$, and $r_b = 1m$, where the resulting state-space equation becomes

$$\begin{bmatrix} \dot{x}_1 \\ \dot{x}_2 \end{bmatrix} = \begin{bmatrix} 0 & 1 \\ 0 & 0 \end{bmatrix} \begin{bmatrix} x_1 \\ x_2 \end{bmatrix} + \begin{bmatrix} 0 \\ 1 \end{bmatrix} u. \quad (5.28)$$

If the eigenvalues of $(A - BK)$, or poles, s , are chosen as

$$s = \begin{bmatrix} -2 & -4 \end{bmatrix}, \quad (5.29)$$

the characteristic equation, $|sI - A + BK| = 0$, can be used to calculate K , or the

place function in Matlab can be used to calculate K to be

$$K = \begin{bmatrix} 8 & 6 \end{bmatrix} \quad (5.30)$$

Figure 5.4 shows the successful convergence of system to the desired values. The

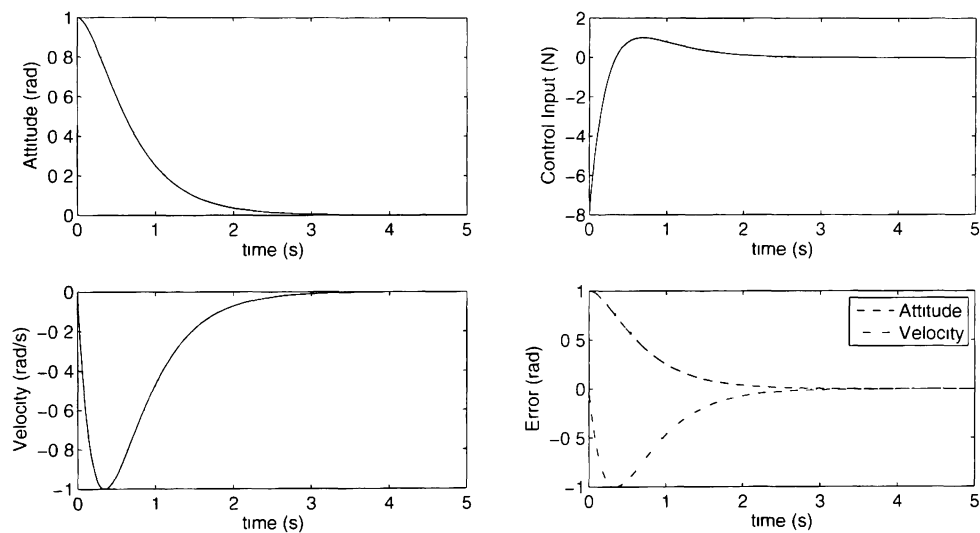


Figure 5.4: Ball control results.

initial conditions for the ball were $\theta = 1rad$ and $\dot{\theta} = 0rad/s$. The desired conditions for the ball were $\theta = 0rad$ and $\dot{\theta} = 0rad/s$.

The full system would include the human arm and joystick dynamics. In this way the control input u would control the torques on the shoulder and the elbow, τ_1 and τ_2 , respectively, which would determine the position and force of the hand which in turn controls the torque placed on the joystick, τ_3 , which determines the angle of the joystick which controls the amount of force produced by the thruster. In this case the joystick control could be considered fly-by-wire. The angle of the joystick is limited to $\pm 0.36rad$ and this may become a limiting factor in the controllability of the system. A proportion gain can be added to increase the sensitivity of the angle of the joystick

to the amount of force produced by the thruster.

Chapter 6

Observers

The methods for designing nonlinear sliding mode observers were discussed in Chapter 2. This chapter will use those methods to design observers for select components of the human-in-the-loop system. Observers will be designed to estimate applied torques to the shoulder, elbow, and joystick. Observers will also be designed to estimate the gains of a PD feedback control law used to control the attitude of a solid ball.

6.1 Sliding Mode Observer for Inverted Pendulum

This section derives a nonlinear sliding mode observer that can estimate the applied torque to a joystick, or inverted pendulum, by measuring the angle of the joystick. As shown in Section 2.4.5, a sliding mode observer can be used to estimate a disturbance to a system. For the case of the joystick, the input disturbance to the system is the applied torque, τ_3 .

The dynamic equation for the joystick as given in Section 4.4.1 is

$$m_3 l_3^2 \ddot{\phi} = m_3 g l_3 \sin \phi - (k_s \phi + k_\mu \dot{\phi}) + \tau_3. \quad (6.1)$$

Equation (6.1) can be re-written by solving for angular acceleration as

$$\ddot{\phi} = \frac{1}{m_3 l_3^2} \tau_3 + \frac{g}{l_3} \sin \phi - \frac{1}{m_3 l_3^2} (k_s \phi + k_\mu \dot{\phi}). \quad (6.2)$$

Equation (6.2) can be written in state-space by defining

$$x_1 = \phi \quad (6.3a)$$

$$x_2 = \dot{\phi}, \quad (6.3b)$$

and so the equations of motions for the joystick become

$$\dot{x}_1 = x_2 = \dot{\phi} \quad (6.4a)$$

$$\dot{x}_2 = \ddot{\phi} = \frac{1}{m_3 l_3^2} \tau_3 + \frac{g}{l_3} \sin \phi - \frac{1}{m_3 l_3^2} (k_s \phi + k_\mu \dot{\phi}) \quad (6.4b)$$

From this the sliding mode observer for the joystick becomes

$$\dot{\hat{x}}_1 = \hat{x}_2 + L_1 \text{sign}(\phi - \hat{x}_1) \quad (6.5a)$$

$$\dot{\hat{x}}_2 = \frac{1}{m_3 l_3^2} L_2 \text{sign}(\dot{\phi} - \hat{x}_2) + \frac{g}{l_3} \sin \phi - \frac{1}{m_3 l_3^2} (k_s \phi + k_\mu \dot{\phi}), \quad (6.5b)$$

where the disturbance τ_3 can now be calculated as

$$\tau_3 = \left[L_2 \text{sign}(\dot{\phi} - \hat{x}_2) \right]_{\epsilon q} \quad (6.6)$$

Equation (6.5) assumes that we can measure both ϕ and $\dot{\phi}$. However it is possible to design the observer such that only ϕ is measured and $\dot{\phi}$ is estimated as v expressed

as

$$\dot{\hat{x}}_1 = L_1 \text{sign}(\phi - \hat{x}_1) \quad (6.7a)$$

$$\dot{\hat{x}}_2 = \frac{1}{m_3 l_3^2} L_2 \text{sign}(v - \hat{x}_2) + \frac{g}{l_3} \sin(\phi) - \frac{1}{m_3 l_3^2} (k_s \phi + k_\mu v), \quad (6.7b)$$

where v can then be calculated as

$$v = [L_1 \text{sign}(\phi - \hat{x}_1)]_{eq}. \quad (6.8)$$

and subsequently τ_3 can then be calculated as

$$\tau_3 = [L_2 \text{sign}(v - \hat{x}_2)]_{eq}. \quad (6.9)$$

This section described an observer that can estimate an applied torque to a joystick by tracking the dynamics of the angle of the joystick. Verification and testing of this observer are shown in Chapter 7.

6.2 Sliding Mode Observer for Human Arm

This section derives a nonlinear sliding mode observer for a human arm, or double pendulum, that can estimate the applied torques to the shoulder, τ_1 and elbow, τ_2 . The equations of motion for the human arm from Section 4.4.2 are presented in the general form

$$M(\Phi)\ddot{\Phi} = C(\Phi, \dot{\Phi}) + T_F(\Phi) + T_A. \quad (6.10)$$

where T_A is the applied to the shoulder and elbow joints and Φ is the angles of the shoulder and elbow joints. Equation (6.10) can be written in state-space by defining

$$x_1 = \Phi \quad (6.11a)$$

$$x_2 = \dot{\Phi}. \quad (6.11b)$$

where

$$\Phi = \begin{bmatrix} \phi_1 \\ \phi_2 \end{bmatrix}, \quad (6.12a)$$

$$\dot{\Phi} = \begin{bmatrix} \dot{\phi}_1 \\ \dot{\phi}_2 \end{bmatrix} \quad (6.12b)$$

The equations of motion for the human arm in state-space then become

$$\dot{x}_1 = x_2 = \dot{\Phi} \quad (6.13a)$$

$$\dot{x}_2 = \ddot{\Phi} = M^{-1}(\Phi) \left[C(\Phi, \dot{\Phi}) + T_F(\Phi) + T_A \right]. \quad (6.13b)$$

From this the sliding mode observer for the human arm becomes

$$\dot{\hat{x}}_1 = \hat{x}_2 + L_1 \text{sign}(\Phi - \hat{x}_1) \quad (6.14a)$$

$$\dot{\hat{x}}_2 = M^{-1}(\Phi) \left[C(\Phi, \dot{\Phi}) + T_F(\Phi) + L_2 \text{sign}(\dot{\Phi} - \hat{i}_2) \right], \quad (6.14b)$$

where the disturbance, or applied torque, T_A , on the system can now be calculated as

$$T_A = \left[L_2 \text{sign}(\dot{\Phi} - \hat{i}_2) \right]_{eq} \quad (6.15)$$

This can be shown individually as

$$T_{\iota} = \begin{bmatrix} \tau_1 \\ \tau_2 \end{bmatrix} = \begin{bmatrix} \left[L_2 \text{sign}(\dot{\phi}_1 - \dot{\hat{\phi}}_1) \right]_{eq} \\ \left[L_2 \text{sign}(\dot{\phi}_2 - \dot{\hat{\phi}}_2) \right]_{eq} \end{bmatrix} \quad (6.16)$$

This section described an observer that can estimate the applied torques to the shoulder and elbow joints by tracking the dynamics of the angles of the joints of the human arm. Verification and testing of this observer are shown in Chapter 7.

6.3 Observer for PD Gains

This section derives a nonlinear sliding mode observer for a PD feedback control system that is controlling the attitude of a simple solid ball as described in Section 5.3. This observer is designed based on the combined system of the solid ball and PD feedback control law, and as such is specific only for this case. The observer will be designed using the general nonlinear observer method from Section 2.4.4. The general form of the observer is given as

$$\dot{\hat{x}} = \left(\frac{\partial H(\hat{x})}{\partial x} \right)^{-1} L(\hat{x}) \text{sign}(V(t) - H(\hat{x})), \quad (6.17)$$

where the nonlinear observer can be designed to observe the states of a system described by

$$\dot{x} = f(x) \quad (6.18a)$$

$$y = h(x). \quad (6.18b)$$

For this case the solid ball control system is given by the equation

$$\ddot{\theta} = \frac{r_b}{J}u. \quad (6.19)$$

where u is the PD control input,

$$u = -K_p\theta - K_d\dot{\theta}. \quad (6.20)$$

By substitution the complete system model becomes

$$\ddot{\theta} = -\frac{r_b}{J}K_p\theta - \frac{r_b}{J}K_d\dot{\theta}. \quad (6.21)$$

Equation (6.21) can be redefined in state-space by letting

$$\begin{aligned} x_1 &= \theta, & \dot{x}_1 &= x_2, \\ x_2 &= \dot{\theta}, & \dot{x}_2 &= x_3x_1 + x_4x_2, \\ x_3 &= -a_1, & \dot{x}_3 &= 0, \\ x_4 &= -a_2, & \dot{x}_4 &= 0, \end{aligned} \quad (6.22)$$

where

$$a_1 = \frac{r_b}{J}K_p \quad (6.23a)$$

$$a_2 = \frac{r_b}{J}K_d. \quad (6.23b)$$

The system can then be put in terms of equation (6.18) where

$$f(x) = \begin{bmatrix} x_2 \\ x_3x_1 + x_4x_2 \\ 0 \\ 0 \end{bmatrix} \quad (6.24)$$

and

$$h(x) = x_1. \quad (6.25)$$

Equation (6.25) represents that the system only measures the state θ . The $H(x)$ vector can then be constructed as the repeated Lie derivatives of $h(x)$ with the form

$$H(x) = \begin{bmatrix} h_1(x) \\ h_2(x) \\ h_3(x) \\ h_4(x) \end{bmatrix}, \quad (6.26)$$

where the components of $H(x)$ are calculated starting with $h_1(x) = x_1$. The rest follow as

$$h_2(x) = \frac{\partial h_1(x)}{\partial x} f = \begin{bmatrix} 1 & 0 & 0 & 0 \end{bmatrix} \begin{bmatrix} x_2 \\ x_3x_1 + x_4x_2 \\ 0 \\ 0 \end{bmatrix} = x_2. \quad (6.27)$$

$$h_3(x) = \frac{\partial h_2(x)}{\partial x} f = \begin{bmatrix} 0 & 1 & 0 & 0 \end{bmatrix} \begin{bmatrix} x_2 \\ x_3x_1 + x_4x_2 \\ 0 \\ 0 \end{bmatrix} = x_3x_1 + x_4x_2. \quad (6.28)$$

$$h_4(x) = \frac{\partial h_3(x)}{\partial x} f = \begin{bmatrix} x_3 & x_1 & x_1 & x_2 \end{bmatrix} \begin{bmatrix} x_2 \\ x_3x_1 + x_4x_2 \\ 0 \\ 0 \end{bmatrix} = x_2x_3 + x_1x_3x_4 + x_2x_4^2, \quad (6.29)$$

so that

$$H(x) = \begin{bmatrix} x_1 \\ x_2 \\ x_3x_1 + x_4x_2 \\ x_2x_3 + x_1x_3x_4 + x_2x_4^2 \end{bmatrix} \quad (6.30)$$

The Jacobian of the vector $H(x)$ can then be calculated as

$$\frac{\partial H(x)}{\partial x} = \begin{bmatrix} 1 & 0 & 0 & 0 \\ 0 & 1 & 0 & 0 \\ x_3 & x_4 & x_1 & x_2 \\ x_3x_4 & x_3 + x_4^2 & x_2 + x_1x_4 & x_1x_3 + 2x_2x_4 \end{bmatrix} \quad (6.31)$$

As described in Section 2.4.4. the observer vector $V(t)$ becomes

$$V(t) = \begin{bmatrix} v_1(t) \\ v_2(t) \\ v_3(t) \\ v_4(t) \end{bmatrix} = \begin{bmatrix} x_1(t) \\ [L_1 \text{sign}(x_1(t) - \hat{x}_1(t))]_{eq} \\ [L_2 \text{sign}(v_2(t) - \hat{x}_2(t))]_{eq} \\ [L_3 \text{sign}(v_3(t) - (\hat{x}_3(t)\hat{x}_1(t) + \hat{x}_2(t)\hat{x}_4(t)))]_{eq} \end{bmatrix} \quad (6.32)$$

With each component defined. the general equation (6.17) can then be simulated.

However in this case, it becomes difficult to accurately observe all of the states of

the system

$$\hat{x} = \begin{bmatrix} \hat{x}_1 \\ \hat{x}_2 \\ \hat{x}_3 \\ \hat{x}_4 \end{bmatrix} \quad (6.33)$$

This is most likely due to the fact that the determinant of the Jacobian of the $H(\hat{x})$ matrix $\frac{\partial H(\hat{x})}{\partial x}$ approaches zero. In this case the attitude and angular velocity, \hat{x}_1 and \hat{x}_2 , respectively, can accurately be estimated as shown in Figure 7.5, in Chapter 7. but the values for $a_1 = -\hat{x}_3$ and $a_2 = -\hat{x}_3$ drastically diverge as shown in Figure 7.6, in Chapter 7.

However it is still possible to observe the angular acceleration \dot{x}_2 from the components of the observer vector $V(t)$. From equation (6.32),

$$v_2(t) = [L_1 \text{sign}(x_1(t) - \hat{x}_1(t))]_{eq} \quad (6.34)$$

and subsequently

$$v_3(t) = [L_2 \text{sign}(v_2(t) - \dot{x}_2(t))]_{eq} = \dot{x}_2. \quad (6.35)$$

Therefore x_3 and x_4 can still be estimated by applying the least square method to the linear equation of the complete system,

$$\dot{x}_2 = x_3 x_1 + x_4 x_2, \quad (6.36)$$

which can also be written as

$$\ddot{\theta} = -a_1 x_1 - a_2 x_2. \quad (6.37)$$

As described in Section 2.5, the least square method can be used to estimate the

values of the constant coefficients of a linear polynomial by using the equation

$$C_{opt} = (X^T X)^{-1} X^T B. \quad (6.38)$$

In this case,

$$C_{opt} = \begin{bmatrix} -\hat{a}_1 \\ -\hat{a}_2 \end{bmatrix}, \quad (6.39)$$

$$X = \begin{bmatrix} x_1(1) & \hat{x}_2(1) \\ \vdots & \vdots \\ x_1(N) & \hat{x}_2(N) \end{bmatrix}, \quad (6.40)$$

$$B = \begin{bmatrix} \ddot{\theta}(1) \\ \vdots \\ \ddot{\theta}(N) \end{bmatrix}, \quad (6.41)$$

where N is the number of time steps.

The PD gains can then simply be calculated as

$$K_P = \frac{J}{r_b} a_1 \quad (6.42a)$$

$$K_D = \frac{J}{r_b} a_2. \quad (6.42b)$$

This section derived an observer that can estimate the gains of a PD feedback controller of the attitude of a solid ball by tracking the dynamics of the attitude of that solid ball. The results of this are shown in Chapter 7.

Chapter 7

Human-in-the-loop With Hardware

As stated before, a human-in-the-loop model aims to simulate a system along with its human controller.

Modeling the system as a vehicle has long been done using the laws of mechanics. This is obviously useful because it provides the ability to predict mechanical behavior, which can allow design corrections to be made before manufacturing and of course provides the ability to design control systems. Understanding the machine is easier than understanding the human because the machine follows the well known laws of mechanics and because the machine was designed from the ground up.

The ability to simulate a human-in-the-loop with hardware provides the ability to predict human behavior, make design corrections, and make a more informed semi-autonomous control system for both systems in conjunction. “Development of human models supports system designs, development and evaluation of dynamic control systems where humans may have manual or supervisory control responsibilities. It is desirable to have a predictive model versus a descriptive model (fitting a model to existing data) so that the behavior of the man machine system may be estimated before the system is built. Prediction may also be based on ideal behavior from an

expert opinion. Simulation and experimental verification become important steps in the validation part of a design process but the information may come too late to significantly affect the design. Thus, the need for accurate human performance models is needed for better insights into new and cost effective design approaches [25]. Simulating the human-in-the-loop allows for the design of observers that could be used to measure whether the vehicle and human controller are in agreement [25].

The models for a human controller, a human arm and a vehicle were discussed in Chapters 3, 4 and 5, respectively. Taking the linear feedback model for the human, the three link model for the arm and the joystick, and the solid ball for vehicle, it is now possible to combine all of these into one model. The observers from Chapter 6 can then be implemented to estimate the unmeasured parameters of the human-in-the-loop with hardware system.

7.1 Results

Sliding mode observers were used to find the gains of a PD feedback control law for attitude control of a solid ball, and to find the applied torques to the joints of the human arm and the joystick. Simulations were run using “Simulink” as a numerical analysis tool. The simulations used an “ODE1” solver (or an Ordinary Differential Equation solver method of order 1) also known as Euler’s method. A sufficiently small time step was needed to provide fast switching in the sliding mode observers. The gains and filters for the observers were tuned manually.

Results of observing arm-joystick torques

The applied torques on the joints of the arm were observed using information about the angles and the angular velocities of the joints. The angles of the joints of the arm

were calculated from the angle of the joystick.

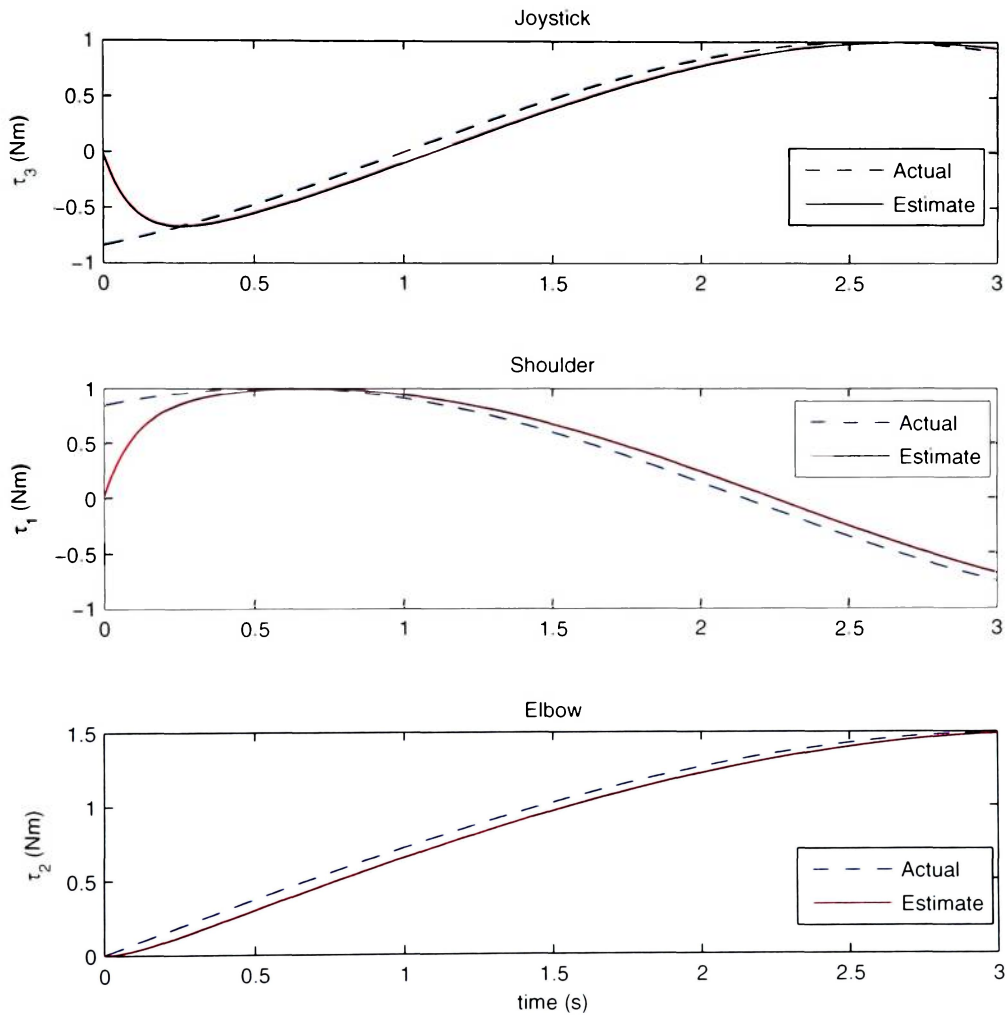


Figure 7.1: Testing results of observers for applied torques.

The accuracy of the sliding mode observers designed to estimate the applied torques were tuned and tested by inputting a known dynamic torque to each joint of the arm-joystick system. The known torques were inputted into a model of the arm and joystick so that the angles could be calculated and then input into the observers. Torques changing as a sin function were input into each of the joints at

different phases. This was chosen arbitrarily for testing. The gains of the observers, L , the filters used to calculate the equivalent values and the time step of the numerical solver were all adjusted until the observed torques matched the input torque. Figure 7.1 shows successful convergence of the estimated torques to the actual torques. It is important to note that the initial condition of the estimate is zero so there is a time t_1 needed for the estimate to converge on the actual torque depending on how far from zero the actual torque is. It is also important to note that although the estimated torques are accurate there is a small lag.

Figures 7.2, 7.3 and 7.4 show the results of the observed applied torques on the arm-joystick system given a change in the angle of the joystick. Figure 7.2 shows three graphs. The top graph, ϕ , represents the measured joystick angle. The angle changes from zero to a positive value where it remains. This represents a pitch-down maneuver a pilot might perform. The middle graph is the angular rate $\dot{\phi}$, which was calculated numerically as the time derivative of the the angle ϕ . It is important to note that for both ϕ and $\dot{\phi}$, the estimate covers the actual trajectories so they are not visible on the graph. This is another indication that the observer is functioning properly. The bottom graph is the observed applied torque τ_3 which was previously unknown. The trajectory of τ_3 makes sense because it starts at zero when the joystick is in equilibrium in the upright position, and then transitions to some higher value where it remains in order to hold the joystick forward against the restoring spring.

Figure 7.3 also shows three graphs. The top graph shows the actual shoulder angle ϕ_1 as calculated from the joystick angle ϕ , along with the estimate trajectory. The middle graph shows the angular rate of the shoulder $\dot{\phi}_1$ calculated numerically as the time derivative of the angle ϕ_1 . Note that for both graphs the estimated values overlap the actual value. The bottom graph is the observed applied torque τ_1 . Note that there is a finite time t_1 needed for the estimated torque to converge.

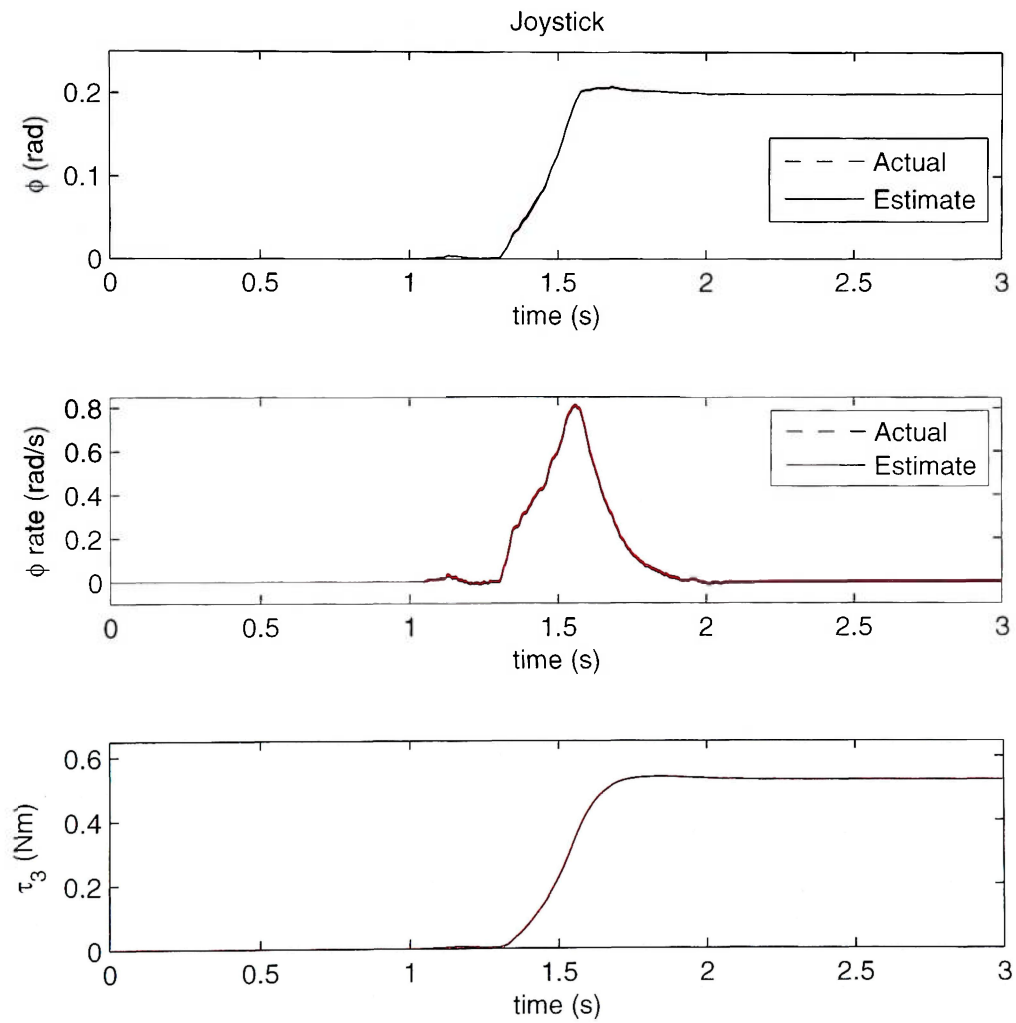


Figure 7.2: Joystick torque observer results.

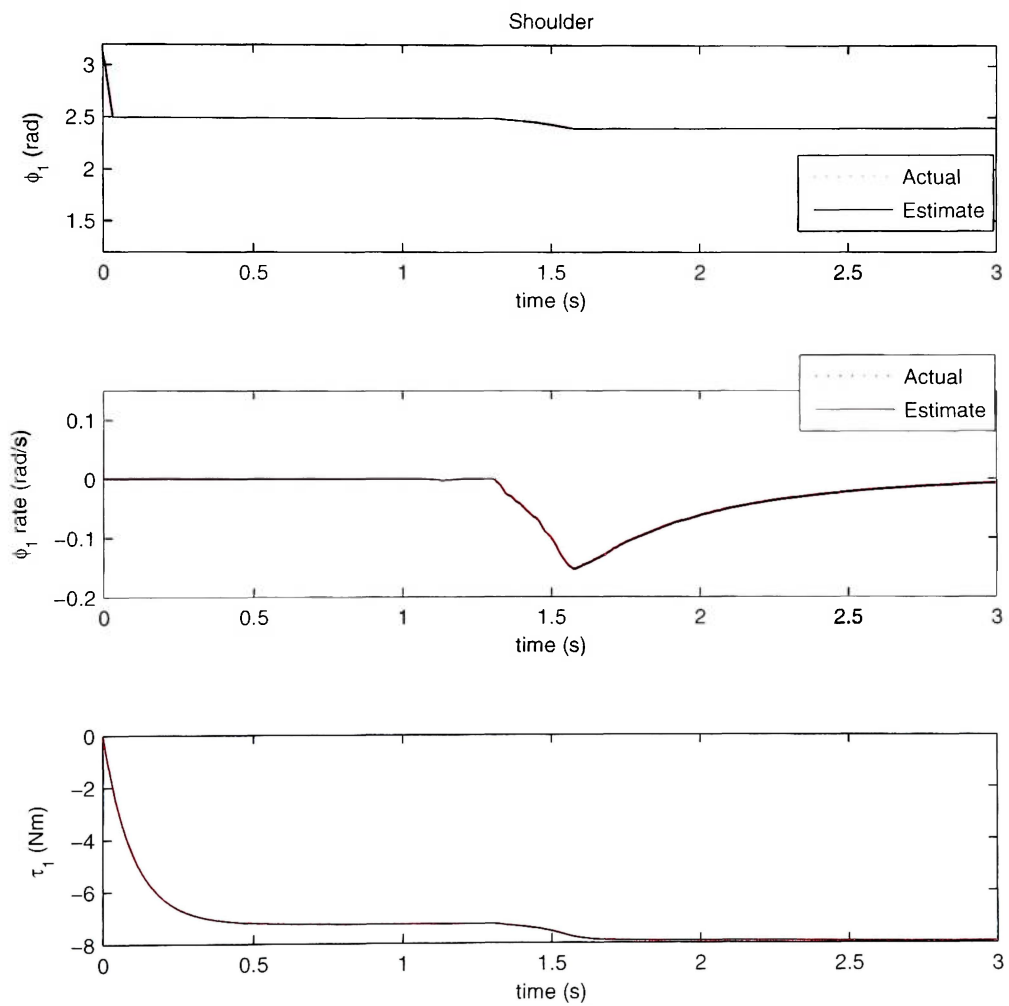


Figure 7.3: Shoulder torque observer results.

The observer was run with enough static time to allow for this convergence before the pitch-down maneuver was performed. The dynamics of the torque makes sense. The initial negative torque shows the torque required on the shoulder to maintain the arm in a position that keeps the hand on the joystick. The change in the torque represents the increase in torque in the negative direction to move the arm forward and also push against the spring of the joystick.

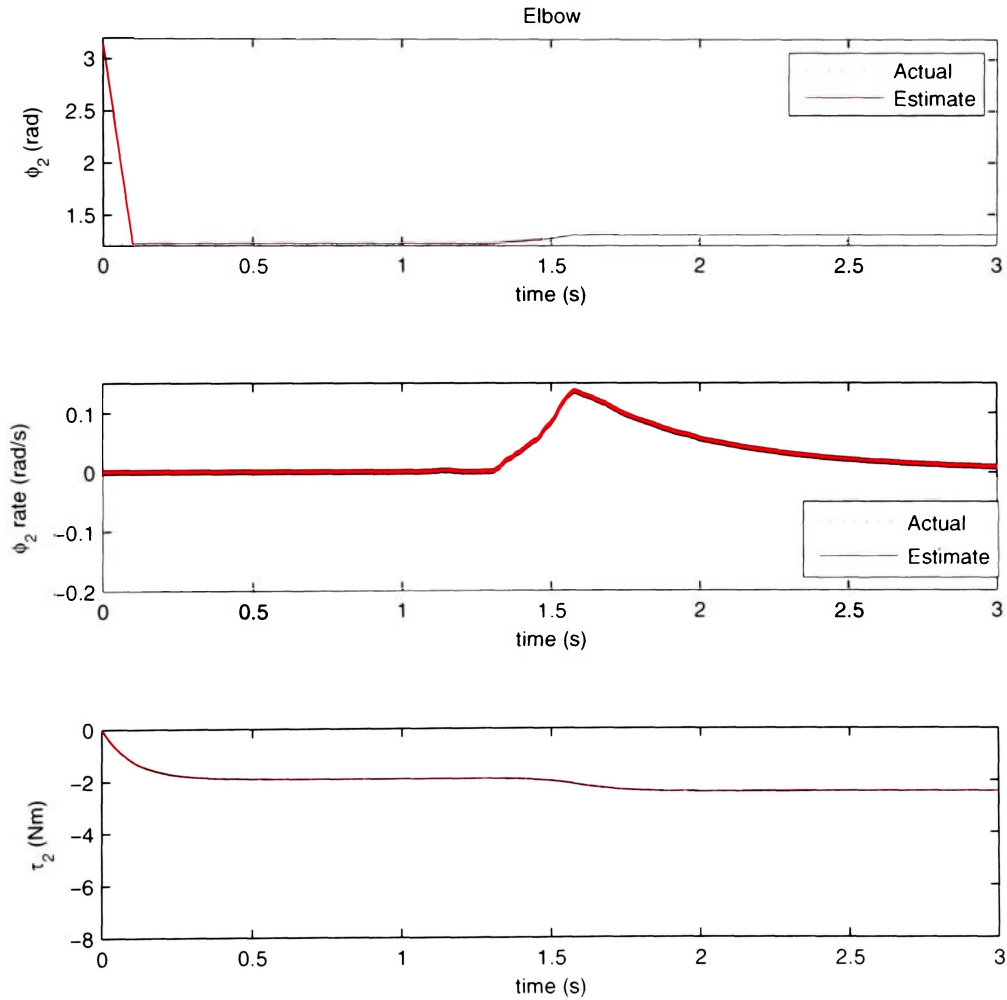


Figure 7.4: Elbow torque observer results.

Figure 7.4 also shows three graphs for the elbow joint and is similar to Figure 7.3. The top graph shows the the elbow joint angle, the middle graph shows the angular rate and the bottom graph shows the observed applied torque τ_2 .

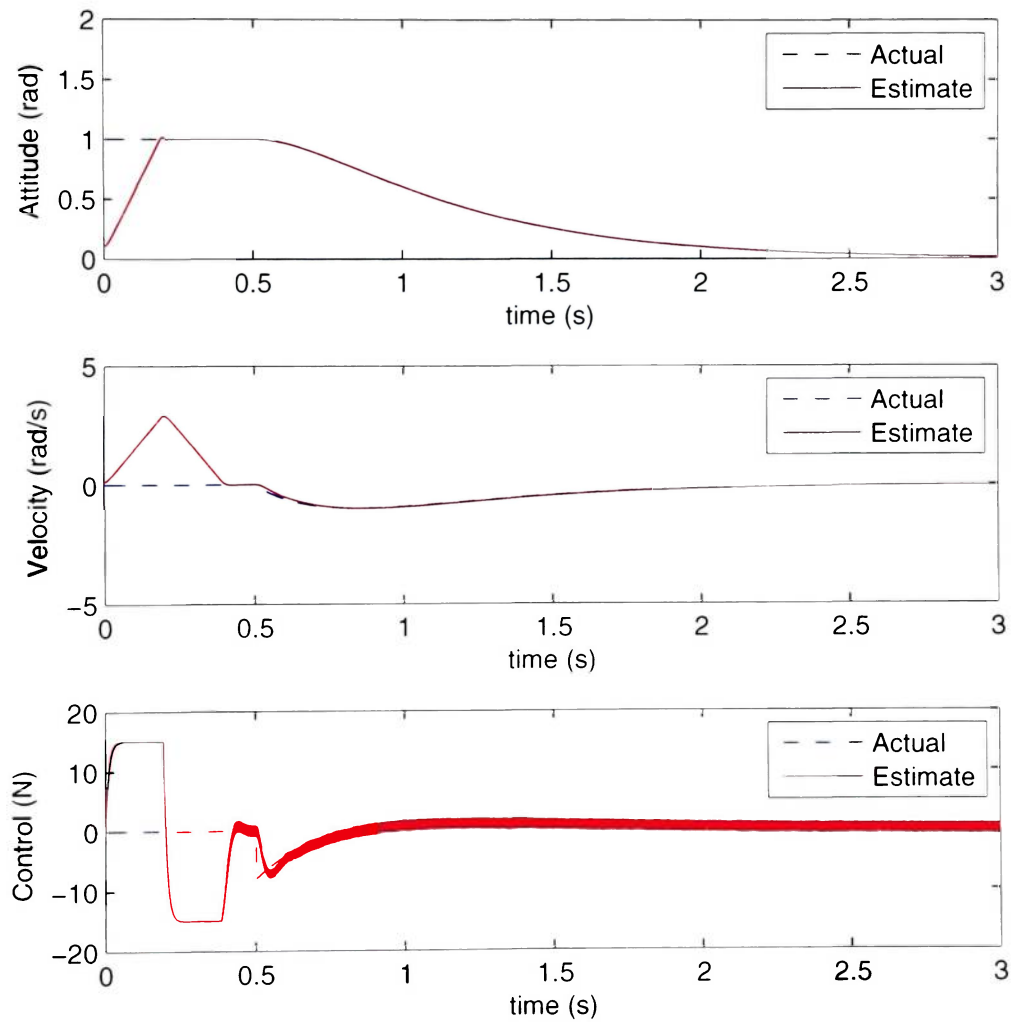


Figure 7.5: Observable states of PD controlling solid ball.

Results of observing PD gains

Figure 7.5 shows the state trajectories that had their estimated value converge to the actual value. The top graph shows the attitude of the ball, θ , and the middle graph shows the attitude's rate of change, $\dot{\theta}$. Both of these values are measured from the system. The bottom graph is the observed angular acceleration, $\ddot{\theta}$. In this case $\ddot{\theta} = u$ since $J = 1$ and $r_b = 1$, so the bottom graph is simply the control input. By the design of the sliding mode observer, it is important to note that each successive higher order state begins to converge only after the previous state has converged and therefore has reached sliding mode. The command to initiate the control of the solid ball to the desired point was therefore delayed until 0.5sec in order to allow time for convergence so that control observer could estimate as much of the maneuver as possible. Once the maneuver began, there was again a delay before the control observer converged because there was such a sharp change in the actual control.

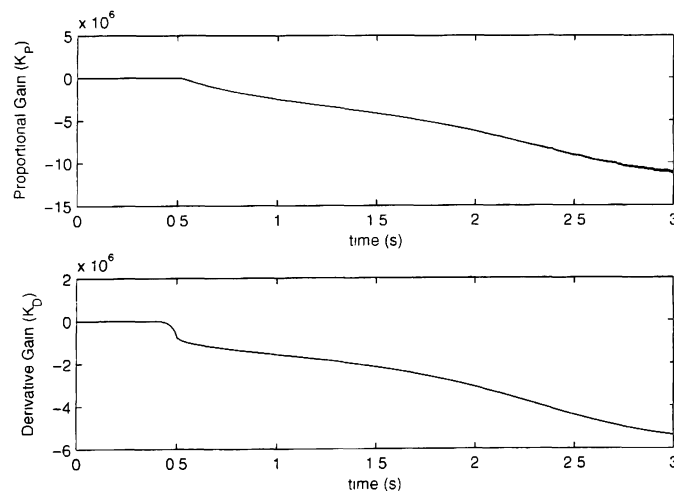


Figure 7.6: Unobservable states of PD controlling solid ball.

Figure 7.6 shows that the observed states \hat{K}_P and \hat{K}_D failed to converge. The feedback control gains K_P and K_D were instead found using the least square method

on the observed control input from Figure 7.5. The least square method was performed on data points of \hat{u} in the range $0.75 \leq t \leq 3\text{sec}$. This was done so the that “best fit” was performed on the data points after the estimated control input had had a chance to converged on the actual control input.

In general the gains of the PD feedback control law used to control the attitude of the sold ball were calculated using the measured attitude of the system. The results are shown in Table 7.1. This shows that the gains of a PD control can be determined

Gain	Actual	Estimate	Error(%)
K_P	8.0000	8.011	0.142
K_D	6.0000	5.860	2.339

Table 7.1: PD gain results.

by just measuring the attitude of the system. The error in the calculated gains are due to the inaccuracy of the observer, which is due to lag time for convergence and chattering from having a finite switching frequency.

7.2 Conclusion

The nonlinear observers developed in this thesis successfully observed parameters of the human-in-the-loop for a simplified model of a human and system. These methods could be generalized to observe more complicated models of a human-in-the-loop with hardware. These observers could eventually be used in conjunction with a semi-autonomous control system that can aid a human-in-the-loop with hardware.

Figure 7.2 shows a human-in-the-loop with hardware. The “Human” can control the “Vehicle” system and receives information about the “Vehicle” system through the “Senses” The “Senses” could be comprised of visual, auditory, and somatic information. The “Vehicle” includes any environmental forces on the vehicle such as atmospheric and gravitational forces. The “Hardware” is comprised of the “Vehicle”

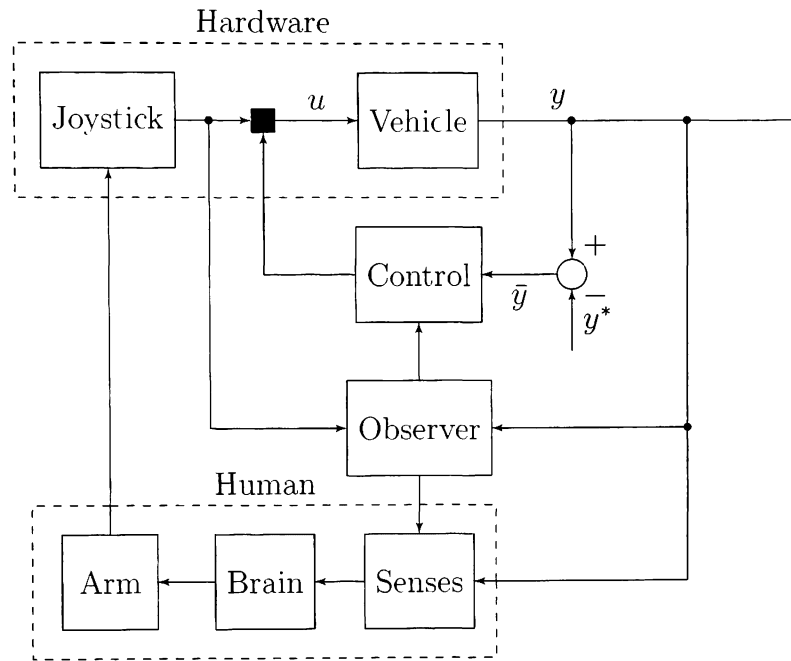


Figure 7.7: Block diagram of human-in-the-loop with hardware.

along with the human interface control input, the “Joystick”, to the vehicle. The “Human” is comprised of the “Senses”, the control processing center in the “Brain” and the mechanical ability to control the machine using the “Arm”. The human-in-the-loop system shows that the “Observer” can estimate parameters of the human controller by tracking the trajectories of the “Joystick” and the “Vehicle” as was shown in this thesis. This information can be used to inform the automatic “Control” of how best to control the “Vehicle” in order to best assist the human operator. The black square where the automatic control and joystick meet represents a “black box” for all the different ways the human and computer control could be mixed to produce the best outcome in different situations. Figure 7.2 also shows that the “Observer” could send information directly to the human to inform them of their performance. The desired output y^* is shown only for the automatic control since the human may calculate the error \bar{y} in a different fashion. However this desired output could perhaps

come from the observer if the desired output should be decided for different situations.

This thesis involved analysis of the dynamics of the mechanical interaction between the human and the system and analysis of the human as a feedback control system. The summation of both of these parts provide a simple model for human-in-the-loop behavior with a system. The use of nonlinear observers provides the ability to calculate unmeasurable parameters of the human arm and the human mind which can be used to gain insight into the condition of a human controller in the loop with a system. These methods were tested on the components of a simplified version of a human-in-the-loop with a system.

Chapter 8

Conclusions and Future Studies

This thesis is only a first step in understanding human-in-the-loop with a system. Only simple models of a human and a vehicle were simulated. More complicated models and more generalized observers should be used to gain insight into human and machine cognition.

8.1 Improve Models

In each case a more complex model is needed to accurately simulate a human-in-the-loop with a system.

Improved Vehicle

The system considered was a simple solid ball with one degree of freedom (only pitch). The control actuator was considered to be a simple thruster of variable thrust which was proportional to the angle of a joystick.

The system should be a complete model of the vehicle the human is controlling, whether it is an aircraft, a spacecraft, or a car. This would include the complete

actuator dynamics between the system and the control input, i.e. the joystick or steering wheel.

Arm

The human arm and joystick dynamical system was considered only as a planer three link chain with a fixed torso position only suitable for pitch control.

The human arm should be modeled in three dimensions. This could be accomplished by modeling a double conical pendulum. More complex dynamics could be taken into account such as joint and muscle dynamics including the wrist and the hand.

There are many cases where it is difficult to assume that the shoulder remains in a fixed position and so it may not be possible to know the angles of the arm just by knowing the position of the control interface. However it is possible to attach lightweight gyros to the wrist and body to measure the angles of the arm more directly.

Joystick

The joystick was modeled as an inverted pendulum with only a restoring spring to keep it upright. This is more indicative of a fly-by-wire system that has no feedback from the controlling surfaces.

The joystick could be modeled as mechanical control input that would be subject to the environmental forces on the controlling surfaces.

Human

The human mind was only considered as a linear PD feedback control system.

This model has the most room for improvement. The complexity could first be increased by modeling the brain as a nonlinear controller. An even more appropriate

model would include a nonlinear feedback controller that could adapt to varying tasks and complexity of tasks. This may include variable gains and even observers that could estimate unforeseen disturbances that the human could then add to their control law and compensate. The control laws designed by the brain should include the human arm as a link to the vehicle control. Different types of inputs should also be considered such as optical, auditory and tactile information. The types of information that would come through each of those channels could be designed into the human model.

And finally, the addition of delay to the humans ability to control should be added into the model. The delay can come from the reaction time of a human and the processing time, or the speed of thinking. These delays should be dependent on the fatigue and stress on the human. The changes in these parameters could be seen in changes in the feedback gains. By observing the feedback gains it is possible to determine if the human is choosing an unsafe or unstable control law due to fatigue or distraction.

8.2 Semi-Autonomous Control

With all of these improvements it is possible to more accurately describe a human-in-the-loop system for a wider range of situations at once. Here again, nonlinear observers, similar to those derived in this thesis, could be developed to estimate all of the parameters of a human-in-the-loop with hardware system.

This provides the opportunity to measure abstract parameters of the human on line, such as fatigue, efficiency, or stability of the control law in use. This information can be used in conjunction with a computer controller. The computer would actually become more like a virtual copilot that could monitor the vehicle and the human

and make decisions in emergency situation where the vehicle or the human has been determined to be unstable. The computer controller could decide to warn the human if they or the vehicle are becoming unstable. If the human does not respond the computer could decide to completely take over, or just control some critical states and allow the human to control the rest.

All of these improvements can make the task of driving a car safer and more enjoyable. It can also make the complex task of flying an aircraft safer, more enjoyable, and more accessible for everyone.

Bibliography

- [1] Anderson, M., (1994) "A Model of the Human Operator Using Sensitivity Function Shaping." *Proceedings of the American Control Conference*, Baltimore, Maryland, June 1994, pp. 1518-1522
- [2] Barger, V. and Olsson, M., (1973) *Classical Mechanics: A Modern Perspective*
- [3] Basar, E. et. al., (2007) "A Breakthrough in neuroscience needs a 'Nebulous Cartesian System' Oscillations, quantum dynamics and chaos in the brain and vegetative system." *International Journal of Psychophysiology*, vol. 64, pp. 108-122
- [4] Campos, F.M.M.O. and Calado, J.M.F., (2009) "Approaches to Human Arm Movement Control – A Review." *Annual Reviews in Control*, vol. 33, pp.69-77
- [5] Chumbley et. al., (2007) "A Metropolis-Hastings algorithm for dynamic causal models." *Neuro Image*, pp. 478-487
- [6] Cohen, M.A. and Grossberg, S., (1983) "Absolute stability of global pattern formation and parallel memory storage by competitive neural networks." *IEEE Transactions on Systems, Man, and Cybernetics*. SMC-13, pp. 815-826
- [7] DeCarlo, R. A., Zak, S. H., Drakunov, S. V., (1996) "Variable Structure, Sliding-Mode Controller Design." *The Control Handbook*, pp. 941-951

-
- [8] Deiderich, A., (1995) "Intersensory facilitation of reaction time: Evaluation of counter and diffusion coactivation models." *Journal of Mathematical Psychology*, vol .39. pp. 197-215
- [9] Drakunov. S.. (1992) "Sliding-Mode Observers Based on Equivalent Control Method." *Proceedings of the 31st Conference on Decision and Control*, Tucson, Arizona; Dec., 1992, pp. 2368-2369
- [10] Drakunov. S. and Utkin. V.. (1995) "Sliding Mode Observers. Tutorial." *Proceedings of the 34th Conference on Decision and Control*, New Orleans, LA; UNITED STATES: Dec. 13-15. 1995, pp. 3376-3378
- [11] Florida Institute for Human and Machine Cognition website. (2010) <http://www.ihmc.us/research.html>
- [12] Freeman, W.. (2000) "Brain Dynamics: Chaos and Intentionality." *Integrative Neuroscience. Bringing Together Biological, Psychological and Clinical Models of the Human Brain*, pp. 163-171
- [13] Friston, K.J., (2001) "Brain function, nonlinear coupling, and neuronal transients." *Neuroscientist*, vol. 7, pp. 406-18
- [14] Grecu, V. et. al., (2009) "Analysis of Human Arm Joints and Extension of the Study to Robotic Manipulator." *Proceedings of the International MultiConference of Engineers and Computer Scientists*, vol. 2 March 18-20. Hong Kong
- [15] Grossberg, S., (1973) "Contour enhancement, short term memory, and constancies in reverberating neural networks." *Studies in Applied Mathematics*, vol. 52. pp. 217-257

-
- [16] Grossberg, S., (1980) "Biological competition: Decision rules, pattern formation and oscillations." *Proceedings of the National Academy of Sciences*, vol. 77, pp. 2338-2342
- [17] Harrison L. M. et. al., (2005) "Stochastic models of neuronal dynamics." *Philosophical Transactions of the Royal Society Biological Sciences*, vol. 360, pp. 1075-1091
- [18] Johannsen, G., (1972) "Development and Optimization of a Nonlinear Multiparameter Human Operator Model." *IEEE Transactions on Systems, Man, Cybernetics*, vol. smc-2, no. 4, pp. 494-504
- [19] Koiwai, K. et. al., (2008) "Design of a Human-Skilled Based PID Controller using CMACs." *International Conference on Control, Automation and Systems, in COEX*, Seoul, Korea, Oct. 14-17, 2008, pp. 64-68
- [20] Landesman, E.M. and Hestenes, M.R., (1992) *Linear Algebra for Mathematics, Science, and Engineering*
- [21] Liao et. al., (2004) "Criteria for exponential stability of Cohen-Grossberg neural networks." *Neural Networks*, pp. 1404-1414
- [22] Nelson, R. C., (1998) *Flight Stability and Automatic Control*, Second Edition
- [23] Pachter, M. and Houppis, C. H., (1996) "Flight Control of Piloted Aircraft." *The Control Handbook*, pp. 1287-1302
- [24] Pamadi, B. N., (2004) *Performance, Stability, Dynamics, and Control of Airplanes*, Second Edition
- [25] Perry, J. F., (2003) *A Tactile Control Prosthesis*, Thesis PhD.

-
- [26] Phatak, A. V and Weinert, H. L., (1976) "Identifiability of the Optimal Control Model for the Human Operator." *Automatica*, vol. 12, pp. 31-41
- [27] Phillips, C. A. and Repperger, D. W., (1999) "An Informatic Model of Human Operator Control." *Proceedings of The First Joint BMES/EMBS Conference Serving Humanity, Advancing Technology*, Atlanta, GA, USA, Oct. 13-16, 1999, pp. 1009
- [28] Rosen, J. et. al., (2005) "The Human Arm Kinematics and Dynamics During Daily Activities Towards a 7 DOF Upper Limb Powered Exoskeleton." *The 12th International Conference on Advanced Robotics*, Seattle, WA. July 2005
- [29] Rubakhin, V.F and Poltorak, M.I., (1974) "A study of the processing of multimodal signals by man." *Voprosy Psikhologii*, Sept-Oct (No.5). pp. 71-80
- [30] Saarinen, A. et. al., (2008) "Stochastic Differential Equation Model for Cerebellar Granule Cell Excitability." *PLoS Computational Biology*, vol. 4
- [31] Sarbanadhikari, S.N. and Chakrabarty, K., (2001) "Chaos in the brain: a short review alluding to epilepsy, depression, exercise and lateralization." *Medical Engineering and Physics*. vol. 23, pp. 445-455
- [32] Stephan, K et. al., (2008) "Nonlinear dynamical causal models for fMRI." *Neuro Image*. vol. 42. pp. 649-662
- [33] Suit, W.T., (1972) "Aerodynamic Properties of the Navion Airplane Extracted from Flight Data." *NASA Langley Research Center*. Report Number. NASA TN D-6643
- [34] Tozeren, A., (2000) *Human body dynamics: classical mechanics and human movement*

-
- [35] Wallace J., (2000) "Unlike Airbus. Boeing lets aviator override fly-by-wire technology." *Seattle Post-Intelligencer Reporter*, March 20, 2000, <http://www.seattlepi.com/business/boe202.shtml>
- [36] Ward, L. M. and West, R. L., (1998) "Modeling Human Chaotic Behavior: Non-linear Forecasting Analysis of Logistic Iteration." *Nonlinear Dynamics, Psychology, and Life Science*, vol. 2, No.4, pp. 261-282
- [37] Ward, L. M., (2002) *Dynamical Cognitive Science*
- [38] Wie, B., (2008) *Space Vehicle Dynamics and Control*. Second Edition
- [39] Zatsiorsky, V. M., (1998) *Kinematics of Human Motion*
- [40] Zatsiorsky, V. M., (2002) *Kinetics of Human Motion*

Appendix A

Constants

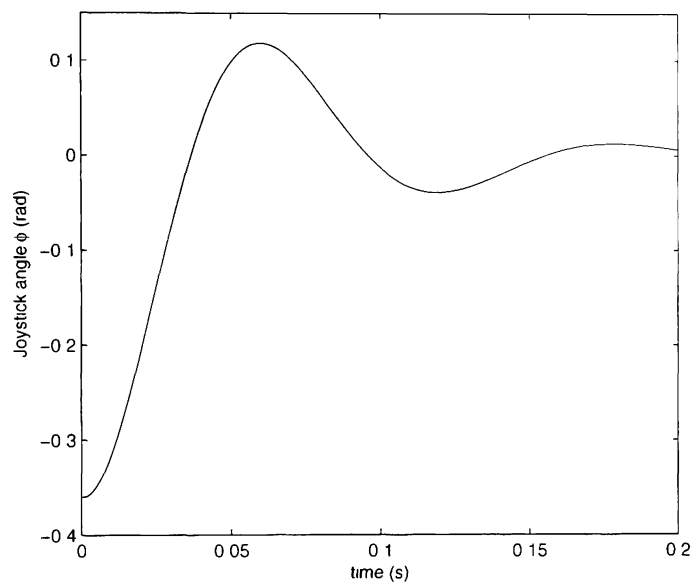
Body Segment	Mass(%)	Length(%)
Whole body	100	100
Upper arm	3.3	17.2
Forearm	1.9	15.7
Hand	0.6	10.4

Table A.1: Relative mass and length of select body segments as a percentage of total body mass and height for adult males [34].

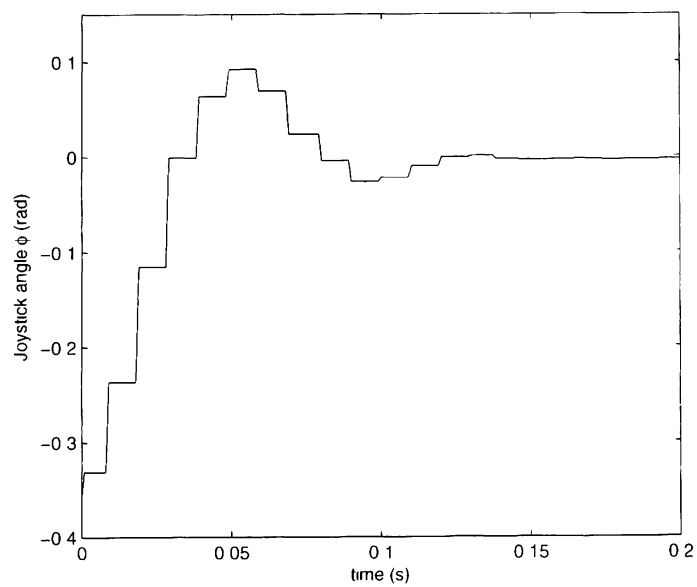
Body Segment	Mass(kg)	Length(m)
Whole body	80	1.8
Upper arm	2.6	0.31
Forearm	1.5	0.28
Hand	0.5	N/A

Table A.2: Mass and length of select body segments as calculated from Table A.1 for typical total body mass and height of adult males.

Reasonable values for k_s and k_μ , shown in Table A.3, were chosen by comparing the motion of a real joystick to the motion of the simulated joystick as shown in Figure A.1. The trajectories shown begin with the same initial condition.



(a) Simulated



(b) Measured

Figure A.1: Simulated and measured results for joystick motion.

Constant	Value	Unit
Mass	0.5	kg
Length	0.15	m
Spring constant (k_s)	12	N/m
Coefficient of friction (k_μ)	0.15	
Range of motion	± 0.36	rad
Base location relative to shoulder	(0.45, -0.3)	m

Table A.3: Joystick constants.

Constant	Value	Unit
Mass	2.5	kg
Radius	1	m

Table A.4: Solid ball constants.

Appendix B

Simulink Models

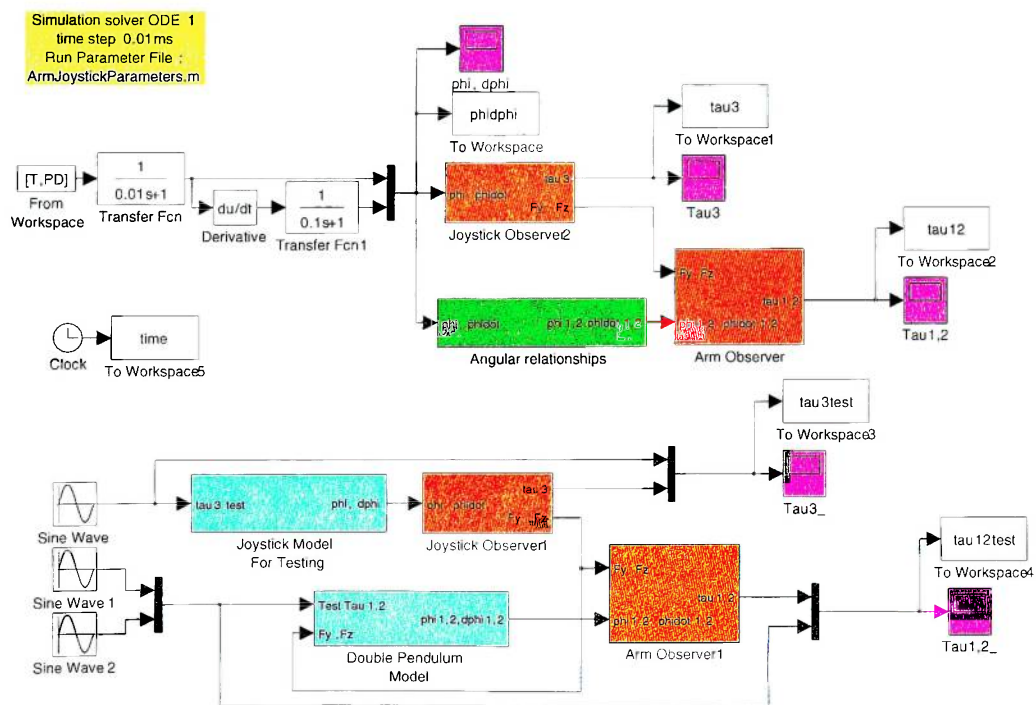


Figure B.1: Arm and joystick models and observers combined.

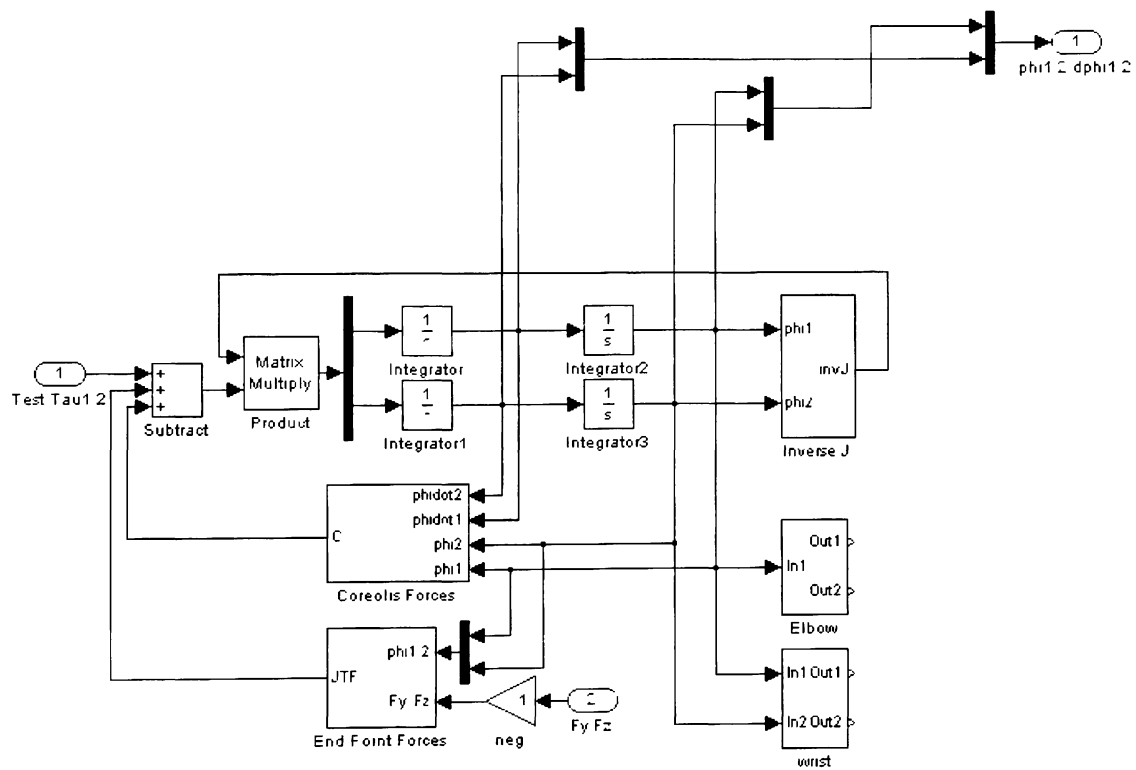


Figure B.2: Arm Simulink model.

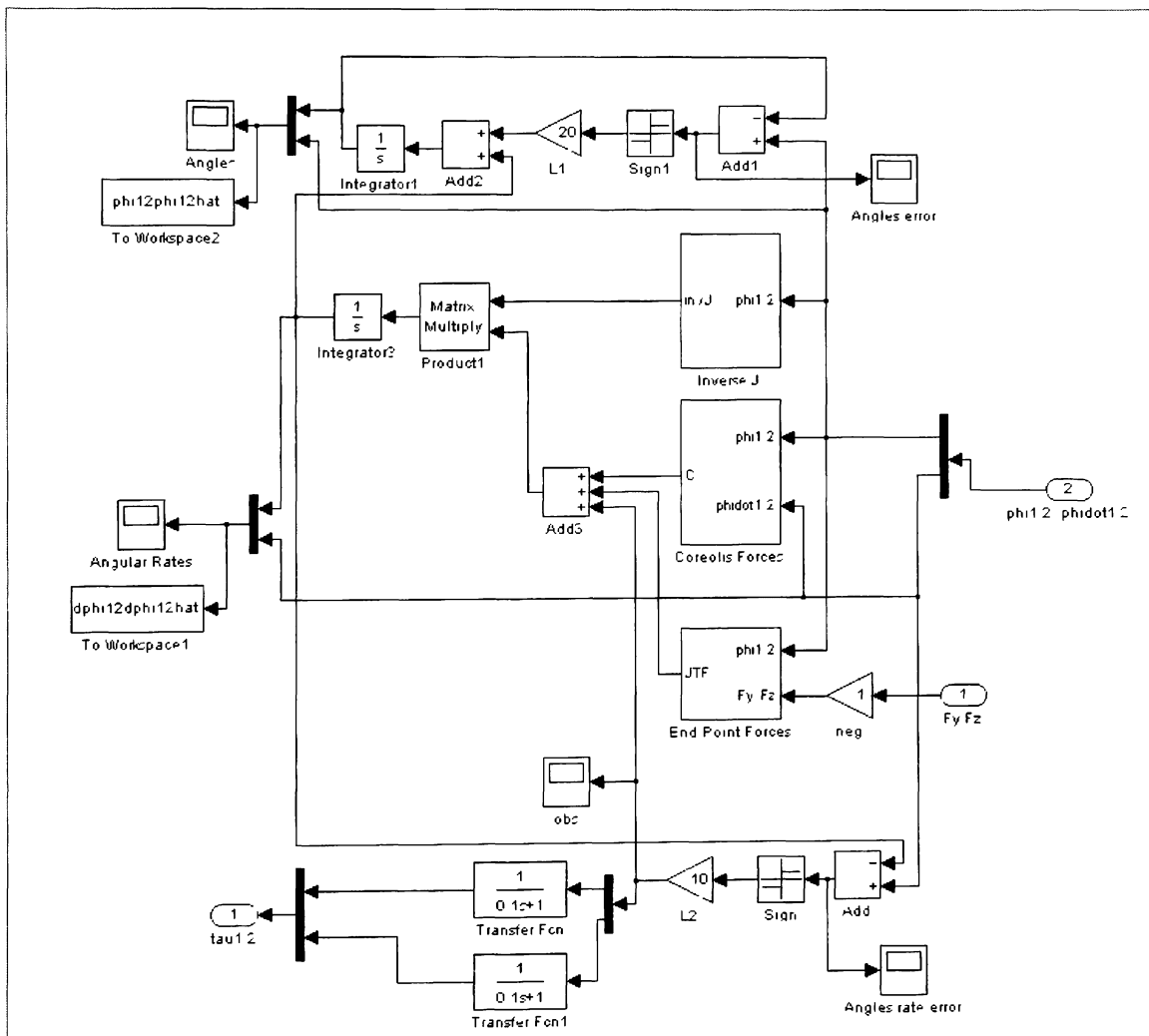


Figure B.3. Arm Simulink observer.

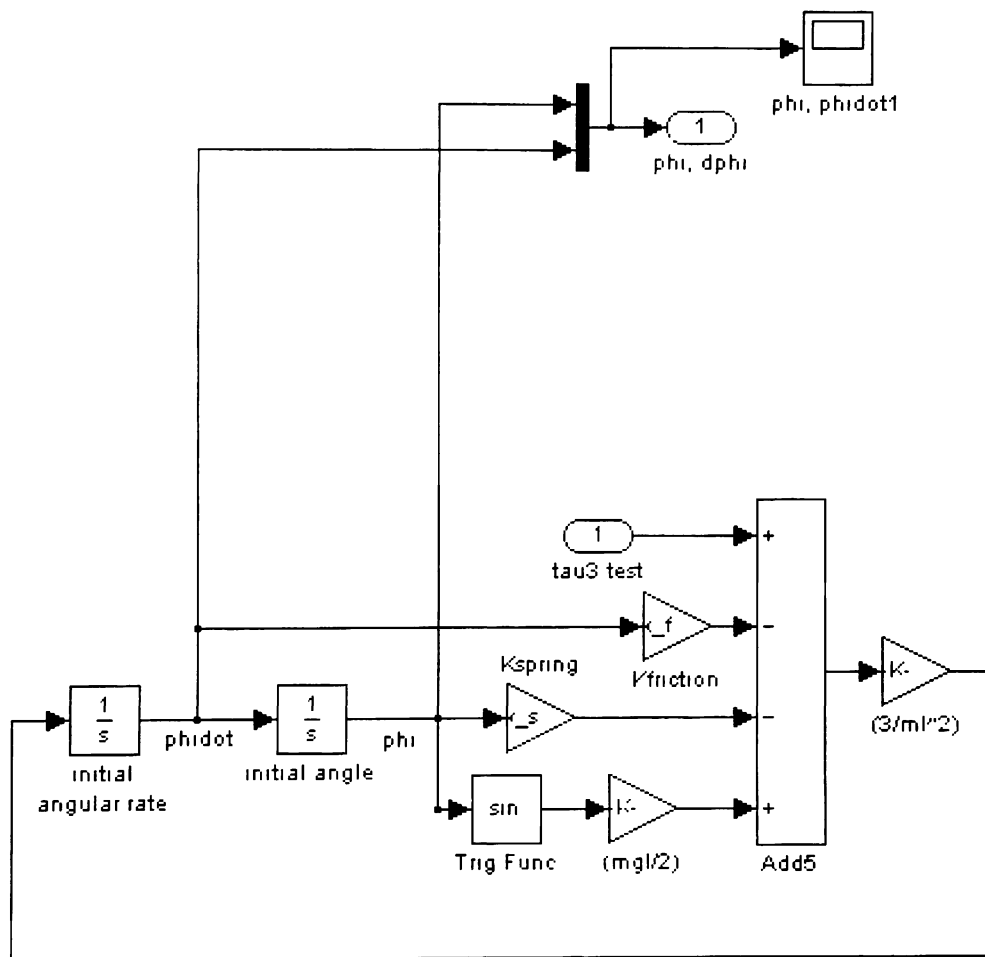


Figure B.4: Joystick Simulink model.

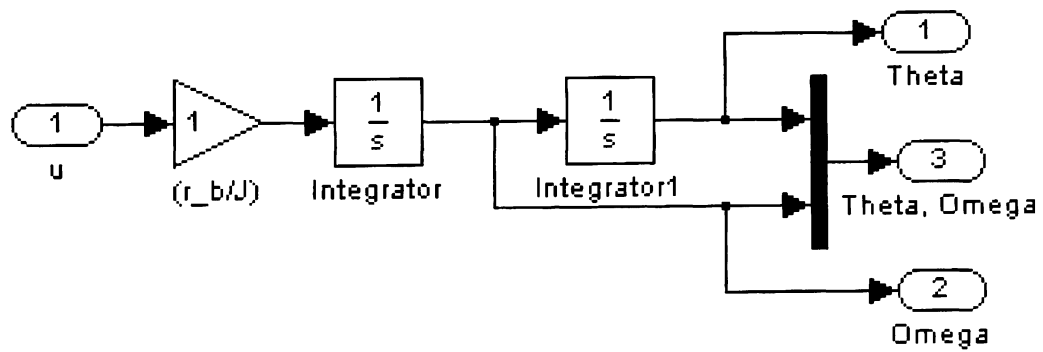
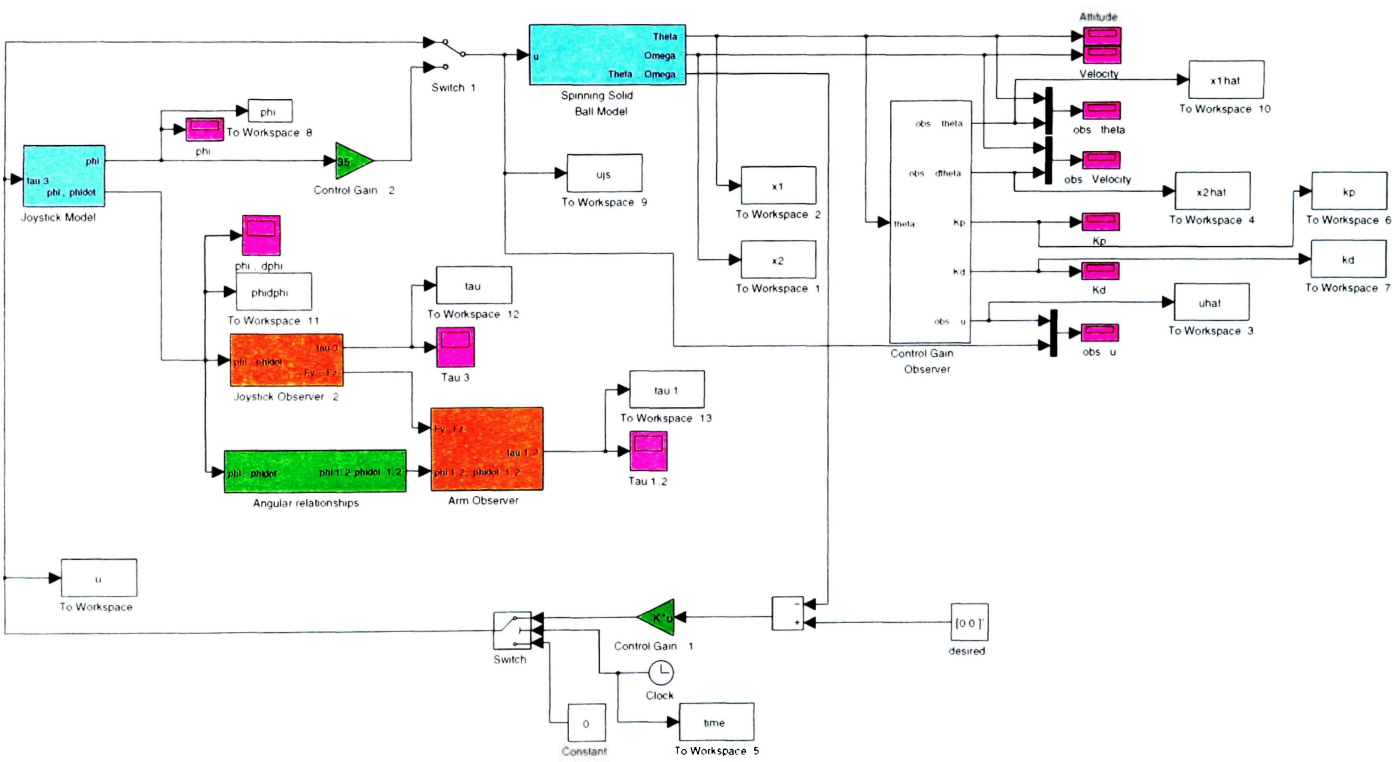


Figure B.5: Solid ball Simulink model.

Figure B.6: Solid ball control with PD and torque observers combined.



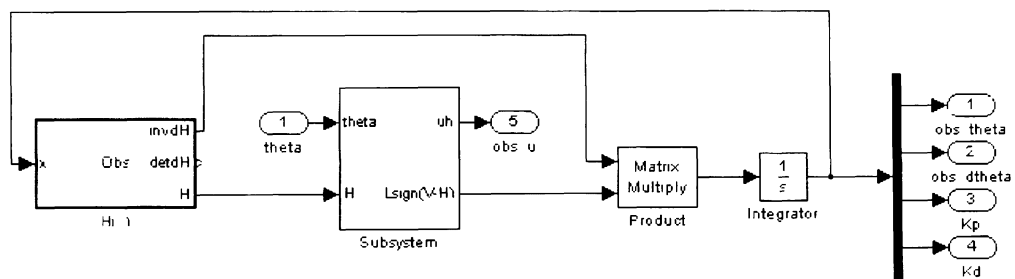


Figure B.7: PD Simulink observer.

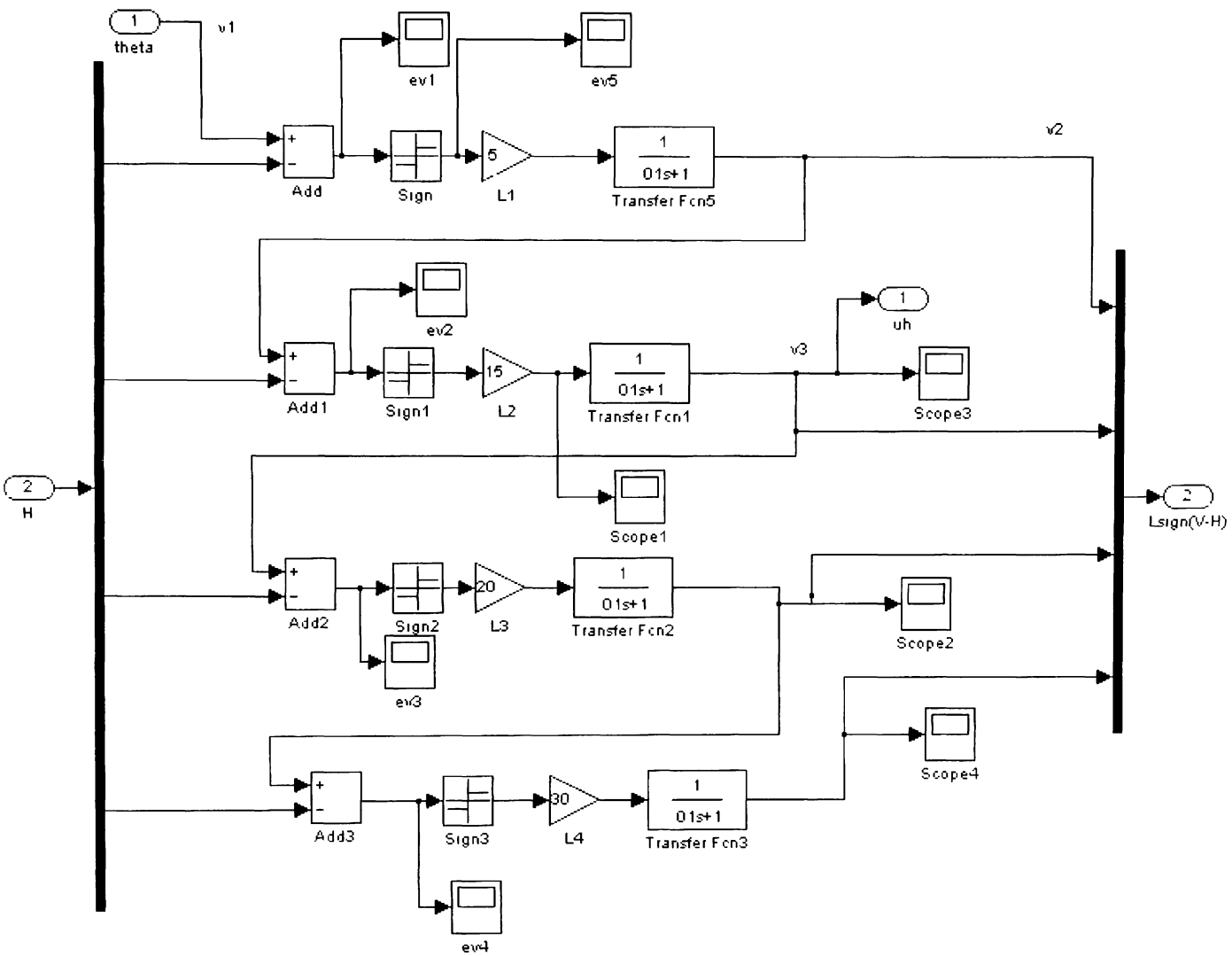


Figure B.8: Observer vector V for PD Simulink observer.

Appendix C

Matlab Code

ArmJoystickParameters.m

```
clear all;

% Joystick
m_j=.5; %mass of Joystick
l_j=.15;%length of Joystick
g=9.8; %gravity acceleration
k_s=3; %spring constant of Joystick
k_f=.1; %friction coefficient of Joystick

% Arm Stuff
m1=2.6;
m2=1.5;
l1=.31;
l2=.28;
l3=.15;
d1=l1/1;
d2=l2/2;
y4=.45;
z4=-.3;

% Pitch Data from wrist gyro
load Joystick_Gyro_Data/HGPD.mat
Time = (x39560917034865-39560917034865).*10^-9;
PD(1:length(Time))=0;
PD(length(Time)+1:2*length(Time)) = -(pitch-pitch(1))*pi/180;
```



```
T(1:length(Time))=Time;
T(length(Time)+1:2*length(Time)) =...
    Time+Time(end)/length(Time)+Time(end);
T=T';
PD=PD';
figure(1);
plot(T,PD,'c')
xlabel('time (s)')
ylabel('angle phi (rad)')
title('Hand Gyro Pitch Down Angle')
legend('pitch')
```

ControlSpinningBallParameters m

```
clc
clear all
close all

%Control delay
T = 1, %1 second
taubias=0; % bias torque

% ball stuff
m_b=1*2.5; %mass of ball
r_b=1*1; %radius of ball
J = (2/5)*m_b*(r_b^2), %Rotational Inertion

% Joystick
m_j=.5; %mass of Joystick
l_j=.15;%length of Joystick
g=9.8; %gravity acceleration
k_s=12; %spring constant of Joystick
k_f=.15; %friction coefficient of Joystick

% Arm Stuff
m1=2.6;
m2=1.5;
l1=.31;
l2=.28;
l3=.15;
d1=l1/1;
d2=l2/2;
y4=.45;
```

```

z4=-.3;

% state space for x1=theta, x2=thetadot, for PD control
A=[0 1;
   0 0];

B=[0; r_b/J];

rank=rank(ctrb(A,B))
eA=eig(A)
p=[eA(1)-2 eA(2)-4]
[Kp,prec,message]=place(A,B,p)
eig(A+B*Kp)
figure(3)
plot(real(eA),imag(eA),'b*');
hold on
plot(real(p),imag(p),'r*');
grid on

    PlottingArm_AngleRelations.m

clc
clear all
close all;

l1=.31;
l2=.28;
l3=.15;
% i=1;
% i=1:100:(length(phi)-1)*.5;
% T=0:.01:10;
phi=-.36:.003:.8;
for i=1:length(phi);
y4=.45;
z4=-.3;
y3=y4+l3*sin(phi(i));
z3=z4+l3*cos(phi(i));

zplus(i)=(1/(2*(y3^2+z3^2)))*(l1^2*z3-l2^2*z3+y3^2*z3+z3^3...
+(-y3^2*(l1^4+(-l2^2+y3^2+z3^2)^2...
-2*l1^2*(l2^2+y3^2+z3^2)))^(1/2));
zminus(i)=(1/(2*(y3^2+z3^2)))*(l1^2*z3-l2^2*z3+y3^2*z3+z3^3...
-(-y3^2*(l1^4+(-l2^2+y3^2+z3^2)^2...

```

```

-2*l1^2*(l2^2+y3^2+z3^2))^(1/2));
%yplus=(1/(2*y3*(y3^2+z3^2)))*(l1^2*y3^2-l2^2*y3^2+y3^4...
% +y3^2*z3^2*-z3*(-y3^2*(l1^4+(-l2^2+y3^2+z3^2)^2...
% -2*l1^2*(l2^2+y3^2+z3^2))^(1/2));

yminus(1)=(1/(2*y3*(y3^2+z3^2)))*(l1^2*y3^2-l2^2*y3^2+y3^4...
+y3^2*z3^2+z3*[-y3^2*(l1^4+(-l2^2+y3^2+z3^2)^2...
-2*l1^2*(l2^2+y3^2+z3^2))^(1/2));
%sqrt=(-l1^4*y3^2+2*l1^2*l2^2*y3^2-l2^4*y3^2+2*l1^2*y3^4...
% +2*l2^2*y3^4-y3^6+2*l1^2*y3^2*z3^2+2*l2^2*y3^2*z3^2...
% -2*y3^4*z3^2-y3^2*z3^4);

phi1(1)=acos(zminus(1)/l1);
phi2(1)=acos((z4-zminus(1)+l3*cos(phi(1)))/l2);
% l1nex1=[0 yminus];
% l1ney1=(zminus/yminus)*l1nex1;
% l1nex2=[yminus y3];
% l1ney2=((z3-zminus)/(y3-yminus))*(l1nex2-yminus)+zminus;
% l1nex3=[y3 y4];
% l1ney3=((z3-z4)/(y3-y4))*(l1nex3-y4)+z4;

% figure(3)
% plot(0,0,'ob',l1nex1,l1ney1,'r',yminus,zminus,'ob',...
% l1nex2,l1ney2,'r',y3,z3,'ob',l1nex3,l1ney3,'r',y4,z4,'ob')
% xlabel('Y')
% ylabel('Z')
% axis([0 .6 -.6 0])
% grid on
% i=i+1;
end

figure(1)
plot(phi(:),phi1(:),'k--',phi(:),phi2(:),'k','LineWidth',1)
xlabel('Joystick angle: \phi (rad)')
ylabel('Shoulder and Elbow angles: \phi_1, \phi_2 (rad)')
legend('\phi_1','\phi_2')

figure(2)
plot(phi(:),zplus(:),'k-.',phi(:),zminus(:),'k')
xlabel('Joystick angle: \phi (radians)')
ylabel('Elbow height position (meters)')
legend('upper solution','lower solution')

```